Design, Fabrication and Control of a Magnetic Capsule Robot for the Human Esophagus

by

Saman Hosseini

A thesis
presented to the University of Waterloo
in fulfillment of the
thesis requirement for the degree of
Master of Applied Science
in
Mechanical Engineering

Waterloo, Ontario, Canada, 2009

AUTHOR'S DECLARATION

I hereby declare that I am the sole author of this thesis. This is a true copy of the thesis, including any required final revisions, as accepted by my examiners.

I understand that my thesis may be made electronically available to the public.

Abstract

Biomedical engineering is the application of engineering principles and techniques to the medical field. It combines the design and problem solving skills of engineering with medical and biological sciences to improve healthcare diagnosis and treatment. As the result of improvements in robotics and micro technology science in the 20th century, micro electromechanical system technology has joined with medical applications which results in micro robotic medical applications.

Drug delivery is one of the most important and controversial topics which scientists and engineers have tried to improve in medical applications. For diseases like cancer, localized drug delivery is a highlight target involving bombarding a small area of a human's body and this technology has not been completely achieved yet.

The ultimate objective of this thesis is the development of wireless capsule robot controlled by a magnetic drive unit. A magnetic drive unit is a system that consists of electromagnets, which produce the magnetic field from outside of the patient's body. The capsule robot, which is the slave robot in the system, moves inside a human's gastrointestinal tract. This project is focused mainly on a human esophagus and all the experiments are done in a prototype of the human's esophagus.

Drug delivery for diseases like cancer is the objective of the capsule robot. The proposed design consists of a slave permanent magnet for the motion of capsule robot in a tube, a reservoir of drug, and a micro mechanical mechanism for drug release. The capsule robot is fabricated and developed in a 12mm length and 5mm diameter with the weight of 1.78 grams without the built-in permanent magnet.

The drug delivery system is a semi-magnetized system, which can be controlled by an external magnetic field. It consists of a mechanical plunger and spring, which can be open and close through an external magnetic field manipulation. The amount of drug for a desired location can be controlled by manipulating the external magnetic field.

To achieve this target, analytical modeling is conducted. A numerical simulation and an experimental setup demonstrate that a capsule robot in a human esophagus in a simple and multi channel system. Horizontal control is set for the capsule robot, using a custom-designed controller and a colored liquid is released with the external magnetic field.

The present study with its fabricated prototype is a research is this area to prove the concept of wireless control of a robot inside a human body and the potential for a drug delivery system. It is

expected that the results achieved in this project will help realize and promote capsule robot for medical treatments.

Acknowledgements

I would like to thank my supervisor, Professor Behrad Khamesee for all their guidance, support, and constant encouragement during my research.

I would also like to express my gratitude to the examining committee members Professor John Medley and Professor William Melek whose comments and suggestions were extremely helpful in improving my manuscript.

Over the last two years, I have been privileged to work with and learn from my colleagues, Andrew Barber, Robert Wagner, Jason Benning, Babak Ebrahimi, Mohsen Azimi Soroosh Hassanpour and Moein Mehrtash.

I wish to express thanks to my family members, Mohammad Hosseini and Zohreh G. Zadeh.

Dedication

To the best creatures of GOD

Mohammad Hosseini

and

Zohreh G. Zadeh

It is them who bestow upon me the character of diligence, resolution and perseverance. Without their never-ending encouragements and support in these years, I could not even consider writing.

Table of Contents

List of Figures

List of Tables

Chapter 1

Introduction

Micro robots are used in various biomedical applications. The presence of a robot often provides accuracy in positioning for the doctors. Also, robots can be used in hazardous environments. Much research on the development of a robotic capsule for the diagnosis of gastrointestinal diseases and drug delivery has been carried out. The powering of these micro systems is becoming very important as the implementation of such systems is limited due to the size and reliability of on-board power supplies.

1.1 Problem definition

The problem is to design a system for accurate drug systems. One of the most exciting topics in drug delivery is local drug delivery for cancer diseases. In these types of diseases, some areas of patient's body need to be bombarded by a drug. In drug bombarding methods such as chemotherapy, a drug is injected into a patient's blood. In this case, large parts of patient's tissues will be affected by the drug not just the desired part.

The human gastrointestinal tract has a peristalsis motion which helps the food or any external object to be digested. It is difficult for doctors to fix any drug delivery system, to stay at a specific location within the gastrointestinal tract to treat the patient.

In some diseases, a drug should be delivered to a selected tissue over a specific period of time. In these types of problems, the tissues should be in contact with drug for enough time to allow chemical reactions to occur.

The focus of the present thesis is to design a capsule robot which can be manipulated in the human esophagus. This robot needs to be able to deliver a drug to a desired location for short or long periods of time. The controller should be a completely wireless system thus eliminating any pain associated with an external wire going inside the human body or avoiding surgical operation such as those involved in classic endoscopy or colonoscopy operations.

The content of the present study is to develop a micro robotic system based on magnetic principles thus eliminating the use of on-board power supplies. The goal is to build a system in which a capsule-robot can be manipulated wirelessly inside human's body.

1.2 Thesis overview

This thesis consists of 6 chapters. After the introductory chapter, the background for the test bed development is presented in chapter 2. Human esophagus in gastrointestinal tract has been explained and resulted to the test bed development. This chapter also includes descriptions of the mechanical properties and medical diseases of the esophagus.

Capsule-robot design and development is presented in chapter 3. After a literature review in section 3.1, the wireless capsule robots have been reviewed. The concept of drug delivery and previous achievements are presented in section 3.2. Mechanical modeling of capsule robots and conceptual designs are reviewed in section 3.3. Following the review this section, capsule-robot development of the present study is described in section 3.4. At the end of this chapter, magnetic field effects on live human tissue have been evaluated to make sure that our method is not damaging to the human body.

Chapter 4 talks about the wireless control system of the capsule robot. In this chapter, the electromagnetic control system has been evaluated to start experiments of drug delivery in designed test bed. The infrastructure has been described in section 4.1. After reviewing all the parts of magnetic setup, system modification has been mentioned in section 4.2. There are some test setup modifications and modeling is explained in this section. Then the pole piece is developed in section 4.2.2. In this section, after finite element analysis of the magnetic drive unit pole piece, the prism theory for the pole piece has been presented. This chapter continues with analytical modeling of magnetic field and force in section 4.2.3. The drag force, friction force and electromagnetic force have been modeled analytically. All the modeling and analysis in this chapter result to design the control system in section 4.2.4. The vertical and horizontal controllers with an open loop and close loop methods are presented in this section. Section 4.2.5 as the last section of this chapter, refers to the finite element modeling of our system which satisfies the controller and analytical modeling we designed.

Chapter 5 presents all the experimental results of the capsule robot. In this chapter, This chapter describes the testing of the controller in Labview and open loop and close loop control system has been tested on the capsule robot. The drug delivery system has been evaluated in this chapter too. The controller performance predictions from Labview are presented along with experimental results that consist of movies of the prototype capsule robot behavior.

Chapter 6, as the last chapter of the present thesis gives the conclusions. It shows that the results address the problem defined at the beginning of the thesis.. The recommendations for the future works on wireless capsule robot and drug delivery system have been presented in this chapter as well.

Chapter 2

Test Bed Development

2.1 Anatomy and Physiology of Gastrointestinal Tract

2.1.1 Gastrointestinal tract

The Gastrointestinal tract of human body which starts from mouth and ends to anus, is a continuous channel through the body with orifices and specific motions for intake and output of external material (2). It consists of a series of organs with the billiard tract as a major side-branch. It should be mentioned here that the structure and function of the gastrointestinal tract differ among animals and humans according to nutritional mechanism. The size of gastrointestinal tract system depends on types of material pass through it in a long term. The wall of passage between the pharynx and the stomach tract has a laminated composite muscle structure, which is called esophagus. (1).

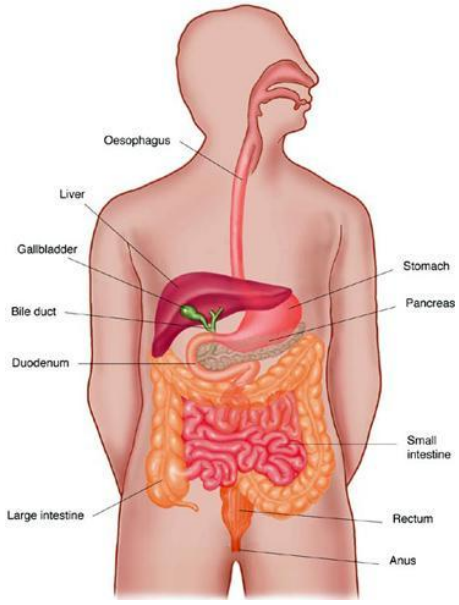

Figure 1 - Gastrointestinal tract (1)

The structure and composition of the muscle layers are listed below:

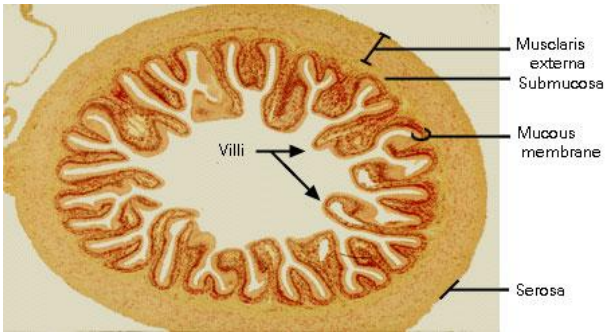

Figure 2 - Structure of muscle in gastrointestinal tract system (1)

1. **The main muscle coat**: The main muscle coat or the muscularis propia has two layers. A network of collagen fibres forms the basic structure or stroma in each layer. They are capable of shortening separately in the contraction process. The two layers of muscle differ in the orientation of their muscle cell (2).

2. **The Muscle of the Mucosa**: A second major layer or third physical layer of muscle is called mucularis mucosae. The submucosa layer is the seperation between this layer and main muscle coat with the same structure as other layers (2).

2.1.2 Esophagus

As it is mentioned in section 2.1.1, the digestive tract (also known as the alimentary canal) is the system of organs within multi cellular animals that takes in food, digests it to extract energy and nutrients, and expels the remaining waste. The major functions of the GI tract are ingestion, digestion, absorption, and defecation. The GI tract differs substantially from animal to animal and human to human. Some of them have multi-chambered stomachs, while some animals' stomachs contain a single chamber. In a normal human adult male, the GI tract is approximately 6.5 meters (20 feet) long and consists of the upper and lower GI tracts. The tract may also be divided into foregut, midgut, and hindgut, reflecting the embryological origin of each segment of the tract.

Figure 3, shows the structure of esophagus that consists of a muscle layer and cells lying in circumferential direction which should tolerate axial and circumferential stresses. This two parts are flexible and enlarges to pass any external objects (2).

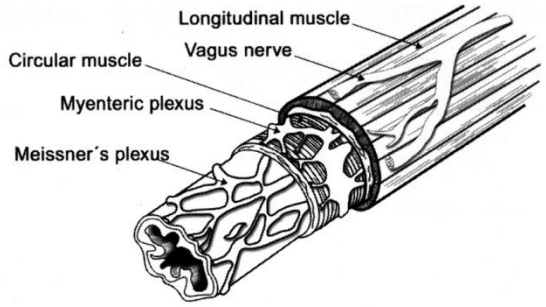

Figure 3 - Esophagus structure (2)

The esophagus, sometimes known as the gullet, is an organ in (Figure 4) which consists of a muscular tube through which food passes from the pharynx to the stomach. The esophagus passes through a hole in the thoracic diaphram called the esophageal hiatus. It is usually 250-300 mm long which connects the mouth to the stomach. It is divided into cervical, thoracic, and abdominal parts.

Food is passed through the esophagus by using the process of peristalsis. Specifically, it connects the pharynx, which is the body cavity that is common to the digestive factory and respiratory system with the stomach, where the second stage of digestion is initiated. The esophagus is lined with mucous membrane, and is more deeply lined with muscle that acts with peristaltic action to move swallowed food down to the stomach (2). The peristalsis process is a substantial problem for any robots wanted to move inside human's GI tract. The human esophagus tends to move any external object down to the stomach. It causes a limitation for any operation by a robot which takes time in esophagus.

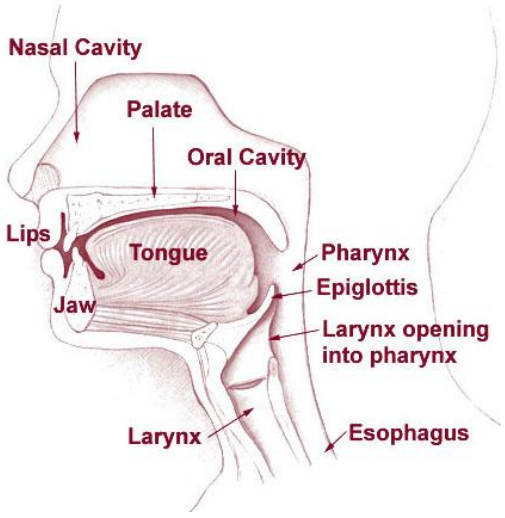

Figure 4 - Human's esophagus (2)

2.1.3 Imaging methods

Endoscopy and colonoscopy are a common procedures in which an optical device is inserted into the gastrointestinal tract through patient's mouth or anus and the patient is viewed by the examiner through the optical cable connecting it to the outside. The need for a cable causes two-thirds of lesions to be un-viewable by this method. Electromagnetically controlled endoscope has been developed and has increased the range into the gastrointestinal tract that the instrument can reach (3)(4) . Computed tomography is used to direct this device. The development of this device demonstrates the ability to magnetically control a device in the gastrointestinal tract and to insert a medical device into it without harming the patient.

2.2 Biomechanics of the esophagus

Mechanics of a material deals with the behavior of a solid bodies subjected to various types of loading. All theories of thin-shell structures have the common objective to represent the three-dimensional structure by a two-dimensional surface. In the classic theory, it is accomplished through the Bernoulli-Kirchhoff hypothesis which states that all points lying on a normal of the neutral surface before deformation do the same after deformation, that for all kinematical relations, the coordinate z of a point is unaffected by the deformation of the shell, and for all considerations of the stress system, the stress σ_z may be ignored. The classical theories use four additional hypotheses:

1. The material is homogenous
2. The strain-stress relationship is linear and elastic
3. The deformation is so small that the strain-displacement relationship is also linear
4. The shell is stress free when all external forces or loads are removed

Biomechanics aims to understand the mechanics of living tissues consist of solid and fluid structure. Biomechanics of esophagus can be used to determine the stresses and strains in this biological structure when forces are acting on them. This is important in the present study for two reasons. First, a test bed can be designed that is similar to the human esophagus and experiments can be run on a prototype capsule robot. Second, the maximum forces acting on a capsule robot can be estimated and used in the prototype design.

Forces applied to solids cause deformation while forces applied to fluids cause flow. Due to the high water content in biological tissues, they have mechanical behavior of both an elastic solid and

viscous fluid and are thus viscoelastic materials. The deformation is time-dependent because of the fluid flow within the tissue. Stress relaxation (when the material is suddenly strained and the strain is maintained constant), creep (when the material is suddenly stressed and the stress is maintained constant) and hysteresis (when the material is subjected to cyclic loading) are features of viscoelasticity such as living tissues. In esophagus the stress in thin-walled cylindrical pressure vessel with linearly elastic material behavior is assumed. Cylindrical pressure vessels having a circular cross-section are found in many industrial settings. Usually the weight of the pressure vessel and its contents can be neglected. In such cylindrical pressure vessels, we deal with radial, circumferential and longitudinal components of stress in the respective direction. The next sections describe the two important stresses components in detail.

2.2.1 Circumferential Stress

In cylindrical pressure vessels, the largest stress induced by distension is in the circumferential direction. According to Laplace's law

$$\tau_{\theta} = \frac{Pr_i}{h} \qquad \textbf{(2.1)}$$

Where $\boldsymbol{P}$ = pressure, $\boldsymbol{r_i}$ = internal radius and $\boldsymbol{h}$= wall thickness.

It should be noted that stress in equation (2.1) is averaged over the thickness of the segment and does not describe any regional distribution of stress across the wall thickness as shown in Figure 5.

2.2.2 Longitudinal Stress

The longitudinal stress is

$$\tau_z = \frac{Pr_i^2}{(r_0^2 - r_i^2)} \qquad \textbf{(2.2)}$$

It should be noted here that the longitudinal force in the esophagus wall $\boldsymbol{\tau_z \pi (r_0^2 - r_i^2)}$ is balanced only by the pressure component $\boldsymbol{P_i \pi r_i^2}$, since all the external forces are assumed to be zero.

Since the wall thickness-to-radius ratio is small, so that $\boldsymbol{r_o = r_i = r}$ and$\boldsymbol{r_o - r_i = h.}$ Then equation (2.2) for longitudinal stress can be simplified to:

$$\tau_z = \frac{Pr_i}{2h} \qquad \textbf{(2.3)}$$

The body-diagram is shown in Figure 5.

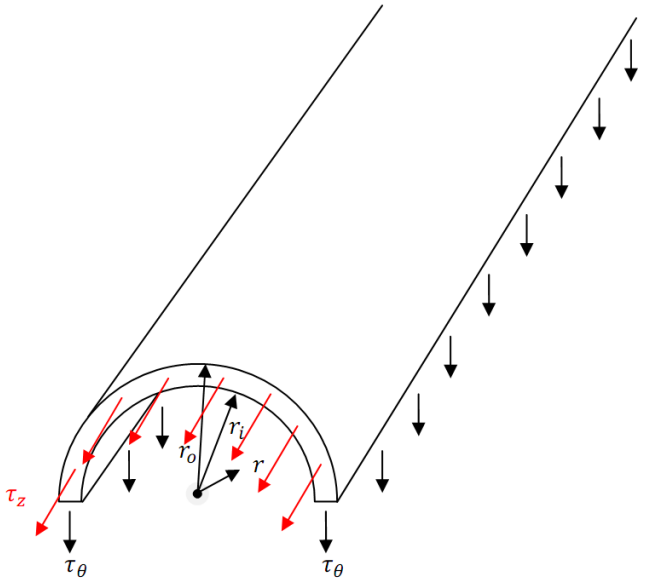

Figure 5 - Esophagus model

2.2.3 The stress-strain relation

In biological tissues the relation between stress and strain is non-linear and the strain is usually large. The non linear mechanical behavior is likely due to the properties of collagen and facilitates stretch in the physiological pressure range and prevents overstretch and damage to the tissue at higher stress level. Over stretch can induce a plastic deformation whereby the tissue can no longer return to its original state when unstressed. The gastrointestinal wall has complex three-dimensional structures that have different material properties in different directions as we call it anisotropy. The constitutive equations of a solid that consists of a homogenous, isotropic, linearly elastic material contain only two material constants:

$$\varepsilon_{ij} = \frac{1}{2\mu}\left[\frac{-\lambda}{3\lambda+2\mu}\tau_{\alpha\alpha}\delta_{ij} + \tau_{ij}\right] \qquad \textbf{(2.4)}$$

Where i and j are indices ranging from integers 1 to 3. The i^{th} index denotes the component in the i direction whereas the j index denotes the surface perpendicular to the j direction.

A uniaxial state of stress with the non-zero stress component $\boldsymbol{\tau_{11}}$ corresponding to the $\boldsymbol{x}$-direction. From equation 1-4 it can be inferred that

$$\varepsilon_{11} = \frac{\lambda + \mu}{\mu(3\lambda + 2\mu)} \tau_{11}$$
$$\varepsilon_{22} = \varepsilon_{33} = \frac{-\lambda}{\mu(3\lambda + 2\mu)} \tau_{11} \quad \textbf{(2.5)}$$

Then the Young's modulus measured in a uniaxial tension test is

$$E = \mu \frac{3\lambda + 2\mu}{\lambda + \mu} \quad \textbf{(2.6)}$$

And Poisson's ratio is given by:

$$\upsilon = \frac{\lambda}{2(\lambda + \mu)} \quad \textbf{(2.7)}$$

Pressure-diameter curves of the esophagus were obtained to define its mechanical properties. The mucosal contribution to the strength of the esophagus was negligible until the outer diameter almost doubled, suggesting that small intraluminal pressures are held by the muscle layer alone. For larger deformations mucosal contribution increased and at failure the mucosa held over one-half of the failure pressure of the esophagus. The paths followed during loading and unloading are different and exhibit hysteresis. They are influenced by the rate of pressure change, being more compliant for low rates of pressure change. They are influenced by the history of loading, being different for successive loading-unloading cycles. If enough loading-unloading cycles are repeated a stable loop is reached, which does not change thereafter. Both the mucosa and the whole esophagus show increasing stiffness with increasing pressure. This behavior can be represented by a simple exponential relationship. However, at rapid rates of pressure increases, the esophageal muscles produce sigmoid loading curves, which gradually become exponential when repeating loading. This results the wave motion of the esophagus. This motion is caused by an external object inside the gastrointestinal tract called swallowing. At the time an external object passes through human's mouth, muscles that mentioned above start to move sinusoidal and helps an object to pass esophagus to the stomach. This is the resistance force applies to the capsule robot during its operation that the magnetic control system is going to produce a locomotive force opposite to peristalsis wave. Regarding this fact, the capsule robot can stay at the specific point to release the drug at that point. A similar method in medical applications like chemotherapy in esophagus cancer is done by delivering the drug through the blood. This destructive drug can then damage all the patient's cells including the targeted cells. On the other hand, drug delivery should be performed in a long time. These two major aims can be

achieved by keeping the capsule at the desired point and release the drug for a long time at that point (2).

2.3 Test Bed

The capsule robot is going to move in the human esophagus. A model of test bed for magnetic drug delivery experiments has been developed. The size of this test bed is modeled with the same size of human's esophagus and the material properties are chosen to be as close as possible to real material. The model of the chamber is shown in Figure 6.

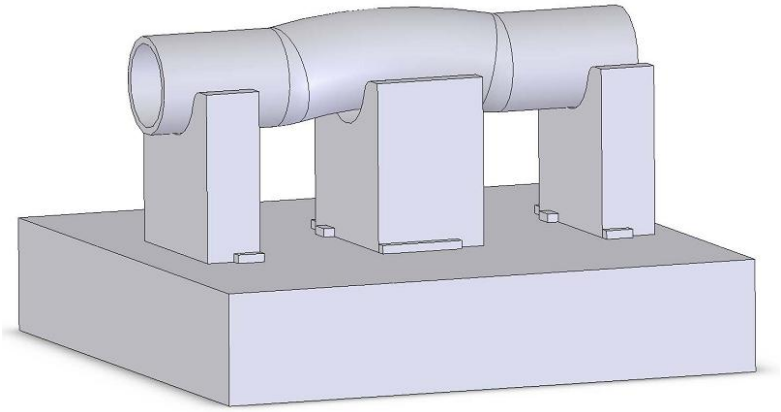

Figure 6 - Drug delivery test bed

All the parts of this test bed except the tube are made of aluminum and the tube is basically made of tuyaux. The size of the test bed is 100 mm by 100 mm and the diameter of tube is 30 mm. The diameter of human's esophagus is between 22.9mm and 49.9mm. The weight of the test bed is 340 grams and is located in the working area of magnetic levitation setup. Test bed and some other prototypes for different experiments are fabricated in the Faculty of Engineering Machine Shop at the University of Waterloo.

Chapter 3

Capsule Robot

3.1 Literature Review

3.1.1 Introduction of capsule robot

A Wireless capsule robot provides a painless method of diagnosis and drug delivery technology in medical applications (7) (8). The first capsule robot was fabricated for diagnosing of gastrointestinal diseases and received approval from the American Food and Drug Administration (FDA). It was used for diagnosing GI bleeding and small bowel tumors as shown in Figure 7.

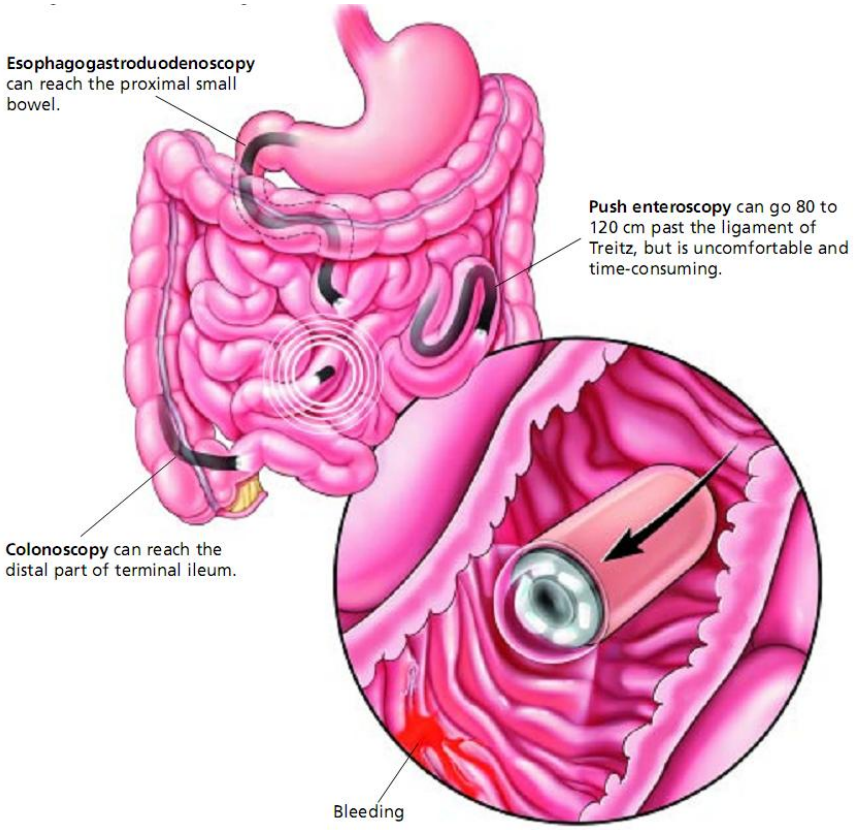

Figure 7 - Capsule robot for endoscopy (9)

In this examination, patients swallowed the pill and after a one night fast, an anti-biotic size capsule which was carried through GI tract. During the transit, the pill takes images which are

transmitted to an array of antennas placed externally at the patient's abdomen and recorded into a portable storage unit attached to a belt, around the patient's waist (Figure 8).

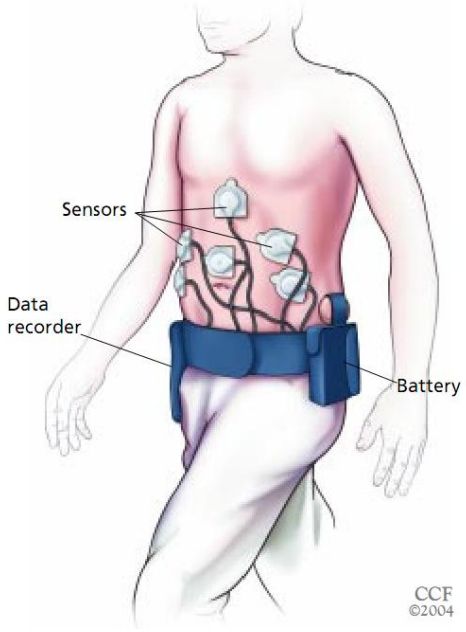

Figure 8 - Setup worn on the patient's waist (9)

The acquisition of images takes 8 hours and during this time patients are free to conduct their daily activities. The device is expelled naturally after approximately 24 hours, if no complications arise. Then, patients return to the physician's office to deliver the pill and the rest of the equipment to download the images into the physician's workstation for review and analysis. This painless procedure has recently extended to the screening of pathologies of oesophagus and colon (10).

The success of wireless capsule has sparked the interest among several research groups, in universities and industries, in order to advance the current practice of wireless capsule robot technology. In fact, at present, the merit of wireless capsule robot is limited to the visualization of the GI mucosa, it is not possible to stop at specific sites of the GI tract for performing biopsy or therapy or for moving independently of peristalsis.

3.1.2 Wireless Capsule Endoscopy (WCE)

The current available device for wireless capsule is Wireless Capsule Endoscopy (WCE). The WCE consists of different component for vision, illumination, power supply and telemetry, as can be seen in Figure 9. This capsule is specifically called M2A and it is known as the first capsule-robot technology in biomedical applications (11)(12). It consists of 1- an optical dome , 2-a lens holder , 3-

a short focal length lens, 4- four LEDs (Light Emitting Diode) , 5- a CMOS (Complementary Metal Oxide Semiconductor) image sensor, 6- two silver oxide batteries, 7- an ASIC radio-frequency transmitter, 8- and an external receiving antenna (13)(14).

Figure 9 - M2A capsule (14)

A number of different patents have been initiated that are related to this capsule robot. The first one is a patent of camera system and was disclosed by Iddan (15). His system includes a light source such as a LED, a viewing window through which the light illuminates the inner portions of the digestive system, a camera system like a charge-coupled device (CCD) which detects the images, an optical system which focuses the images onto the CCD camera system, a transmitter which transmits the video signal of the CCD camera system, a power source such as a battery to provide power to all electrical elements of the capsule, and a data processing system which generates tracking and video data from the single data stream. The parts listed above are for the purpose of image processing in capsule robot. Although the images are not well-qualified but the technology of image processing in capsule robot has been initiated from his patent. In particular, the CCD chip includes the camera and the electronics for producing a video signal from the output of the CCD device. There is a mirror that transmits the light from the LED to the walls of the GI tract via the viewing window and also deflects the light reflected from the GI tract towards the lens which then focuses the light onto the CCD camera system. Up to date more than 500,000 patients have experienced the benefits of WCE (15).

The next generation of wireless capsule robots is the PillCam ESO designed and manufactured exclusively in the United States by InScope, a division of Ethicon Endo-Surgery, a Johnson & Johnson company. This capsule has the same dimensions (26 mm x 11 mm), but has a better image processor with rate is 14 images/sec. This means that, during WCE, PillCam can process 2,600 images in an 8 hour operation. The PillCam body is shown in Figure 10.

Figure 10 - PillCam ESO (15)

A recent market analysis by Millenium Research Group on sales of Given Imaging has indicated that the field of WCE is growing at a tremendous pace (15). The first competitor of Given Imaging was Olympus Corporation (Tokyo, Japan) which disclosed an endo capsule for treating digestive disease, a pill for the inspection of the small intestine. This device has also the same dimensions as PillCam (26 mm x 11 mm) and frame rate (14 images per second) [12]. Olympus Corporation has been selling capsule robot for the first time in Europe since 2005. Olympus capsule is shown in Figure 11. The device got clearance from FDA in September 2007 (16).

Figure 11 - Olympus Endo capsule (15)

3.1.3 Supplementary patents related to the capsule robot

3.1.3.1 Patents on Localization

In 2006, a method for determining the path length of an endoscopic pill through a body lumen was proposed (15). This was called a patent in localization of wireless capsule designs. Based on this invention, a recorder was installed in the capsule which was receiving signals from antennas. In this way they could track the path of the capsule robot.

In 2007, a method for determining position and orientation, by means of X-ray radiation, of an endoscopic capsule, driven by an external magnetic field (17). In this case, the determination of the

position and orientation of the capsule is helpful to generate the correct magnetic field for the purpose of capsule navigation. In this invention, an X-ray was used for both exact positioning and elimination of interfering the signals of position tracking and magnetic field. This patent includes an endoscopic capsule, a navigation device for generating the magnetic field and an X-ray machine for recording radiation images. In the capsule is shown, with an assigned image processing device for automatically determining position and data orientation.

3.1.3.2 Patents on energy management

In December 2007, an endoscopic capsule with a built-in power generator was presented. The power inside the pill was generated by coils installed inside the capsule robot, while an external power source of a time varying magnetic field supplies energy to the coils (6). The system is presented in Figure 12. By the change of the external magnetic field, each of the coils inside the pill generates electromotive force through the current produced in them.

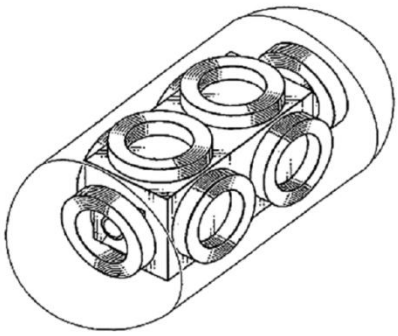

Figure 12 - Patents on energy management (15)

After this invention, a method to provide an endoscopic capsule with a wireless power supply was presented by means of an energy supplying coil sending power to the capsule, based on a magnetic coupling power supply (18) Figure 13. This invention was very close to magnetic control system which is used in the present thesis to control a capsule robot.

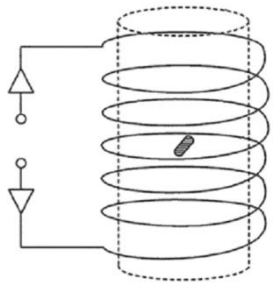

Figure 13- Invention of Nakamura (15)

3.1.4 Micro-robot propulsions

A 1 mm diameter, magnetic field driven robot has recently been developed to move in human veins. Its driving force is enough to allow it to move against the blood stream. It was considered a semi-active capsule because of the blood flow in veins. The magnetic driving force allows control of the robot inside the veins (19). The robot uses small powerful arms which protrude from its central hub to maintain a specific position for prolonged observation (20) (21).

Similar designs have used a mechanical flagellum (22) (23). One such design developed in 2007 has a diameter of 250 μm and moves the flagellum using a piezoelectric motor (24). The design is planned for use in minimally invasive surgery on areas including the heart. It was studied in the lab but never commercialized for medical applications. This device would enter the body through a syringe and return to an extraction point at the end of its operations to be removed in the same way.

Another possibility for micro-robot propulsion is to use of a spiral shaped exterior of the capsule which directs surrounding fluid when the robot rotates, pushing the capsule forward. A magnetic film deposited on the capsule rotates the robot when a rotating external magnetic field is applied, allowing the motion of the robot to be controlled. The frequency of rotation is directly related to the speed of the robot. Olympus is developing a capsule that is propelled by this principle (25).

Some researchers have proposed use of insect mimicking micro-hooks to grip surfaces and propel the robot forward. One suggestion is to use micro-hook pads that are moved by activating shape memory alloy (SMA) springs. The micro-hooks are at approximately 45° to the wafer they are attached to, allowing them to slide across tissue in one direction while gripping it in the reverse direction. This conceptual design is further explained in chapter 3.3. Another suggestion is to coat the wafer with a magnetic material to move hooks back and forth using an external magnetic field. The hooks can be as small as 40 μm, which apparently does minimal damage t the human tissue. Figure 14 presents a few of the possible propulsion principles for capsule robots (26).

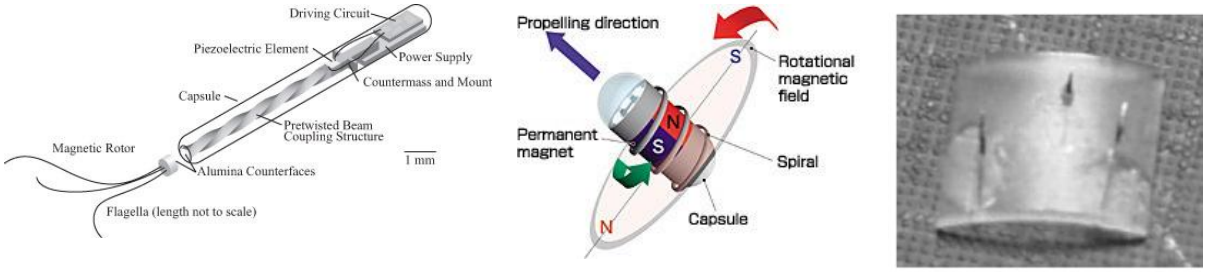

(a) **(b)** **(c)**

Figure 14 - Developmental capsule robot propulsion systems. (a) piezoelectric flagellum (24) (b) external spiral (25) and (c) microneedle wafer (26).

3.2 Drug delivery

AS mentioned in chapter 1.1, the purpose of the present research is to design a wireless medical capsule robot to function inside human esophagus, and an *in vitro* simulating environment to test a robot prototype. The present research project has been separated into two parts: capsule robot modeling plus experiment, wireless control with wireless drug delivery system. When treating conditions such as small cell cancer, chemotherapy is usually administered intravenously or through pills (27). These methods do not specifically target the cancerous cells, damaging healthy cells and reducing the effectiveness of the treatment. Delivering drugs to specific sites can improve the effectiveness of treatment and reduce the adverse effects of the chemicals. Capsule robots could deliver medication to specific targets. This would be a further improvement over many existing capsule robots which merely observe the affected areas.

Periodic drug release for a longer time is another goal of drug delivery system of capsule robot. In some GI diseases, drug delivery need to be achieved several times during 24 hours. In order to perform it, different injection or pills need to be used. This goal can be achieved by using capsule robot.

3.2.1 Concept of drug delivery

Biomedical, mechanical and materials engineers have performed advance techniques for drug delivery. Polymer-drug matrices are the first method of drug delivery which has been considered in the present project. In this technique, sol-gel transitioning materials are combined with medication (28) (29). An external magnetic, electric, or ultrasonic trigger is then used to control the swelling of the polymer, releasing the drug (30). Most of this work has dealt with the ultrasound trigger because it is similar to established medical procedures and ultrasound increases the tendency of tissue to absorb medication (28) (31) (32).

Another promising drug release technology is a microchip etched with small reservoirs containing drugs and covered with gold membranes. An electric potential is created between an anode of the chip and the gold membrane. The electrochemical reaction converts the gold into gold chloride, which dissolves allowing the drug to release (34) (35). A drug release microchip is presented in Figure 15.

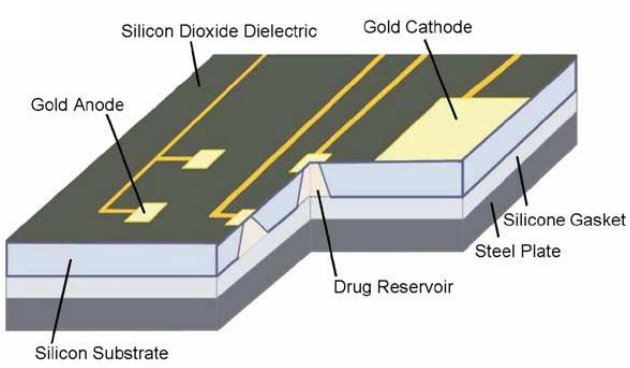

Figure 15 - Drug release microchip (36)

Shape memory alloys have been used in micro-manipulation systems for their high force to weight ratio and simple structure. Olympus is developing a capsule robot that releases drugs from a balloon when it receives a signal which opens a shape memory alloy micro-valve. Sampling of fluid is possible by a similar valve balloon principle, except prior to opening the valve, the balloon holds a negative pressure (37).

One of the wireless controllers, proposed in 2001 was used radio frequency to release drug. The RF Systems Lab has developed a capsule robot called Sayaka, which contains a camera and releases drug wirelessly (38) (39). This improves visibility of the wall tissue over a frontal camera. This robot is externally powered, reducing the risk of harmful battery the same as our capsule and contents being released into the patient 40. The Sayaka robot is presented in Figure 16.

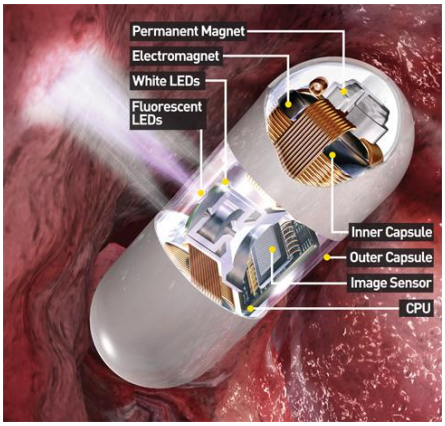

Figure 16 - Rendering of Sayaka capsule robot (41)

3.2.2 Conceptual designs for drug delivery

3.2.2.1 Pressurized tube

The drug delivery system is to function by storing powdered medication in stretched balloons and upon triggering expels the drug by allowing the balloons to contract. Designs operating on a similar principle use micro valves. A search was conducted for a suitable commercially available micro value however no such device was found. As an alternative a design was envisioned in which a piston acts to hold the drugs in the balloon. A solenoid would then move the piston to release the drugs as the balloon contracted. This design is presented Figure 17. The outer cylinder would be wrapped in wire. When the wire conducts current the piston would be moved by the magnetic field generated by the wire. This design was determined to be infeasible because the number of turns of wire would be too high. It was decided that use of a commercial solenoid would be a better choice.

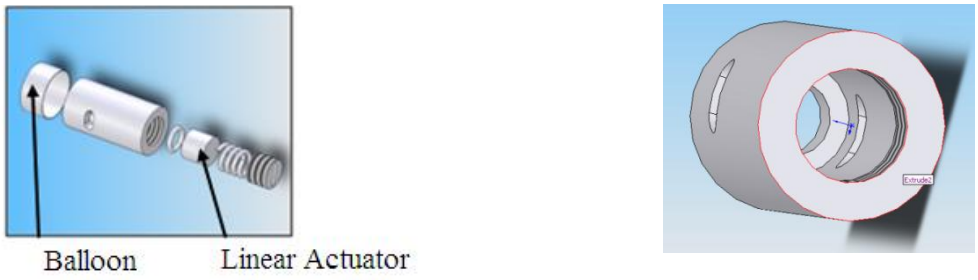

(a) (b)

Figure 17 - First iteration of drug delivery system (a) overall exploded view (b) main cylinder

In order to avoid the limitation of solenoid, shape memory alloy is recommended for drug delivery. In this iteration of drug delivery, the plastic tube of pressurized drug is located inside the capsule robot. The SMA is located at the position that touches this plastic reservoir with minimum force applying to this reservoir. SMA is connected to the internal circuit which can apply voltage to its both ends and change its length. Therefore, it makes a hole on pressurized tube and drug will be released there. The goal for drug delivery in our system is to have a wireless actuation of releasing the drug the same as wireless magnetic control system. Designing the circuit as a power transmission system for drug delivery is explained as power transmission design (42) (43).

Power Transmission Design

The power transmission system was designed based on a design of a power transmission system for a gastrointestinal capsule robot (44) in biomedical applications. There was an external transmitting coil, driven by sinusoidal current, generates a varying magnetic field. This varying magnetic field shown in Figure 18 produced by AC voltage induced in the receiving coil. Then the AC voltage is rectified and filtered to DC voltage powering the micro system.

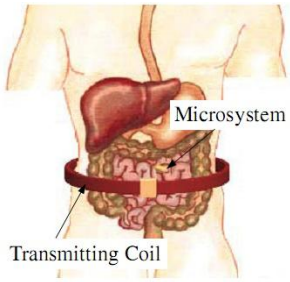

Figure 18 - Sketch of a power transmission system (42)

The power transmission circuit is shown in Figure 19. Note that using a capacitor, C_2, on the receiving side in series instead of in parallel reduces the need to tune the circuit parameters for different loads, which is best for this design as the change in load when the solenoid turns on could be detrimental to the secondary voltage otherwise.

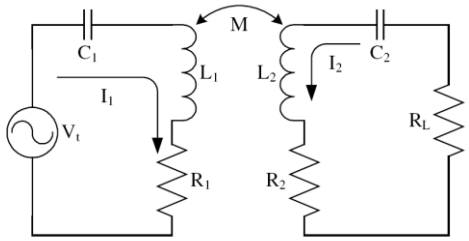

Figure 19 - Power transmission circuit (42)

The concept of using capacitor in the design is to eliminate the wire of controlling the drug release and use a wireless actuation. These two circuits shown in Figure 19, are installed separately inside the capsule robot and on the human's body. By applying the voltage on master circuit the current will be induced in the slave circuit.

3.2.2.2 Micro fabricated and permanent magnet arrangement for drug delivery

The second drug delivery design presents using micro-fabrication technology in drug release. In this system a wafer is fabricated with a pattern of small holes in it and the drug release rate can be controlled by the diameter of holes. The drug delivery mechanism is the polyethylene wafer 0.02m by 0.01m with the holes of 50 micrometers. The design of this wafer is shown in Figure 20 (a).

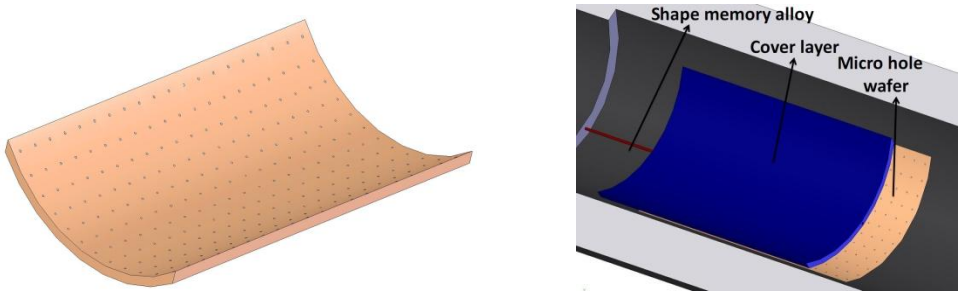

(a) **(b)**

Figure 20 – (a) Micro fabricated poly ethylene wafer, (b) drug delivery mechanism with micro fabricated wafer

This micro-fabricated wafer could be achieved in micro fluidics lab in the Department of Mechanical and Mechatronics Engineering at the University of Waterloo.

Drug can pass through the holes and the concept of long term drug delivery can be achieved too. This system proposes to use two wafers of the same size on top of each other. The upper one can be moved along the other one by a shape memory alloy shown in Figure 20 (b). This mechanism for drug delivery is one degree of freedom motion controlled by shape memory alloy and lets the drug pass through holes by moving the layer on top of it. The problem in this conceptual design is the leakage between two layers. Accuracy of mechanical design in infinitesimal size and micro meter tolerances is not applicable easily. On the other hand, the power transmission for shape memory alloy requires a circuit with power supply which increase the weight of the capsule robot.

Regarding the wireless drug delivery concept, a second design was using the arrangement of permanent magnets work both for manipulation and drug delivery. In this system, three arc magnets are covering three holes on the body of capsule robot. The combination of magnets is shown in Figure 21.

(a) **(b)**

Figure 21 - Arc magnets design

The permanent magnets used in this method are arc magnets which have been magnetized radially. As it is shown in Figure 21 (a), the distribution of permanent magnets is in the way that two of them are opposite to the third one. The magnetic field of the magnetic drive unit produces a magnetic force which absorbs these two magnets and moves the capsule robot vertically. To release the drug, the second coil can be used from the bottom of the capsule. With an impulse of current applied to this coil, the arc magnet can be separated from the capsule robot. Liquid drug can be released through this hole.

3.3 Mechanical Design of a Capsule Robot

Mechanical modeling of capsule robot is related to motion part of the capsule and drug delivery mechanism. Drug delivery designs including a mechanism of drug release and drug reservoir are explained in section 3.2.2. In this section, different parts are presented to show the capsule movement inside human's GI tract. All designs have dimensional limitation and so, manufacturing and design features are for small dimensions. Most of mechanical joints and connections cannot be achieved through classic manufacturing and modern methods of manufacturing such as micromachining and micro fabrication need to be used. It should be mentioned here that, although conceptual designs are presented for a capsule robot, but it is going to build in the UW machine shop entirely.

The first design, illustrated in Figure 23 uses shape memory alloy (SMA) and micro fabricated motion part. In this method, wormy motion for capsule robot is proposed. Based on limitation in MEMS and micro-robotic applications, shape memory alloys as small actuators with high response are recommended. In this design 2 SMA with 2 clamps move capsule robot. The most important point in producing locomotive force is displacement, power and safety of the SMA. The strain of SMA is 2

- 3 % of its length, but if it is shaped into spring, strain can be increased into 80 times more than that. SMA has a nominal length in its memory, after any temperature difference, it can return to its nominal length when the original temperature is restored.

In order to explain the mechanism of locomotive force, the set of SMA are used shown in Figure 22.

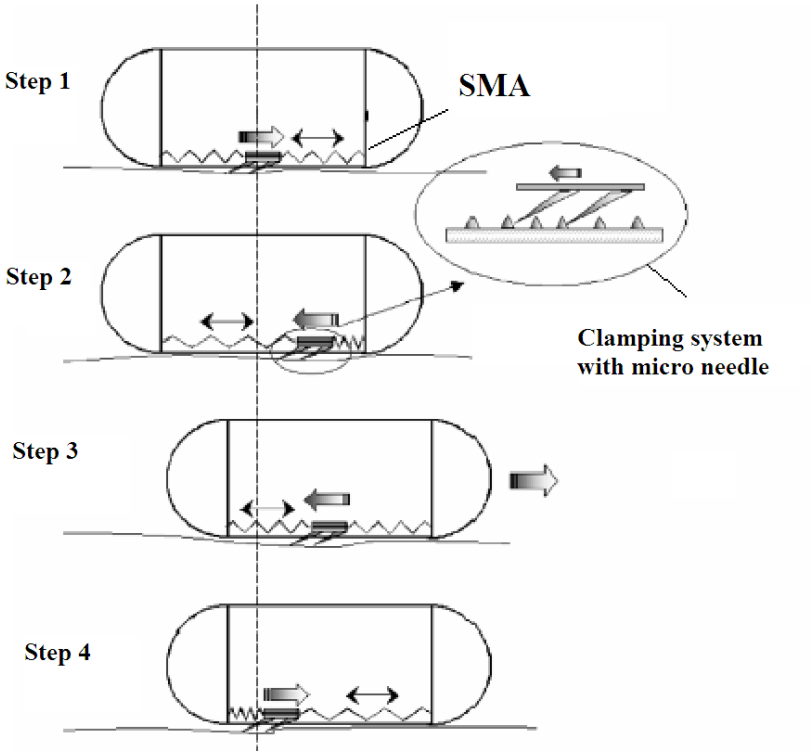

Figure 22 - connection of 2 SMA for locomotive force

The clamp connects two SMA to each other. It can be inferred that by actuating each SMA, the clamping position changes and if the clamping location moves close to the GI tissue and two other parts placed on capsule body, the capsule robot can crawl inside esophagus. On the other hand, it can be expressed that the set of SMA are fixed at two points, one point is the body of capsule robot and the other one is the clamp plain. By actuating SMA, the point that is connected to capsule's body is fixed and clamp can move the capsule. This cycle of movement is shown in Figure 23.

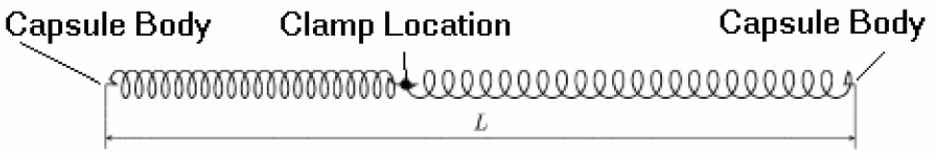

Figure 23 - The 4 steps of capsule robot movement

There is a micro needle plane connected to the clamping system. Micro needle plane can be fabricated using wet etching. The wafer is made of PET (Poly-Ethylene tetraphlyte). It is shown in Figure 24.

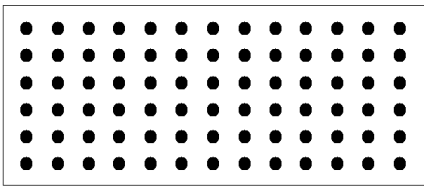

Figure 24 - Lithography mask

3.4 Capsule Robot Development

A capsule robot was developed in the Maglev Lab at the University of Waterloo by the present author with the same size as the classic capsules described previously in this chapter. The capsule robot consists of a permanent magnet for positioning and a drug delivery chamber with wireless drug delivery system. After 7 iterations of micro machining the capsule was developed using Aluminum. The body of the capsule was shown in Figure 25. The capsule robot is finally developed in 18×5 mm. The middle part of the capsule was used for the permanent magnet and it was separated from reservoir with the circle plate. The body has either a 0.25 or a 0.75 mm thickness and the whole weight of the capsule robot was 1.78 grams regardless the permanent magnet. Two end caps were fitted to finish the capsule's body.

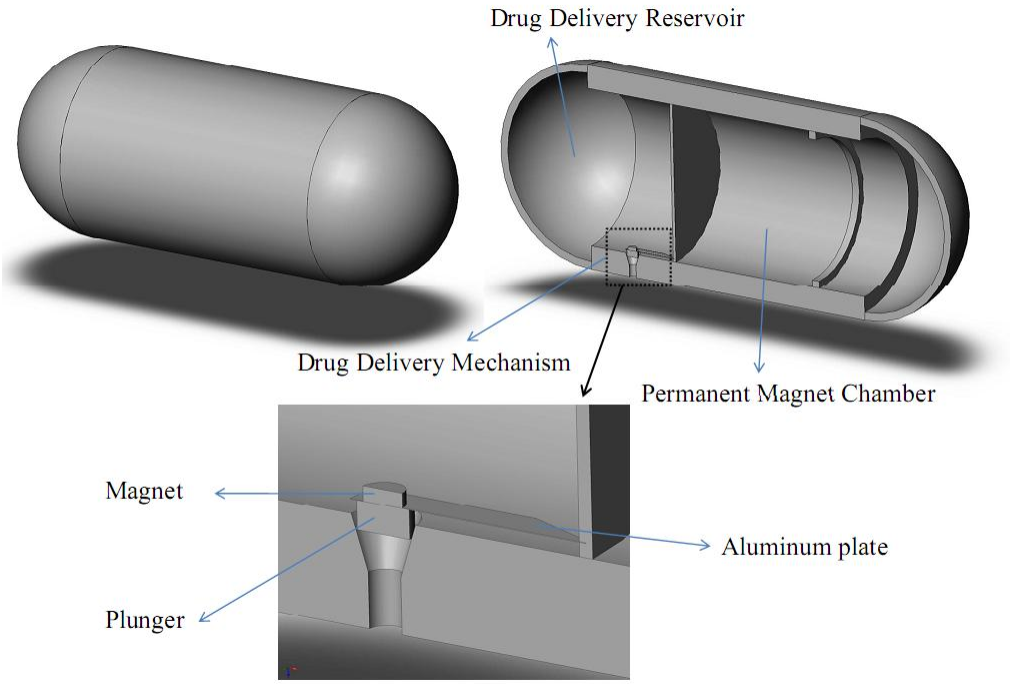

Figure 25 - Capsule Robot Components

The drug delivery mechanism consisted of a wireless magnetic plunger that lets the drug be released from the hole. The most challenging part of the present project was the drug delivery mechanism manufacturing. According to the size of plunger, aluminum plate and the hole on the capsule body, assembling needed to be accurate. In other words, tolerances played a serious role in drug delivery system. The hole had to be completely sealed with the plunger.

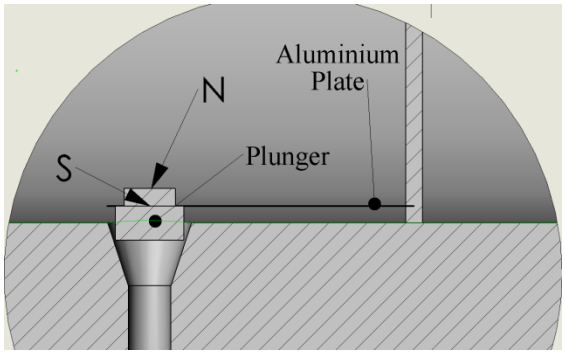

Figure 26 - Drug delivery mechanism

In this mechanism, an external magnetic field from the bottom of the capsule moves the plunger up and let the drug to pass through the hole. The external electromagnetic field for drug release can be provided through another set of coils located on the bottom of the patient's body. According to the poles of permanent magnet for drug delivery, this external field pulls the whole capsule down and opens the hole for drug release. This mechanism satisfies the concept of accurate local drug release system by allowing the capsule to stay at a specific location. The sinusoidal current signal is supposed to control the amount of drug for a specific point. By adjusting the frequency of signal, the opening and closing time for the plunger can be evaluated and closing process and control the amount of drug release. The force required to release the drug can be calculated according to the cantilever beam shown in Figure 27.

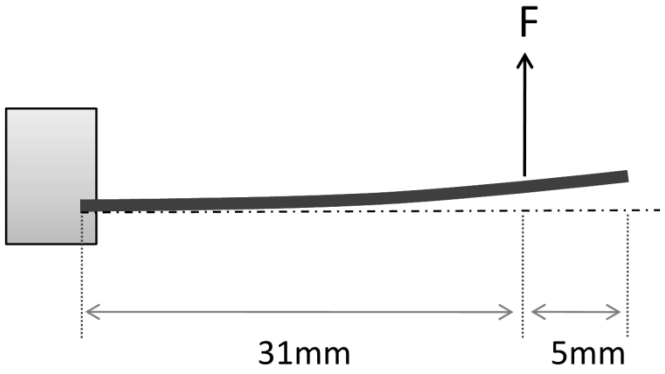

Figure 27 - Drug release beam

This force must displace the cantilever by 0.1 mm to move the plunger enough to release the drug. For this displacement, the force can be calculated as:

$$y = \frac{FL^3}{6EI} \tag{3.1}$$

And

$$\begin{aligned} \mathrm{I} &= 8.33\ \mathrm{e}-16\ \mathrm{m}^4 \\ E_{Al} &= 70Gpa \end{aligned} \tag{3.2}$$

Therefore, the force required for 0.1mm displacement is

$$F_z = 1.18e-2N \tag{3.3}$$

Magnetic field distribution for external electromagnet to release the drug is shown in Figure 28. The amount of force applied to the plunger would be at *z=0.035m*. Electromagnetic force at this height is

$$F_z = M \frac{\partial B_z}{\partial z} \tag{3.4}$$

This can be evaluated from the magnetic field versus height diagram. According to the Figure 28, it can be inferred that at *z=-0.04m* (the distance between the external field source and the capsule robot)

$$\frac{\partial B_z}{\partial z} = 1.25e-8 \tag{3.5}$$

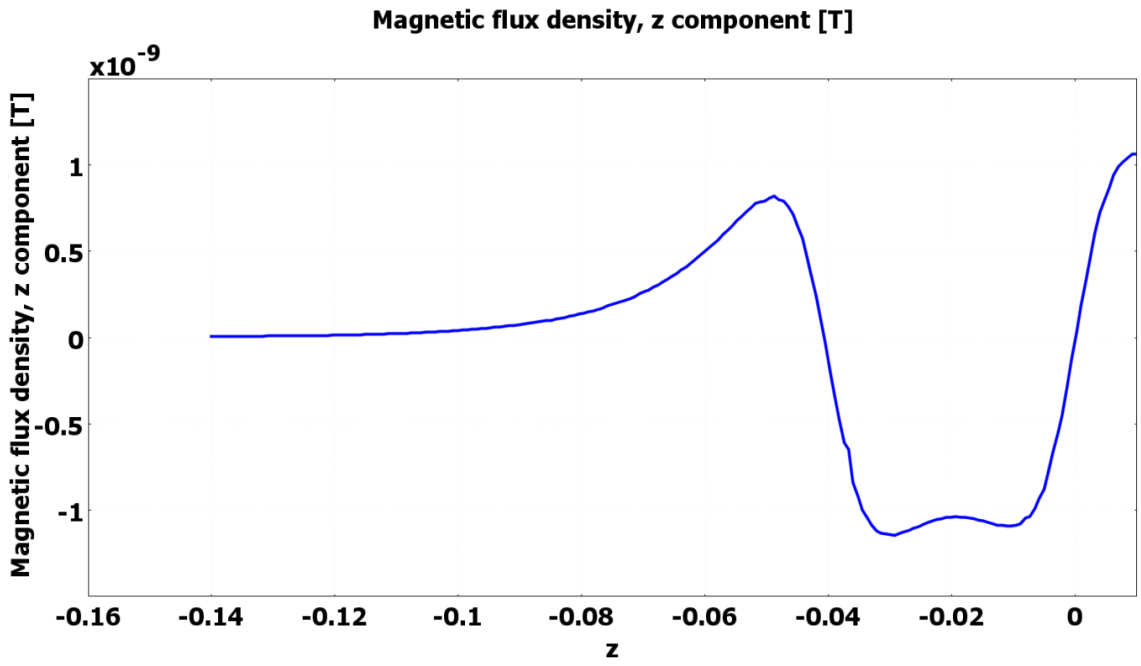

Figure 28 - Magnetic field distribution for external coil

The magnetization of permanent magnet is *1e6 A/m*, based on the model of permanent magnet (N42). Therefore, the force would be

$$F_z = 1.25e-2N \tag{3.6}$$

Therefore, the difference between the required force and the force available from the magnetic field is negligible which satisfies the concept of this drug release system. The external electromagnet for drug release is located at *z=-40 mm* under the capsule robot. The volume of the drug chamber is 200 cubic millimeter.

3.5 Magnetic field effect on live tissue

Magnetic manipulation system is proposed to move the capsule robot inside the human GI tract and release drug there. In this section the effect of magnetic field produced by electromagnets which is explained in Chapter 4, has been analyzed. Avoiding one type of damage to healthy human cells from electromagnetic field is the purpose of this analysis. To achieve this, the ferrohydrodynamic model of blood in the electromagnetic field induced by a coil has been evaluated. The solution of this model is based on Maxwell's equations and the Navier-Stokes equations. The solution has been done in two different physics for the system. The largest effect of the magnetic field is concentrated on blood vessels. (43) (42) Therefore, the analysis is done on vessel containing blood in human's body. The FEM modeling of magnetic field on live tissue in presented in the sofware package called COMSOL.

The 2D model of human vessels represents the blood vessel with coils and surrounding tissues. Blood feeds to the vessel from the left side as it is shown in Figure 29.

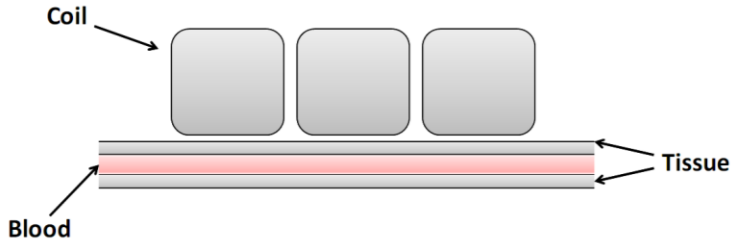

Figure 29 - Geometric representation of vessel model

The magnetic part of this problem is static; Maxwell-Ampere's law for the magnetic field **H** (A/m) and the current density **J** (A/m^2) applies

$$\nabla \times H = J \tag{3.7}$$

Furthermore, Gauss' law for the magnetic flux density **B** (Vs/m^2) states that

$$\nabla . B = 0 \tag{3.8}$$

The constitutive equations describing the relation between **B** and **H** in the different parts of the modeling domain read

$$\begin{aligned} B_{permanent\_magnet} &= \mu_0 \mu_{r,mag} H + B_{rem} \\ B_{blood\_stream} &= \mu_0 (H + M_{ff}(H)) \\ B_{human\_tissue} &= \mu_0 H \end{aligned} \tag{3.9}$$

It should be mentioned here that μ_0 is the magnetic permeability of vacuum $(Vs/(A.m))$; μ_r is the relative magnetic permeability of the permanent magnet (dimensionless); B_{rem} is the remanent magnetic flux (A/m); and M_{ff} is the magnetization vector in the blood stream (A/m), which is a function of the magnetic field, **H**. (44)

Defining a magnetic vector potential **A** such that

$$\begin{aligned} B &= \nabla \times A \\ \nabla . A &= 0 \end{aligned} \qquad \textbf{(3.10)}$$

and then substituting this in Eq. (3.7) through Eq.(3.9), gives the following vector equation to solve

$$\nabla \times \left(\frac{1}{\mu} \nabla \times A - M \right) = J \qquad \textbf{(3.11)}$$

Simplifying to a 2D problem with no perpendicular current, this equation reduces to

$$\nabla \times \left(\frac{1}{\mu_0} \nabla \times A - M \right) = 0 \qquad \textbf{(3.12)}$$

Note that this equation assumes that the magnetic vector potential has nonzero component only perpendicularly to the plan, $A = (0, 0, A_z)$.

For the fluid flow analysis, the navier-stokes equations describe the time dependant mass and momentum balances for an incompressible flow

$$\begin{aligned} \rho \frac{\partial u}{\partial t} - \nabla . \eta (\nabla u + (\nabla u)^T) + \rho u . \nabla u + \nabla p &= F \\ \nabla . u &= 0 \end{aligned} \qquad \textbf{(3.13)}$$

In this equation η is the dynamic viscosity $(kg/(m.s))$, **u** the velocity vector (m/s), ρ the fluid density (kg/m^3), p the pressure (N/m^2), and **F** a volume force (N/m^3).

In this equation, it is assumed that the magnetic nanoparticles in the blood do not affect on each other and the magnetic force can be estimated as

$$F = M \nabla H \qquad \textbf{(3.14)}$$

To evaluate this force, magnetization vector in blood stream should be achieved. According to Eq. **(3.12)**, magnetization vector can be written as

$$M_x = \frac{\chi}{\mu_0}\frac{\partial A_z}{\partial y}$$
$$M_y = -\frac{\chi}{\mu_0}\frac{\partial A_z}{\partial x} \qquad \textbf{(3.15)}$$

where χ is the material parameter that characterizes the induced magnetization $M_{induced}(x,y) = (M_{induced\_x}, M_{induced\_y})$ of the ferrofluid (blood).

Therefore, ***F*** can be written as

$$F_x = \frac{\chi}{\mu_0 {\mu_r}^2}\left(\frac{\partial A_z}{\partial x}\frac{\partial^2 A_z}{\partial x^2} + \frac{\partial A_z}{\partial y}\frac{\partial^2 A_z}{\partial x \partial y}\right)$$
$$F_y = \frac{\chi}{\mu_0 {\mu_r}^2}\left(\frac{\partial A_z}{\partial x}\frac{\partial^2 A_z}{\partial x \partial y} + \frac{\partial A_z}{\partial y}\frac{\partial^2 A_z}{\partial y^2}\right) \qquad \textbf{(3.16)}$$

On the vessel wall, a no-slip condition is assumed and velocity is zero. At the inlet boundary, it can be said that there is a parabolic flow profile with the maximal flow velocity of V_m. Regarding the heart beat, the inflow velocity follows a sinusoidal expression in time. Therefore, the inlet velocity will be

$$V_0 = 2V_m s(s-1)(\sin(\omega t) + \sqrt{\sin(\omega t)^2}) \qquad \textbf{(3.17)}$$

That *s* is a boundary segment length parameter that goes from 0 to 1 along the inlet boundary segment.

The model data are shown in Table 1.

Quantity	**Description**	**Value**
$\mu_{r,mag}$	Relative permeability, magnet	5000
B_{rem}	Remanent flux density	0.5 T
χ	Ferrofluid (Blood) magnetization parameter	3×10^{-7}
ρ	Density of Blood	$1003 kg/m^3$
η	absolute viscosity Blood	$5\times10^{-3} kg/(m.s)$
u	Velocity at vessel wall	0

Table 1- Model data and description of human's vessel filled with blood

All of the analysis mentioned above has been modeled in COMSOL, and solved in magneto static and fluid flow physics. Since magneto static problem is a stationary nonlinear problem that is independent of the fluid flow problem, it has been solved only once. The fluid flow is a time dependant problem with the velocity of the blood and is solved for 2 seconds. It used a time dependant solver of COMSOL. Distribution of magnetic potential has been shown at t=0.6s after 2 amps passes through coils in Figure 30.

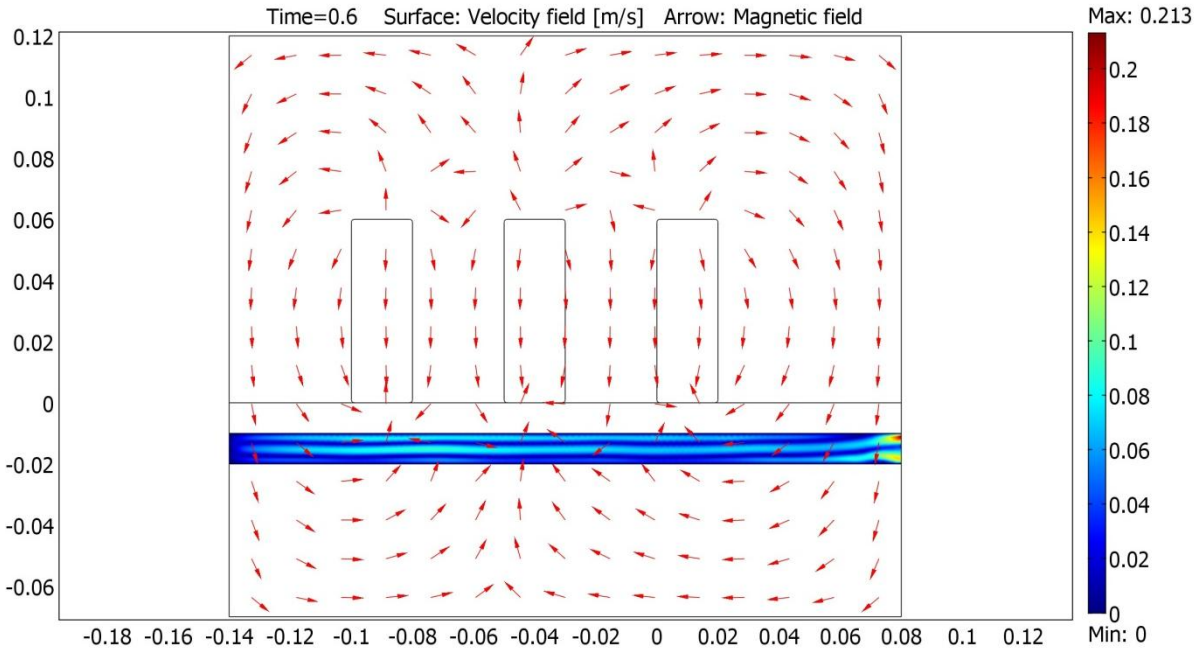

Figure 30 - Finite element model of coils and human's vessel at t=0.6s

The moderate adult blood pressure is 160 mm HG or 21346 Pascal. For pressures more than this, there would be a risk of vessel tear. Pressure distribution on the wall of vessel has been evaluated. The distribution of pressure for t=0 sec, 0.5 sec, 1 sec, 1.5 sec, and 2 sec is shown in Figure 3131. The negative and positive pressure on the wall of the vessel is because of the net force direction in the vessel. Since blood has an initial velocity in vessel, an external magnetic field in any vertical strip of vessel has a direction of force applies to either top or bottom layer. The net pressure, regardless of the direction, can be the critical blood pressure for human's vessel. It can be inferred that the maximum pressure on vessel wall is 380 Pascal that is still less than critical pressure. The pressure is dependent on the velocity of blood and flux density produced by electromagnets

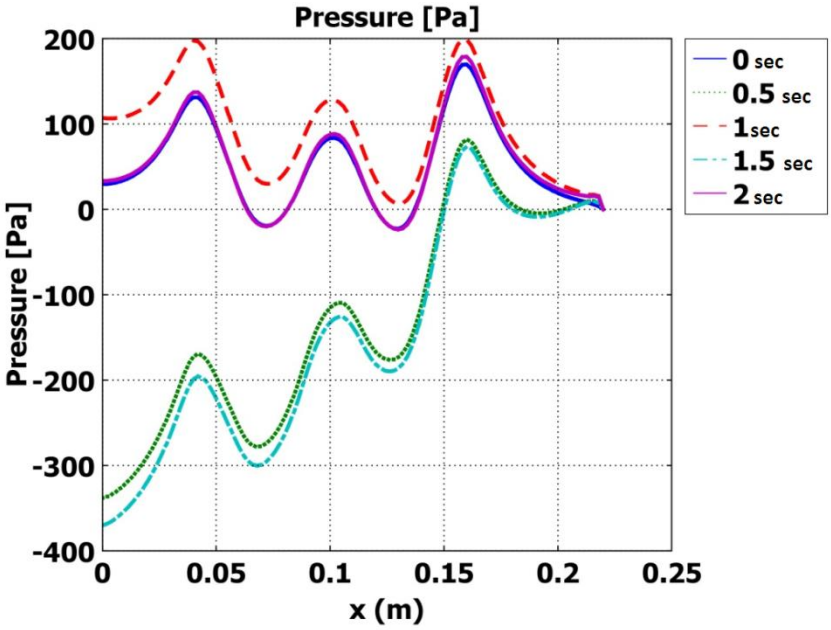

Figure 31 - Pressure distribution on vessel wall

It means that the capsule robot is ready to get manipulated and moved in the test bed by magnetic control system without any destructive effect on human's body. Magnetic field along human's vessel filled with blood is shown in Figure 32.

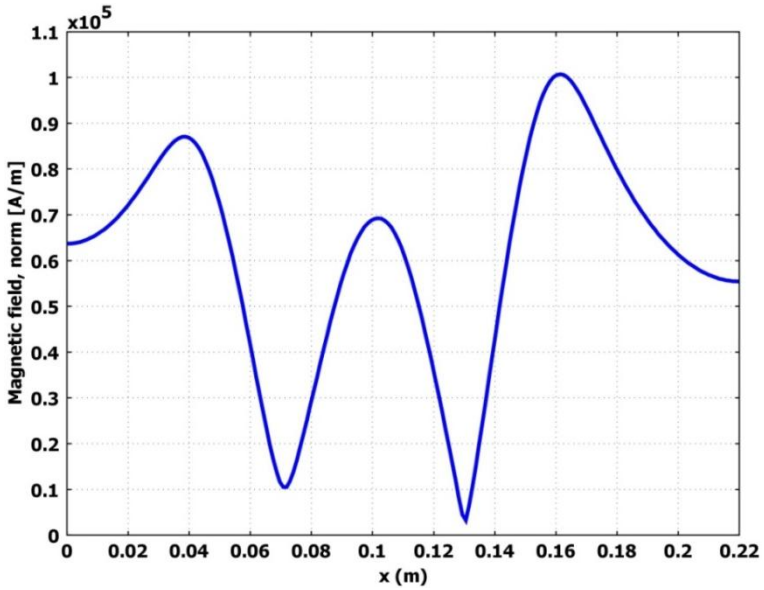

Figure 32 - Magnetic field along human's vessel

3.6 Conclusion

Considering the different capsule robot which had been studied before and the ones made by Olympus, some conceptual designs have been presented in the present chapter. There were couples of iteration in student machine shop and UW machine shop in the University of Waterloo. At the end the final design for capsule robot and drug delivery prototype is selected. This capsule robot is fabricated and used for the experimental results of this project. At the end, the effect of magnetic field on human's live tissue and blood pressure has been modeled in COMSOL. It is shown that the magnetic field produced by our system does not increase the blood pressure more than the maximum allowed pressure. Finally, the capsule robot is ready to get manipulated and moved in the test bed by magnetic control system without any destructive effect on human body.

Chapter 4

Electromagnetic Control System

4.1 Infrastructure description

Current in any conducting medium produces a magnetic flux density ***B*** in the space around it. From the application of Bio-Savart law, for any element of ***dl*** in the space carrying current ***i***, the field ***dB*** at desired point ***P*** can be founded by:

$$dB = \frac{\mu_0}{4\pi} \frac{i\vec{dl} \times \vec{R}}{|R|^3} \quad \textbf{(4.1)}$$

Here ***R*** is the vector between element ***dl*** and the point ***P*** and μ_0 is the permeability of free space, 1.26e-6 Wb/(A m). The magnetic flux density for the Magnetic Drive Unit (MDU) has been evaluated from Eq. (4.1).

Magnetic levitation is achieved through the interaction between the flux density field ***B*** and the magnetic dipole moment ***D*** of the levitating object (45).

The magnetic dipole moment of a system is a measure of the strength and the direction of its magnetism. More technically, the term magnetic moment of a system (such as a loop of electric current or a bar magnet) usually refers to its magnetic dipole moment, and quantifies the contribution of the system's internal magnetism to the external dipolar magnetic field produced by the system (45). The magnetic dipole moment is modeled as

$$D = \left(\frac{B_s}{\mu_0} \right) V \quad \textbf{(4.2)}$$

Where B_s is the value of the flux density field at the surface of the object, μ_0 is the permeability of free space, and V is the volume of the object. For permanent magnet, B_s is assumed as B_r, where B_r is the remnant flux density of the magnet provided by the manufacturer. A typical magnetic levitation setup is shown in Figure 33.

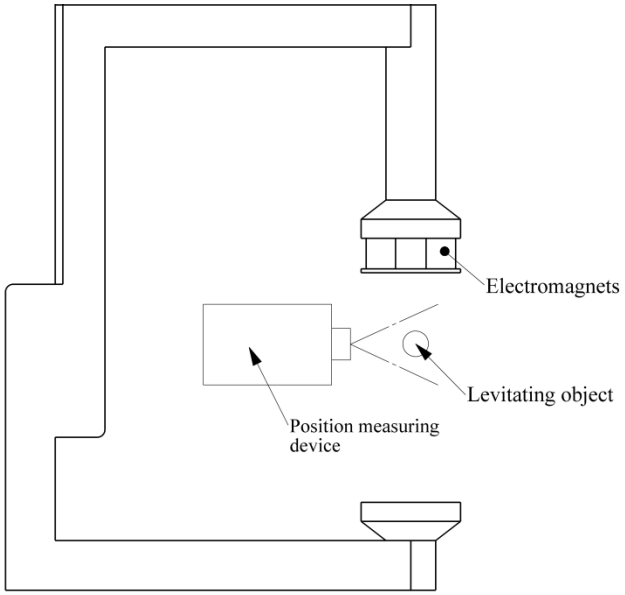

Figure 33 - One dimensional magnetic levitation system

The resultant force acing on the object is

$$\vec{F} = (\vec{D}.\nabla)\vec{B} \tag{4.3}$$

When the dipole moment, D= *(0, 0, D),* the resultant force becomes

$$\vec{F} = (D\frac{\partial B_x}{\partial z}, D\frac{\partial B_y}{\partial z}, D\frac{\partial B_z}{\partial z}) \tag{4.4}$$

For the current free space, it can be presented as

$$\begin{aligned} &\nabla \times B = J = 0 \Rightarrow \\ &\frac{\partial B_z}{\partial y} - \frac{\partial B_y}{\partial z} = 0 \\ &\frac{\partial B_x}{\partial z} - \frac{\partial B_z}{\partial x} = 0 \\ &\frac{\partial B_y}{\partial x} - \frac{\partial B_x}{\partial y} = 0 \end{aligned} \tag{4.5}$$

Therefore, the force can be written directly as a function of the *z* component of the flux density gradient.

$$\vec{F} = (D\frac{\partial B_z}{\partial x}, D\frac{\partial B_z}{\partial y}, D\frac{\partial B_z}{\partial z}) \tag{4.6}$$

From Eq. (4.6), the vertical force ***F*** acting on the levitated object is

$$F = \left(D \frac{\partial B_z}{\partial z} \right) \quad \textbf{(4.7)}$$

This force acts toward the electromagnets that are generating the magnetic field. According to Figure 33, the magnetically suspended object incorporates permanent magnets inside the capsule robot that interact with generated magnetic field to produce full spatial motion. In order to achieve full spatial motion, several electromagnets are arranged in an array configuration of 6 coils arrange in a circle, tangent to each other and one coil in the middle of them. The pole piece is attached to the electromagnets and is used to both unify and strengthen the individual fields that are produced by each electromagnet. The yoke fixture is made of iron and this further amplifies the field strength.

Vertical motion of the capsule robot is achieved by applying equal power to each electromagnet in the array. In this way the value of $\frac{\partial B_z}{\partial z}$ changes which results the increase of the vertical force applied to the capsule robot.

Horizontal motion is achieved by varying the amount of power each of coils receives. However, the total power applied to the coils remains constant. In this way the resultant force is kept constant but a shift in the equilibrium point results in a horizontal force being generated. Electromagnets need to have infinite dimensions for electromagnets studies. This means that the electromagnet models are not “REAL” electromagnets, rather than it is more appropriate to consider them as long rectangular iron bars with straight current carrying wires running alongside them (45). The system can be studied using finite element methods to demonstrate the behavior of flux density field produced by the magnetic drive unit. However, some simplified models need to be evaluated to analyze the electromagnets. The distribution of electromagnets can be only modeled in 3D system and most of finite element software have some limitations in 3D analysis.

The experimental setup consist of amplifier to produce current, controller to feed the amplifier and control the voltage for magnetic levitation, magnetic drive unit (MDU) to produce the magnetic field and the capsule robot as the final target of the project to be developed. The whole system is shown in Figure 34. The different parts of magnetic system are explained in the following section.

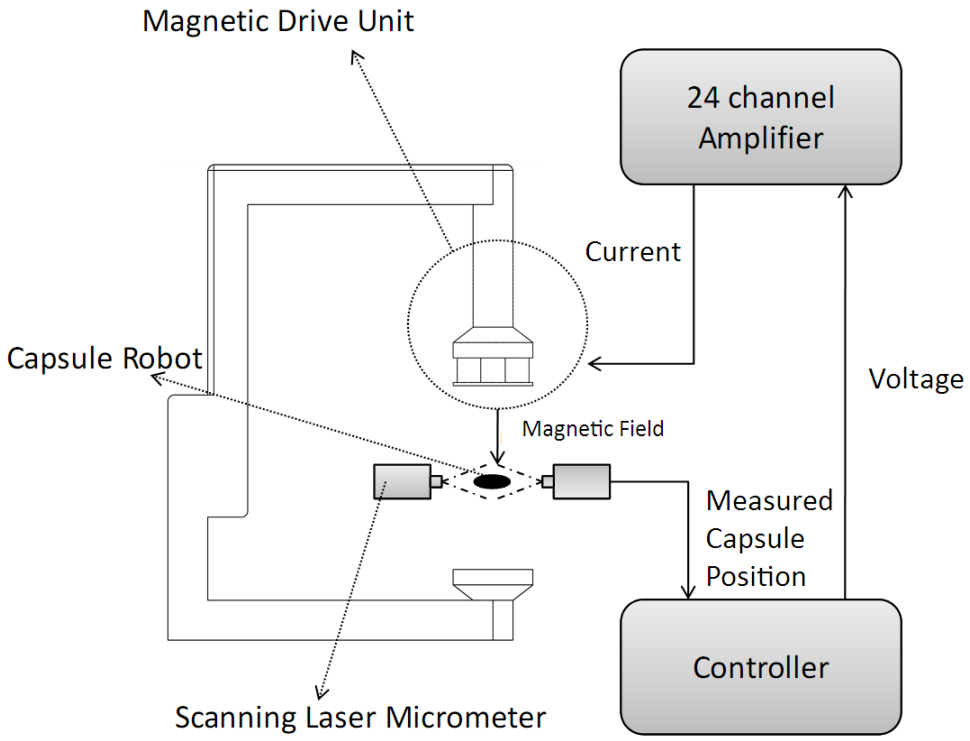

Figure 34 – Schematic representation of the micro robot control loop

4.1.1 Yoke

The yoke and pole piece (Figure 34). They are made from soft iron and help to improve the strength of the magnetic field. The yoke individually plays the role of conducting the magnetic field streamlines. It closes the circuit in a circular path which helps the object to get controlled. The system is designed that electromagnets can be installed on the top and bottom of the yoke. Different parts of the yoke can be adjusted to change the air gap in order to manipulate different type of objects and also in different environments.

4.1.2 Electromagnet

For the amplifier used in the setup, up to 24 electromagnets can be installed in the MDU. Currently, 7 electromagnets are used for the levitation and horizontal control system. The distribution of these 7 electromagnets is shown in Figure 35. The centre position electromagnet is only used for vertical manipulation.

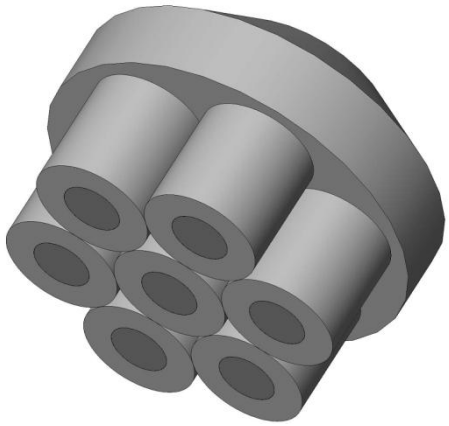

Figure 35 - Electromagnets distribution on bracket

Each electromagnet is handmade and has 840 turns of #22 AWG wire and the nominal parameters for both calculation and finite element modeling is shown in Figure 35.

Table 2 - Electrical and geometric parameters of electromagnet

Coils	Resistance	Inductance	Number of turns	Core diameter	Coil diameter	Wire specification	Length of coil
1-7	4.25 ohm	29 H	840	20 mm	40 mm	AWG	40 mm

4.1.3 Laser Sensor

The lasers are used to read the position of the object in the working space. Three KEYENCE LS-5000 scanning laser micrometers are used to measure *x, y,* and *z* position of the levitating object. The lasers are installed on a hexagonal aluminum ring that surrounds the air gap workspace of the yoke. The brief characteristic of laser is shown in

.

Table 3 - Brief characteristics of the laser

Measuring Range	Scan Rate	Analog Output Range	Analog Output Resolution

0.2-40 mm	1200 Hz	+/- 10 V	5 mV

The micrometer laser is programmed to measure the location of the capsule robot that is nearest to the zero mm position which is set on the bottom bracket. The amount of current drawn from the power supply is sent to the amplifier which was built in the Faculty of Science at the University of Waterloo. The amplifier has 3 inputs of connectors with power supply. The approximate gain equation mapping the input voltage *v* to the output current *i* for the amplifier is

$$i = 0.355v \tag{4.8}$$

The laser calibration is achieved using the adjustable laser stand shown in Figure 36. The global term of *z* (mm) in term of laser voltage is obtained as

$$z = (20 - V_L) - d + 188 \tag{4.9}$$

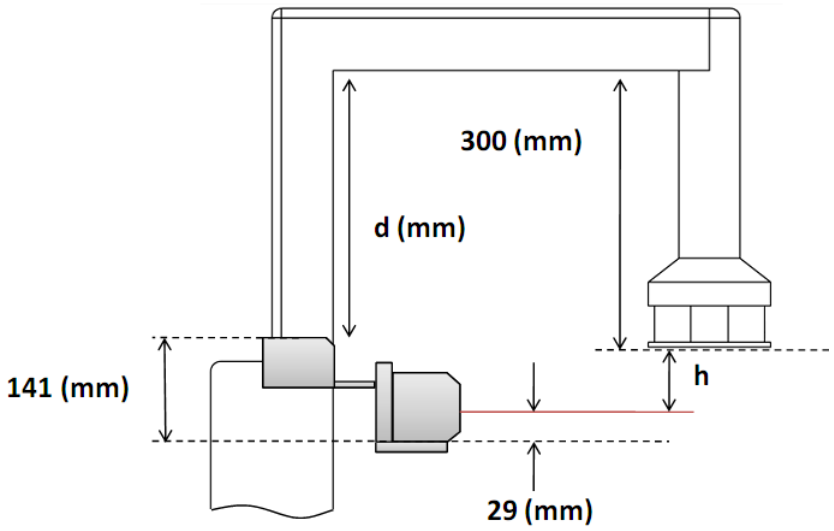

Figure 36 - Laser measurement frame

4.1.4 Power supplies and Amplifier

Two Sorensen DCS40-30E DC power supplies are used to provide power to the electromagnets. Only one of the power supplies is currently in use since only 7 electromagnets are installed on the MDU. The maximum output of voltage is 40 volts, and the maximum output current is 30 Amperes (46).

4.2 System modification

To control the capsule robot in the human esophagus some modifications are needed for the new environments. Some of the features of this new environment are as follows:

1. There would be no position feedback from the system. Thus, the capsule robot is moving inside human's esophagus and the MDU would need to control the capsule without any position feedback.
2. The capsule robot may be in contact with the tissue of the GI tract and this may produce quite high friction forces. Therefore, the amount of magnetic field produces by electromagnets may need to be increased significantly.
3. Liquid inside human esophagus produces a drag force during capsule robot movement. This drag force would be another resistance force for capsule manipulation. This is another reason for increasing the amount of magnetic field produced by the electromagnets.

To increase the amount of magnetic force we can modify the terms of Eq. (4.10).

$$B_{coil} \propto \frac{\mu_0 NI}{L} \tag{4.10}$$

The amount of current applies to coils can be increased by 30% . The maximum amount of the coil is limited by the thermal resistance of wires. The specification for the electromagnets of MDU is 750 turns with the length of 40 cm made of copper. The maximum amount of current for this specification is 10 Amps in each coils which produces approximately B=0.02 T. The only way to increase the magnetic field is increasing the number of coils in the system. The sketch of magnetic drive unit is shown in Figure 46.

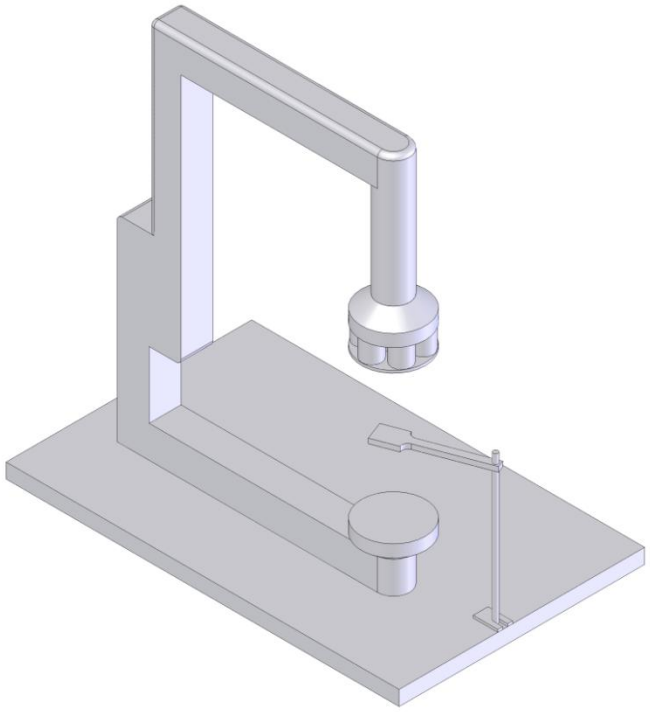

Figure 37 - Magnetic Drive Unit Infrastructure

Three different concepts have been proposed to increase magnetic field produce by electromagnets in MDU in order to move the WatCapsule. The first one was to add other coils in *x* and *y* directions as well. However, this approach would require the position feedback from the laser micrometers which is not available for a capsule robot in the GI tract. Thus,, the method of control should be focused on the magnetic field controls. Therefore, 3D coils produce a complicated field that is very hard to be evaluated. The second idea was to add another set of electromagnets fixed on the bottom face of MDU shown in Figure 46 and apply the opposite current to them. In this case, the field produced by the new set of coils empowers the first field. The problem of this idea was the distance between the bottom face and the working space. The order of magnetic field produces by electromagnets is mili-Tesla fields that the distance of our real-size model are large enough to reduce the effectiveness of adding these extra electromagnets.

4.2.1 Test setup modification

In this section, the magnetic field produced by the electromagnets has been evaluated both analytically and modeled in finite element analysis software (COMSOL). Magnetic field modification is performed to optimize the magnetic drive unit for capsule robot's manipulation targets. The

magnetic field distribution produce by coils, need to be optimized for magnetic control system. Magnetic flux density for the system (7 electromagnets) has been determined when we move along the line (x=0.1) shown in Figure 38.

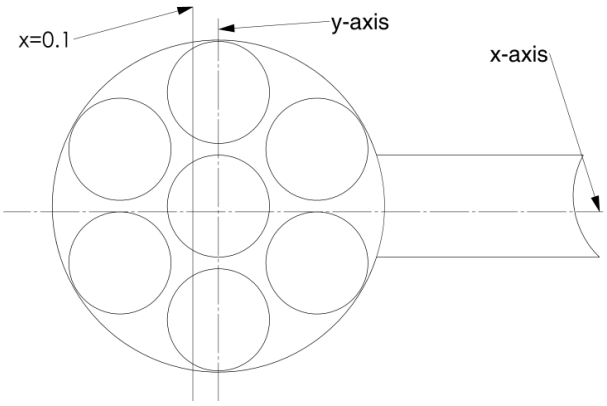

Figure 38 - Section view of electromagnets with yoke

The magnetic flux density along the line x=0.1m can be achieved from superposing the magnetic field produced by each coil is the working space. Working space for the magnetic control system is the cylindrical space under the pole piece where the magnetic particle can be levitated. In order to model the electromagnets in COMSOL, permanent magnets must be substituted instead of electromagnets.
For the purpose of the calculation of the fields in permanent magnets, an output is sought in terms of equivalent currents instead of magnetization. The reason to model the permanent magnet with coils is that, the magnetic field produced by the coil can be evaluated in both Cartesian and cylindrical coordinates. Magnets are not different than solenoids and they can always be replaced by equivalent current densities. In our specific problem that electromagnets have been distributed in x-y plane, the only way to analyze this infrastructure in finite element software, is to solve it in 3 dimensional models. In order to solve the 3D model in Cartesian coordinates, coils need to be equivalent with permanent magnets, because of the circular current density in 3D coils (that cannot be applied in 3D model of electromagnet).

An electromagnet and a permanent magnet can be equivalent to each other if the same current density pass through an outer surface of the rod as shown in Fig Figure 39.

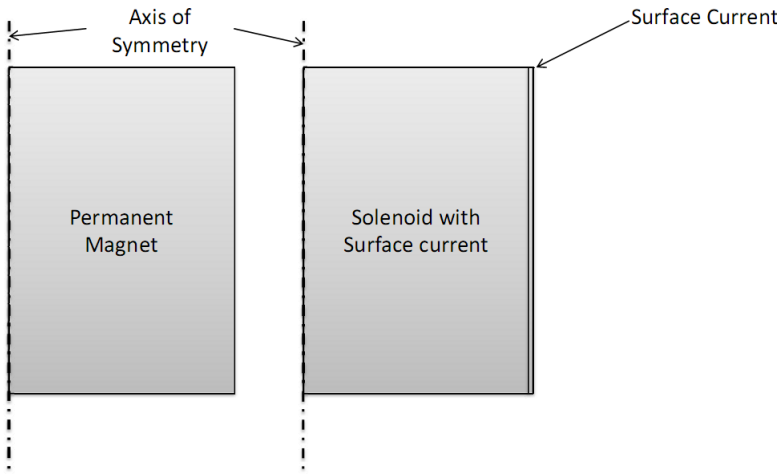

Figure 39 - Permanent magnet with equivalent solenoid

A permanent magnet with a magnetization of ***M*** is equivalent to the solenoid with a current density ***J*** passing through its surface with thickness ***t*** then we have

$$J = \frac{M \times L}{A} \tag{4.11}$$

Where ***L*** is the length of the coil or magnet and ***A*** is the cross section of current plate. Flux density for both electromagnet and permanent magnet is shown in Figure 40. It can be seen here that magnetic flux density is completely the same and the permanent magnet model can be used for capsule robot manipulation significantly.

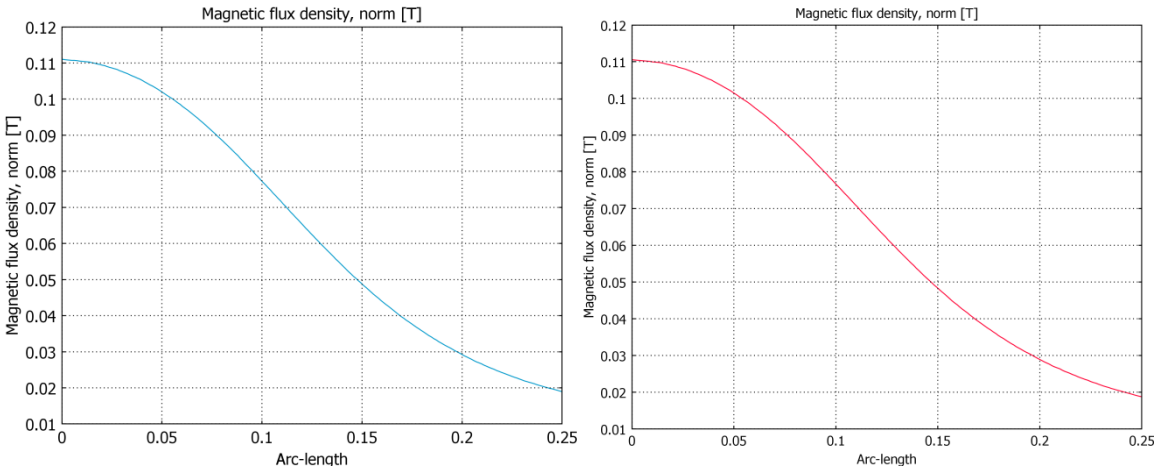

(a) **(b)**

Figure 40 – (a) Magnetic flux density for permanent magnet (b) Magnetic flux density for equivalent solenoid with surface current density

The real coil in our magnetic drive unit has the dimensions of 40 mm long, 20mm diameter of core and 20 mm thickness of wires around the core. Evaluation of magnetic field cannot be possible from surface current density model. Now there is a case with volume current density instead of surface current density. According to the geometry of the electromagnet, the curl in cylindrical coordinates is the volume current density as it is presented in Eq. (4.12).

$$J_m = \nabla \times M = -\hat{\phi}\frac{\partial}{\partial r}M \qquad \textbf{(4.12)}$$

In this case, magnetic flux density is maximum at the centre of the magnet and goes down linearly at $r=a$. Since the current density is uniform, it produces a linear magnetization which is highest on the axis of the magnet and zero at its outer surface, as required. Magnetic flux density for this model is shown in Figure 41. It can be seen that the trend of magnetic flux density is the same in both and it is possible to use PM instead of electromagnets in modeling. It should be mentioned here that magnetic flux density should be applied only along the axis of the cylindrical PM. This design of equivalent PM or the combination of PM which produce the same flux density of solenoid, magnetic drive unit can be analyzed in finite element software too, and then the results can be compared with the analytical solution of the coils. The reason for modeling magnetic drive unit is because of pole piece.

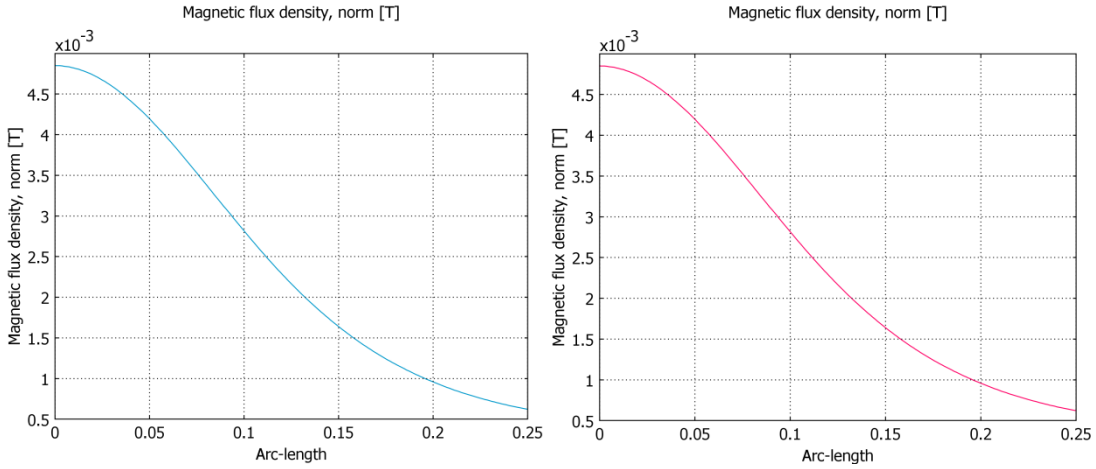

(a) **(b)**

Figure 41 (a) Magnetic flux density for permanent magnet (b) Magnetic flux density for equivalent solenoid with volume current density

To summarize, one of the concepts to improve the magnetic field for capsule robot manipulation is to add permanent magnets on the bottom mounting bracket. Regarding to the poles of permanent magnets on this bracket, the constant magnetic field can be applied to any objects in the system and

there could be an initial force always applies to particle in the working space. Also, the magnetic field can be controlled by designing adjustable height for the permanent magnets. We had two problems to use this concept for magnetic field empowering. First, providing the magnets of sufficient size that affect the magnetic particle was not possible. These rod magnets should be the same size of the electromagnets with radial magnetization that is not easy to purchase. Second, not only adjusting the height of the permanent magnet on the bracket is not easy, but also the range of magnetic field is not so large.

4.2.2 Pole piece Analysis

The pole piece analysis is to make an optimize pole piece to produce a field for magnetic control of capsule robot. The first assumption to solve this problem is to suppose the field as a uniform magnetic field. Suppose that a certain magnetic induction B_0 exists in a region of empty space initially. A permeable body is now placed in a region which is uniformly magnetized cylinder in an external field. The lines of magnetic induction are modified. As we know from magnetic field boundary conditions, for a media of very high permeability, the field lines would tend to be normal to the surface of the body. The field inside the magnetic material is smaller than the source field outside of it. Such a reduction in field is said to be due to the magnetic shielding provided by the permeable material. It is of considerable practical importance, since essentially field-free regions are often necessary or desirable for experimental purposes. The magnetized cylinder in an external field is evaluated in Appendix B.

It can be inferred that for the magnetic drive unit, magnetic field streamlines, pass from iron to air. The ratio of permeability makes large amount of deflection from one environment to the other. As it is explained before, the perpendicular streamlines to the pole piece, pass without any deflection which refers to the middle area of the pole piece.

All explained above were the effect of pole piece on magnetic field in working space. The reason of using pole piece is to modify the magnetic field into the constant field area which makes the magnetic manipulation stable enough. The pole piece on the magnetic drive unit is a cylinder of 132mm in diameter and 6mm thick.

4.2.3 Analytical modeling of the magnetic field and its force

In this section, the magnetic field and its force applied to capsule robot based on electromagnets are analytically modeled. Then, the combination of electromagnets is modeled in COMSOL and finite element analysis for magnetic field has been done in COMSOL to calculate electromagnetic force for capsule robot manipulation.

4.2.3.1 Capsule Robot Force Analysis

There are different forces that apply to a capsule robot when it moves inside human GI tract. When the capsule touches the tissue of the human body, a free body diagram can be drawn to show all of the forces acting on the capsule. Friction force is related to the contact of the capsule with the GI tissue. Drag force also acts because of the liquid inside human's esophagus. Therefore, the magnetic force needs to overcome friction force, drag force and weight of the capsule robot. The capsule free body diagram is shown in Figure 42. It needs to be mentioned here that the horizontal diagram of esophagus is because of the operation environment for local drug delivery. The esophagus is vertically oriented but the patient lies down under the MDU and the esophagus would be in horizontal direction.

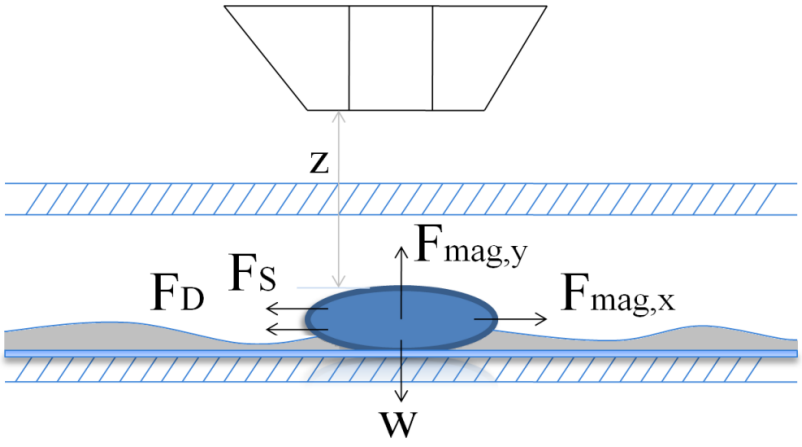

Figure 42 - Capsule body diagram

4.2.3.1.1 Electromagnetic force

In order to calculate the electromagnetic force, magnetic field produced by coils should be evaluated. The field of a current ring needs to be achieved to find the magnetic field produce by coil. To evaluate this magnetic field, the field of a current ***I*** is considered flowing on a ring of radius ***R*** as shown in Figure 43. In order to simplify the calculation of magnetic field, it is convenient to relate

the current distribution to a potential and then calculate the magnetic field from the potential. For this purpose, vector potential ***(A)*** is defined in what is called the coulomb gauge:

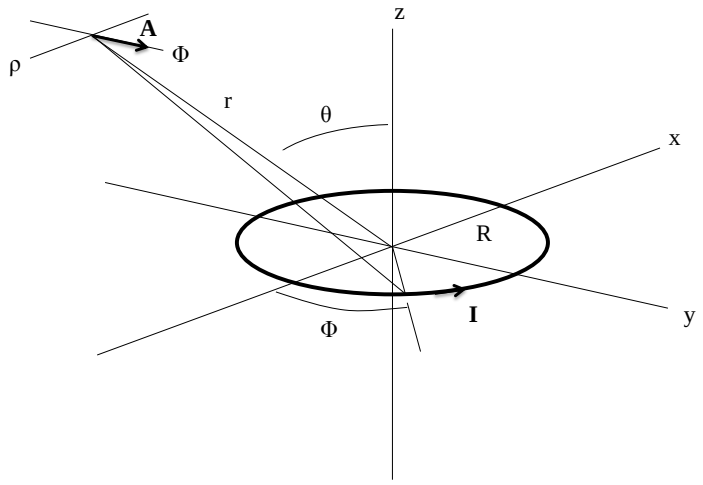

Figure 43 - Field of current ring

According to Bio-savart law, vector potential can be calculated as

$$A(r) = \frac{\mu_0 I}{4\pi}\left(\int_{C_1} \frac{dl}{r_1}\right) \qquad \textbf{(4.13)}$$

r_1 here denotes the distance between the source element dl at r_1 and the desired point in the space. Because of the symmetry, the magnetic field is obviously independent of the angle φ of the field point. According to Figure 43, dl can be developed as

$$dl = (-a_x \sin\varphi + a_y \cos\varphi) R d\varphi \qquad \textbf{(4.14)}$$

The law of cosines gives

$$\frac{1}{r_1} = \frac{1}{r}\left(1 + \frac{R}{r}\sin\theta\sin\varphi\right)\sin\varphi d\varphi \qquad \textbf{(4.15)}$$

Since dl is an even function of a_y, the radial component of A integrates to zero and we left only with the radial part of vector potential. We first find the vector potential and then determine B by $\nabla \times A$. According to the concept of vector potential the coil need to be modeled as a ring with 2 different diameters as shown in Figure 44.

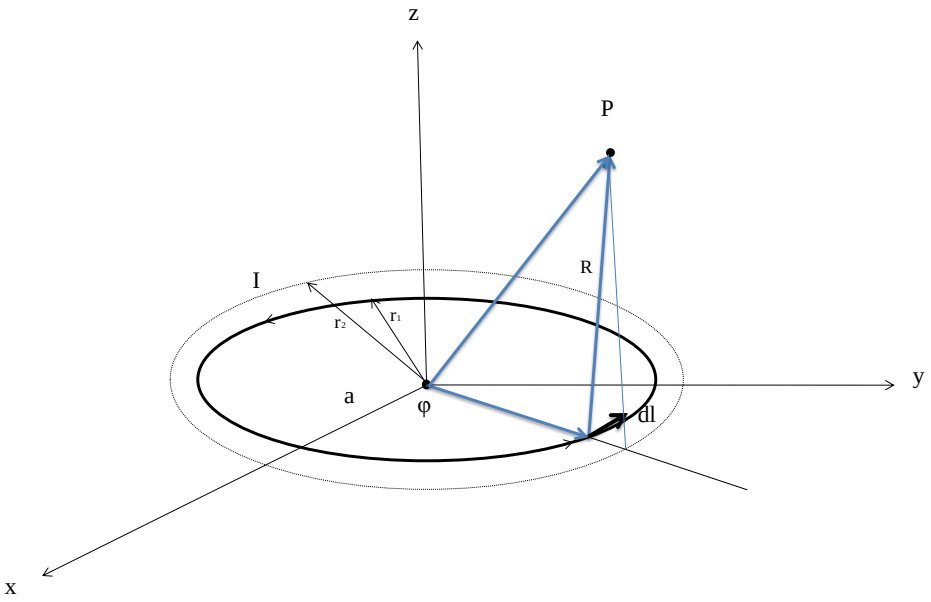

Figure 44 - One section of coil

According to Bio-savart law explained for vector potential and curl of vector A, magnetic field can be written as

$$B = \frac{\mu_0 m}{4\pi} \int_C \frac{Idl \times R}{R^3} \tag{4.16}$$

dl and R can be developed as

$$dl = a\left(-sin\varphi i + cos\varphi j\right) d\varphi \tag{4.17}$$

And

$$R = \left(x - acos\varphi\right) i + (y - a\sin\varphi) j + \left(z - h\right) k \tag{4.18}$$

Now, the magnetic field produced by coil at a desired point in the space can be achieved through the integration of a ring shown in Figure 44 from r_{in} to r_{out}, $-L/2$ to $L/2$ and 0 to 2π. The scheme of electromagnet is shown in Figure 45. Magnetic field produced by this coil in desired location in the space like P can be written as

$$B(x, y, z) = \frac{\mu_0 m}{4\pi^2 a} \int_0^{2\pi} \frac{(-\sin\varphi i + \cos\varphi j) \times R}{|R|^3} d\varphi \tag{4.19}$$

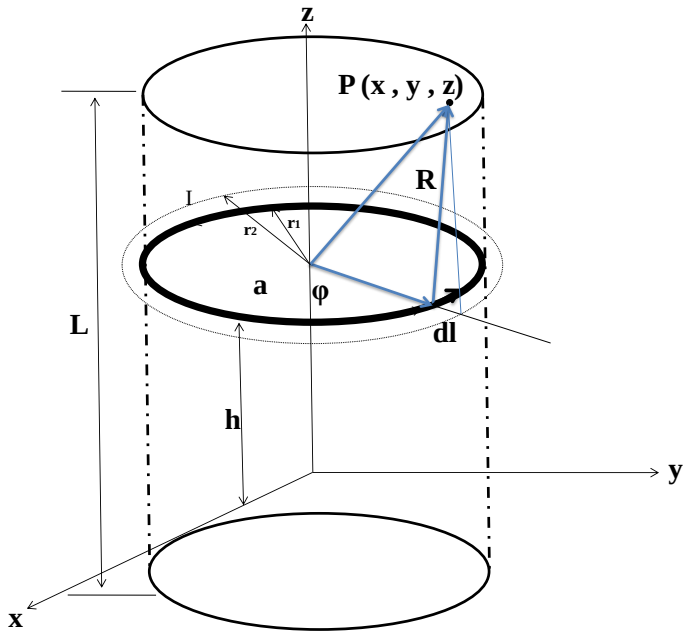

Figure 45 - electromagnet scheme (Coil)

If σ is a winding density of wire per unit area, the magnetic dipole moment for a filamentary element of radius *r*, thickness *dr* and height *dz* is defined as:

$$m_v = \sigma I \pi r^2 dr dz \tag{4.20}$$

Therefore

$$B(x,y,z) = \frac{\mu_0 \sigma I}{4\pi} \int_{r_{in}}^{r_{out}} \int_{-L/2}^{L/2} \int_{0}^{2\pi} \frac{r(-\sin\varphi i + \cos\varphi j) \times R}{|R|^3} d\varphi dz dr \tag{4.21}$$

This integration has been solved numerically in MATLAB. By integrating *B* along the line at desired height, the vector of *B* for each coil can be achieved. This numerical method is used because of the working height of magnetic field is limited. At different heights, the magnetic field can be achieved along the desired line of capsule movement. The components of magnetic field vector are shown below.

$$B_x = \frac{\mu_0 \sigma I}{4\pi} \int_{r_{in}}^{r_{out}} \int_{-L/2}^{L/2} \int_0^{2\pi} \frac{[r\cos\varphi(z - z_1)]i}{|R|^3} d\varphi dz dr \quad \textbf{(4.22)}$$

$$B_y = \frac{\mu_0 \sigma I}{4\pi} \int_{r_{in}}^{r_{out}} \int_{-L/2}^{L/2} \int_0^{2\pi} \frac{[r\sin\varphi(z - z_1)]j}{|R|^3} d\varphi dz dr \quad \textbf{(4.23)}$$

$$B_z = \frac{\mu_0 \sigma I}{4\pi} \int_{r_{in}}^{r_{out}} \int_{-L/2}^{L/2} \int_0^{2\pi} \frac{[\cos\varphi(x - r\cos\varphi) + \sin\varphi(y - r\sin\varphi)]k}{|R|^3} d\varphi dz dr \quad \textbf{(4.24)}$$

Now, the superposition method is used to develop magnetic field provided by all the electromagnets of magnetic drive unit. The distribution of electromagnets is shown in Figure 46.

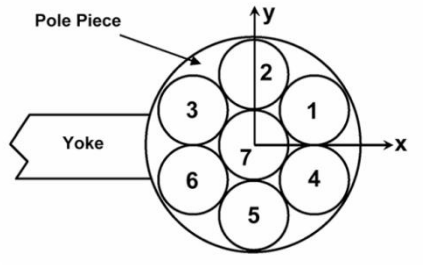

Figure 46 - Electromagnets distribution

If we suppose that the global coordinate system is in the middle of coil 7 then the superposed of magnetic field for this point can be written as

$$\begin{aligned} B_x(x) &= B_{1x}(x - r\sqrt{3}) + B_{2x}(x) + B_{3x}(x + r\sqrt{3}) + B_{4x}(x - r\sqrt{3}) \\ &+ B_{5x}(x) + B_{6x}(x + r\sqrt{3}) + B_{7x}(x) \end{aligned} \quad \textbf{(4.25)}$$

And

$$\begin{aligned} B_y(y) &= B_{1y}(y - r\sqrt{3}) + B_{2y}(y) + B_{3y}(y + r\sqrt{3}) + B_{4y}(y - r\sqrt{3}) \\ &+ B_{5y}(y) + B_{6y}(y + r\sqrt{3}) + B_{7y}(y) \end{aligned} \quad \textbf{(4.26)}$$

Therefore, the magnetic field along the first line is achieved and shown below.

Electromagnetic force produced by coils move the capsule robot in *x* and *y* directions. Distribution of coils is the way that their axis are perpendicular to pole piece which produce electromagnetic field in *z* direction. According to Eq.(4.7), the growth of magnetic field in vertical direction produces vertical force applied to the permanent magnet. Horizontal forces produce by coils, the same as vertical force, are function of magnetic field presented in Eq. (4.27) and(4.28).

$$F_x = D\frac{\partial B_x}{\partial x} \quad \textbf{(4.27)}$$

And

$$F_y = D\frac{\partial B_y}{\partial y} \quad \textbf{(4.28)}$$

Horizontal forces are much smaller than vertical force produce by electromagnets for two main reasons. First, the distribution of electromagnets produces magnetic field in the *z* direction and the gradient of this field in *x* or *y* directions are very small. Second, permanent magnet in capsule robot is magnetized only in one direction, and the dipole moment of permanent magnet is parallel to electromagnets. Therefore, horizontal forces are times smaller than vertical ones and the manipulation the capsule robot in horizontal plane is more difficult than in the vertical plane.

4.2.3.1.2 Drag Force

One of the first analysis tasks was to estimate the drag force on the capsule robot produced by the fluid flow in the GI tract. This was done to know if any special efforts should be taken on the motion system for stability or in integrating components to withstand the force produces by gastrointestinal tract movement. The capsule was approximated as a cylinder in parallel flow. The curvature on the front of the actual capsule will serve to reduce drag, making this estimate conservative. For a capsule diameter of 11 mm and a length estimated as 20 mm, the ratio of length to diameter is available. The drag coefficient based on frontal area for this geometry and length to diameter ratio can be achieved through shape coefficient [63].

After these calculations we need a model to evaluate the force diagram of capsule robot. Therefore, the model for the vertical force of the magnetic field is needed to get used in experiment. Then, the experimental and numerical model for force can be compared with each other. In the present section, the power amplifier is analyzed. This amplifier receives the input command from the controller which controls the current for vertical and horizontal movement of the capsule robot. The range of the voltage for this amplifier is 0 - 10 volts.

The output is set to the current in the coil with the controller command as the input for frequency response of the amplifier and the coil. As it is shown in Figure 47, amplifier is almost a linear gain for frequencies less than 2 kHz.

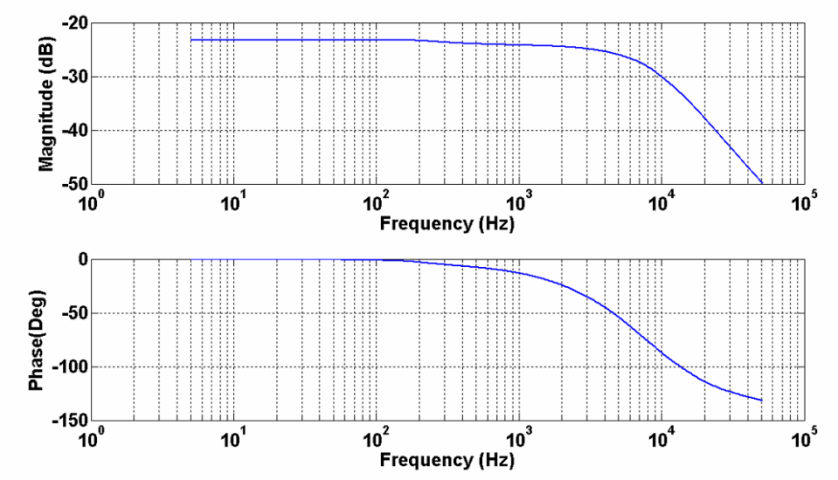

Figure 47 – Frequency response of the amplifier

Then, it can be assumed that, amplifier has a linear gain as the model of the amplifier in the magnetic control system. This gain can be explained as the transfer function *G*.

$$G_{amp}(s) = \frac{I(s)}{V(s)} = K_{amp} \tag{4.29}$$

And in this equation ***I(s)*** is the current in the coil, ***V(s)*** is the voltage fed to the amplifier and K_{amp} is a constant number presented as amplifier gain. The vertical force in the capsule body diagram is related to the *z* component of magnetic field only. A set of experiments were done at different heights below the pole piece for frequency response. According to these experiments the first order for transfer function between field and current was presented which we used for magnetic force simulation.

$$G_B(s) = \frac{B_z(s)}{I(s)} = \frac{k}{1+\tau s} \tag{4.30}$$

Where *k* and τ are two function coefficients as presented here

$$K = 0.073(T/A)$$
$$\tau = 0.0037(s) \tag{4.31}$$

Substituting Eq. (4.29) in Eq. (4.30) then we have

$$G_B(s) = \frac{B_z(s)}{V(s)} = \frac{k_{amp}k}{1+\tau s} \tag{4.32}$$

In this step, we need to recognize the relationship between *k* and height. A second order of polynomial was fit on the gain plot results the general form of magnetic model presented here.

$$G_B(s) = \frac{B_z(s)}{V(s)} = \frac{k_{amp}(c_1 z^2 + c_2 z + c_3)}{1+\tau s} \quad \textbf{(4.33)}$$

where c_1, c_2 and c_3 are found experimentally. With magnetic field model, magnetic force can be found easily. Therefore, the magnetic field can be found through Eq. (4.7) and is presented

$$F_z(s) = |P|\left(\frac{2c_1 z + c_2}{1+\tau s} k_{amp}\right) V(s) \quad \textbf{(4.34)}$$

And $|P|$ is a constant equal to the magnetic dipole moment of the levitated capsule robot in z direction. Then the magnetic force is

$$F_z(s) = (\alpha z + \beta)\left(\frac{V(s)}{s + 1/\tau}\right) \quad \textbf{(4.35)}$$

That $\alpha = |P|(2c_1 K_{amp})/\tau$ and $\beta = |P|(c_2 k_{amp})/\tau$. Therefore, the magnitude of force for the constant voltage as the magnitude of controller command in term of an analog voltage can be calculated as

$$F(t) = (\alpha z + \beta)(1 - e^{\frac{-1}{\tau}})V \quad \textbf{(4.36)}$$

This equation of force shows the experimental model for force in magnetic control system which was done based on experimental data we have from amplifier and controller. The analytical solution for force has been presented as well. In this way, charge model is used to calculate the magnetic force apply to the capsule robot in an external field. It is assumed here that the volume of the capsule robot as the object in the system has a negligible effect compared with the magnetic field as constant magnet and produce from a long distance source. The charge model is a method to analyze permanent magnet. In this method magnet is supposed as equivalent "magnetic charge". According to current model the force can be determined using

$$F = \int_V J_m \times B_{ext} dv + \oint_S j_m \times B_{ext} ds \quad \textbf{(4.37)}$$

That *V* and *S* are the volume and surface of the magnet. J_m and j_m are volume and surface current density. To solve this equation, we start with equivalent current and magnetization in current model as presented in Eq. (4.38)

$$J_m = \nabla \times M$$
$$j_m = M \times n \qquad \textbf{(4.38)}$$

Then Eq. (4.37) can be written as

$$F = \int_V (\nabla \times M) \times B_{ext} dv + \oiint_S (M \times \hat{n}) \times B_{ext} ds \qquad \textbf{(4.39)}$$

A vector identity can be used to solve this equation as

$$\int_V (V \times U) \times V dv - \oiint_S (n \times U) \times V ds = \int_V [U \times (\nabla \times V) - U(\nabla . V)] dv + \int_V (U . \nabla) V dv \qquad \textbf{(4.40)}$$

Now if substitute $U=M$ and $V = B_{ext}$, gives

$$F = \int_V (M . \nabla) B_{ext} dv \qquad \textbf{(4.41)}$$

Because the first integration will be zero on left side of Eq. (4.40). Therefore regarding the fact that $\nabla . B_{ext} = 0$, force can be evaluated as

$$\begin{aligned} (M . \nabla) B_{ext} &= (M_x \frac{\partial}{\partial x} + M_y \frac{\partial}{\partial y} + M_z \frac{\partial}{\partial z}) B_{ext_x} \hat{x} \\ &+ (M_x \frac{\partial}{\partial x} + M_y \frac{\partial}{\partial y} + M_z \frac{\partial}{\partial z}) B_{ext_y} \hat{y} \\ &+ (M_x \frac{\partial}{\partial x} + M_y \frac{\partial}{\partial y} + M_z \frac{\partial}{\partial z}) B_{ext_z} \hat{z} \end{aligned} \qquad \textbf{(4.42)}$$

Therefore, force density in the volume of 1 cubic meter, that is valuable for us can be presented as

$$f = (M . \nabla) B_{ext} \qquad \textbf{(4.43)}$$

This equation can be expanded as

$$f = (M . \nabla) B_{ext} = (M_x \frac{\partial}{\partial x} + M_y \frac{\partial}{\partial y} + M_z \frac{\partial}{\partial z}) . [B_x \quad B_y \quad B_z]^T \qquad \textbf{(4.44)}$$

According to the real model of electromagnets, there can be an acceptable assumption as

$$M_x \cong M_y \cong 0 \qquad \textbf{(4.45)}$$

Therefore

$$f_z = M_z \frac{\partial B_z}{\partial z} \qquad \textbf{(4.46)}$$

On the other hand the force can be written as

$$F = \int_V \rho_m B_{ext} dv + \oiint_S \sigma_m B_{ext} ds \quad \textbf{(4.47)}$$

4.2.4 Vertical and Horizontal Control System

4.2.4.1 Introduction

After analyzing the magnetic drive unit and designing the capsule robot, there is a control system required for capsule movement. It is noted that, more than half of the industrial controllers in use today utilize proportion-integral-derivative (PID) or modified PID control schemes. When the mathematical model of the plant is not known and therefore analytical design method cannot be used, PID controls prove to be most useful. In these cases, an analytical approach to the design of a PID controller is not possible. Then we must resort to experimental approaches to the tuning of PID controllers. Magnetic control loop is shown in Figure 48.

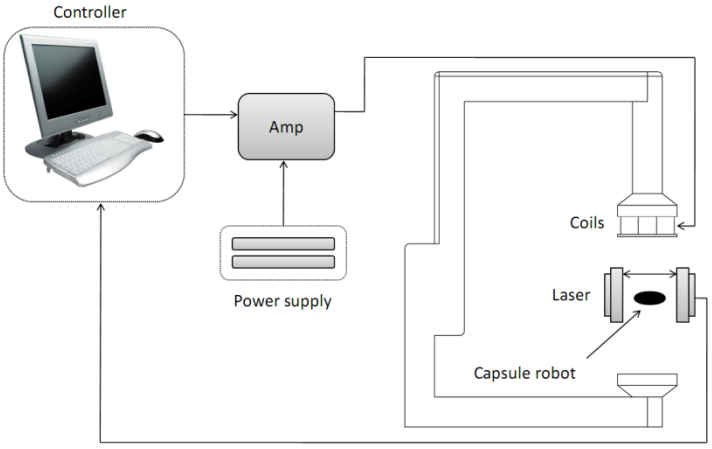

Figure 48 - Close loop control of magnetic control system

The magnetic control setup in Figure 48 is the computer which receives the position signal from lasers, runs the Labview program and controls the output signal for our system. The controller's task it to receive the real position of the capsule robot and compare it with the input command position. The difference between these two data is the error of the controller. Then, controller calculates this difference and applies an appropriate analogue voltage to the amplifier. The voltage produces by power supply is between 0 to 10 volts. For the vertical position of the capsule, the only force applies to the capsule is the gravity force. For horizontal control of the capsule or *x* and *y* directions, some other forces would be involved in various situations..

4.2.4.2 First order control system for horizontal manipulation

To design the controller, dynamic behavior of the system should be predicted from the knowledge of the components. For magnetic drive unit, first-order system is selected for the dynamic behaviour of the system. The block diagram for the first-order system is shown in Figure 49.

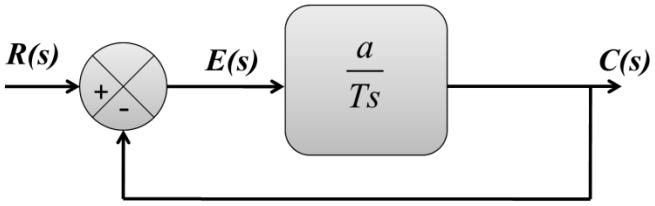

Figure 49 - block diagram for the first-order system

To evaluate input and output relationship of this system, the transfer function can be written as

$$\begin{aligned} C(s) &= E(s)\times\frac{a}{Ts} \\ E(s) &= R(s)-C(s) \\ \Rightarrow C(s) &= [R(s)-C(s)]\times\frac{a}{Ts} \\ \frac{C(s)}{R(s)} &= \frac{a}{Ts+a} \end{aligned} \qquad \textbf{(4.48)}$$

Now, the unit step response for this function can be achieved through Laplace transform function of the unit step. For the unit step of $R(s) = 1/s$, it can be written as

$$C(s) = \frac{a}{Ts+a}\times a/s \qquad \textbf{(4.49)}$$

By expanding Eq. (4.49) into partial fraction gives

$$C(s) = \frac{a}{s} - \frac{aT}{Ts+1} = \frac{a}{s} - \frac{a}{s+(\frac{a}{T})} \qquad \textbf{(4.50)}$$

And the inverse Laplace for Eq. (4.50) will be

$$c(t) = a(1-e^{-\frac{1}{T}t}) \qquad \textbf{(4.51)}$$

Which *a* is the control command of our system. For the horizontal control system, the command of *x* and *y* is in the range of millimeter. In Eq.(4.51), *c (t)* is zero at *t=0*, and finally *c (t) =a*. The time constant *T* is set to 1 and for *a=2.5 mm,* the exponential response curve is shown in Figure 50. The

slope of the tangent line at t=0 of exponential response curve is related to time constant and in this case is 0.1.

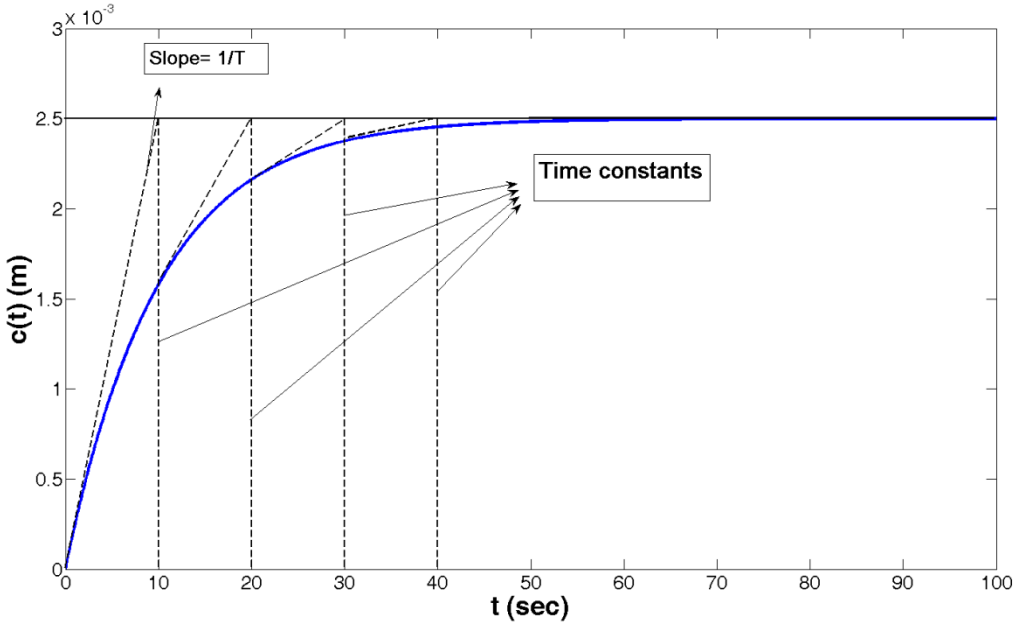

Figure 50 - Exponential response curve

It should be mentioned here that the smaller time constant *T*, the faster the system response.

The horizontal position of the capsule robot is achieved through mathematical method. The horizontal control system is set for both closed loop and open loop control system. The close loop control of *x* and *y* is used to move the capsule robot for very small displacement in the range of 1mm. On the other hand, the open loop control strategy is used to move the capsule for larger displacement in the range of 10 mm. The concept of the horizontal movement of the capsule robot comes from the change of the ratio of current in the electromagnets without any change in the net amount of input current. According to Professor Khamesee and Dr. Shameli's research on the same project, it is proven that if the net total current in electromagnets keeps constant, when changing the ratio of this amount in different coils, the vertical position of the capsule robot does not change. The same strategy is used for the mathematical model of capsule's motion in horizontal plane by position and/or current command. In this system of control, there are two different sets of commands for the current. The first set, *u* is the same current for all the electromagnets, and the second is the current that makes the change in ratio for horizontal movement.

4.2.4.3 Open loop control system

There is a principle of movement in horizontal plane. This principle explains the task of each electromagnets in *x* and *y* directions. This distribution is presented in Table 4.

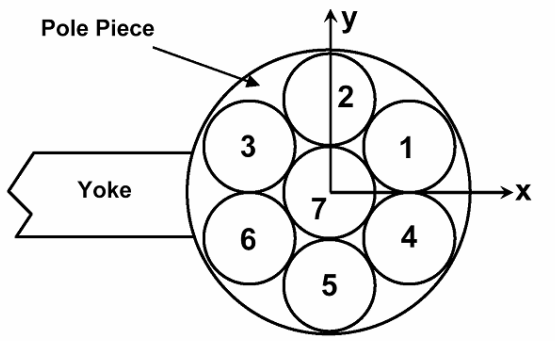

Figure 51 - Electromagnets distribution for horizontal control system

Table 4 - Current distributions in electromagnets for *x* and *y* motion

Motion of the capsule robot	Current increase in electromagnets	Current decrease in electromagnets
+x	1,4	3,6
-x	3,6	1,4
+y	1,2,3	4,5,6
-y	4,5,6	1,2,3

According to the principle of movement, there are three different type of current applies to the electromagnets. The first one is I_z, which is the same for all the coils that are used for *z* manipulation. There are two different currents, I_x and I_y for the *x* and *y* manipulation that are applied based on the distribution explained in . I_z applied to all electromagnets and I_x and I_y are applied to change the ratio of current between electromagnets. The current ratio algorithm is presented as:

$$\begin{aligned} I_1 &= I_z(1+I_x)(1+I_y) \\ I_4 &= I_z(1+I_x)(1-I_y) \\ I_3 &= I_z(1-I_x)(1+I_y) \\ I_6 &= I_z(1-I_x)(1-I_y) \end{aligned} \quad \textbf{(4.52)}$$

According to Figure 51, distribution of current showed in Eq. (4.52), is used to move the capsule robot in *x* direction. The same distribution can be written for electromagnet 2 and 5 but the point here is that it was supposed that the ratio of current changes for horizontal distribution but the total current is the same. Regarding to these two principles, current for electromagnets 2, 5 and 7 is:

$$\begin{aligned} I_2 &= \frac{(6I_z - I_1 - I_3 - I_4 - I_6)(1 + I_y)}{2} \\ I_5 &= \frac{(6I_z - I_1 - I_3 - I_4 - I_6)(1 - I_y)}{2} \\ I_7 &= I_z \end{aligned} \quad \textbf{(4.53)}$$

The current term explained above can be replaced by a position command and then move the capsule robot based on position feedback. In this method of horizontal manipulation, the real esophagus for human is considered as environment and so there is no feedback of laser commands. In this manner, the concept of capsule robot manipulation in *x* and *y* is demonstrated.

By substituting *x*, *y* and *z* instead of I_x, I_y and I_z, the same concept of manipulation can be achieved for horizontal manipulation with laser feedback. Ehsan Shameli and David Craig showed that, there could be a ratio factor *n* multiplied by I_y which increases the rate of *y* manipulation.

In this method of horizontal control, the capsule robot moves based on current ratio changes. The total current in the electromagnets which produce the magnetic field is constant. The value of this current is calculated as:

$$I_{sum} = 7I_z \quad \textbf{(4.54)}$$

There are steps of movement in this mathematical method. By Increasing I_x or I_y, there will be a command of current which moves the capsule robot one step in the *x* or *y* direction. The exactness of the motion is related to the number of steps for one displacement. According to the electromagnets distribution, there is magnetic field produced in *z* direction and the gradient of this field in *x* and *y* which provides the force in *x* and *y* directions, is very small. This gradient is shown in chapter 4.2.5. The limitation of command is because of the lack of coils in *x* or *y* directions. This infinitesimal force can move an object with the minimum resistance force. The minimum resistance circumstance for this system is levitation. To prove the concept the capsule robot can move inside human's body without any feedback, the new method of control is explained in the present chapter. Although without any position feedback, the exactness of the control is not as good as with the PID control system, but the proof of concept for wireless motion without feedback is reasonable.

In this case, capsule robot is inside the tube as shown in Figure 52.

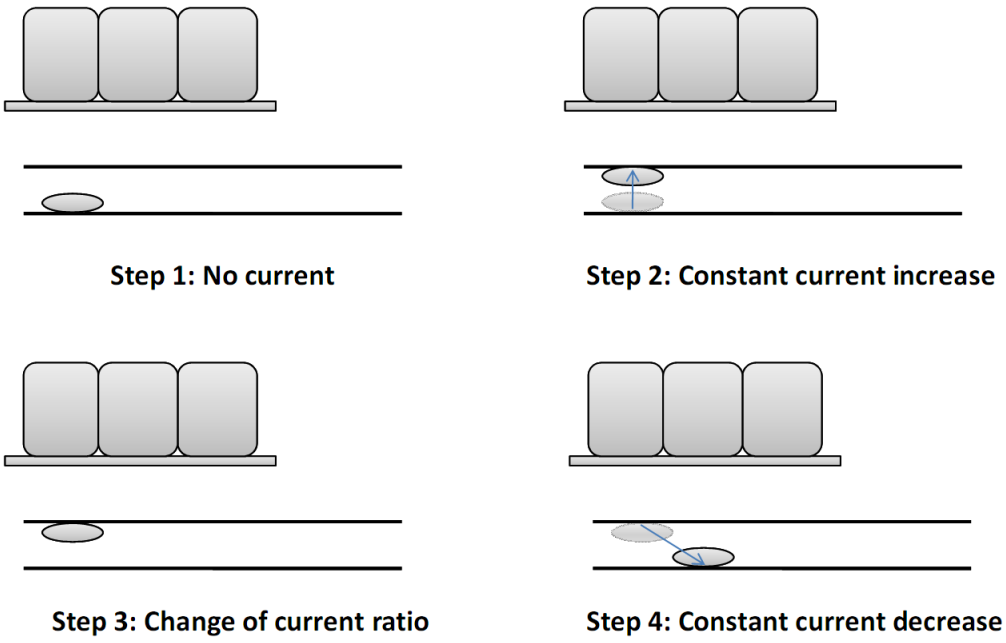

Figure 52 - Step of movement for open loop control system

There are four steps of movement are designed to move the capsule robot forward. These four steps are explained below.

- **Step 1.** In initial step movement, capsule robot does not move and there is no current in electromagnets. Capsule robot located at the bottom layer of esophagus.
- **Step 2.** Second step of movement, has a vertical motion only. In this step by increasing the amount of I_z, capsule is levitated. Since there is no feedback of position in this control system, instability of capsule robot cannot be controlled and it cannot stay levitated inside the esophagus. Capsule position is on the top layer of the esophagus and the amount of current is the same in all electromagnets.
- **Step 3.** In this step capsule robot stays at its location and does not move. By changing I_x and I_y in this step the ratio of current will change rather than step 2. Because of the friction force between the capsule and inner layer of esophagus, although the ratio has changed, the capsule stays at the top layer and does not move. At the end of this step, maximum magnetic field are has transferred to the right side.

- **Step 4.**The last step of movement is the horizontal motion of capsule robot. In this step, the amount of I_z is decreased without any changes on I_x and I_y. By decreasing the amount of I_z, after the specific amount, capsule robot start to move down. The point here is that, because of the ratio of current inside electromagnets, the capsule moves down and follows the maximum point of the magnetic field area which was moved right in step 3. Therefore, capsule robot has both horizontal and vertical movement in this step. At the end, all 4 steps should be repeated again for the next horizontal movement.

These four steps of movement provide the horizontal motion for capsule robot. By controlling increase of I_x and I_y, the exactness of movement can be evaluated. The position command in this control system is divided to different steps and this method is repeated for each of them. By increasing the steps of movement between desired points "A" and "B", the accuracy of the system will be increased as it is shown in

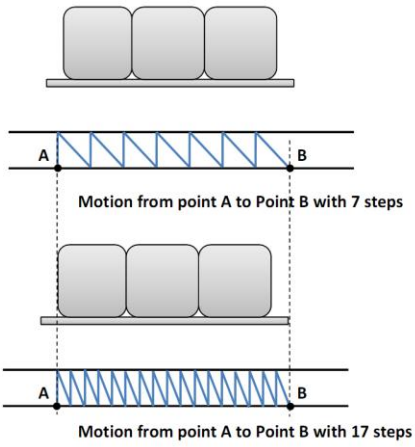

Figure 53 - Open loop control for horizontal direction for two different accuracies

4.2.4.4 PID control for the horizontal manipulation

A PID controller is the strategy to move the capsule horizontally. PID controller attempts to decrease the error between the measures or actual variable that is position in our system and a desired variable. Three specific gains should be set for PID control signal as proportional gain, integral gain and derivative gain. Control signal with these gains is shown in Eq (4.72).

$$u(t) = K_p e(t) + K_i \int_0^t e(\tau) d\tau + K_d \left(\frac{d}{dt} e(t)\right) \quad \textbf{(4.55)}$$

That *e (t)* is the error of the system. It can be calculated through the difference between the command position and measured position of the magnet. As it is mentioned in this chapter, in order to control the capsule robot motion, a mathematical model of the system should be evaluated. According to section 4.2.3.1, the dynamic modeling of the capsule robot was evaluated from 2 different approaches. The experimental approach of force is used for mathematical model as:

$$(\alpha z + \beta)(1 - e^{\frac{-1}{T}t})u - mg = m\ddot{z} \quad \textbf{(4.56)}$$

Term $(1 - e^{\frac{-1}{T}t})$ in Eq.(4.56) is evaluated through the first-order system development in this chapter. α and β are the experimental coefficients which can be evaluated from the experiments as explained later in this chapter, *m* is the mass of the capsule. *g* is the acceleration of gravity, *z* is the vertical position of the capsule. As levitated object always tends to move toward the maximum point of the magnetic field, the control system in the horizontal direction is using this following for manipulation of the capsule robot.

The centre electromagnets does not affect on horizontal movement. In this system there is the command of *u* for all electromagnets that is set for the *z* command. Then, there is ratio of the current changes based on the strategy listed above. On the other hand, there is always a feedback from *z*-controller to keep the total current the same for the vertical equilibrium of force.

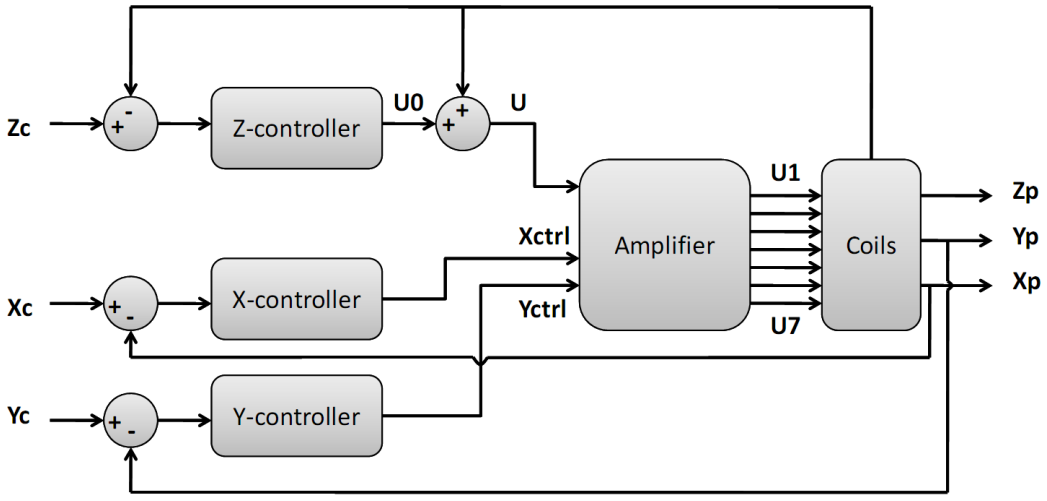

Figure 54 - Schematic of horizontal control system

The schematic of control system is shown in Figure 54.

Due to the modeling uncertainties an open loop controller contains a steady state error which is going to be eliminated in PID control system.

Using PID control law, the *x* and *y* position can be calculated as

$$x_{ctrl} = K_p(x_{command} - x_p) + K_i\int_0^t (x_{command} - x_p)d\tau + K_d((\dot{x}_{command} - \dot{x}_p)$$
$$y_{ctrl} = K_p(y_{command} - y_p) + K_i\int_0^t (y_{command} - y_p)d\tau + K_d((\dot{y}_{command} - \dot{y}_p) \quad \textbf{(4.57)}$$

4.2.5 Finite element modeling

4.2.5.1 Introduction

It is explained in Chapter 4 that magnetic drive unit provides the magnetic field to control the capsule robot as a wireless control system. This magnetic field is produced by current passing through 7 coils that forms the magnetic field source of the present system. In the present section, the magnetic field produced by this system has been analyzed and the optimum distribution of the pole piece has been evaluated. All the magnetic analysis is done in COMSOL. Geometry of electromagnetic system is compatible with 3D modeling in the finite element analysis (FEA). Because of the limitation of COMSOL in 3D modeling, the model of permanent magnet has been evaluated for electromagnets. According to section 4.2.1, each coil has been modeled with permanent magnet and the magnetic field produced by either electro magnet or radially magnetized permanent magnet are close enough to each other for the present analytical purposes. It is good to mention here that there is a virtual cylinder with the same diameter of the pole piece and a length of coil under the electromagnets, supposed as the working space of the magnetic drive unit. All the analysis of magnetic field and force are done in this space.

4.2.5.2 Coil and Pole piece effect

In this section, the magnetic field produced by coil and the effect of pole piece has been evaluated. The same method that has been used in chapter 4.2.1 that explains permanent magnet with magnetization of $\boldsymbol{M}$ is equivalent to the solenoid with the current density $\boldsymbol{J}$ passing through its surface with thickness $\boldsymbol{t}$ has been used.

$$J = \frac{M \times L}{A} \quad \textbf{(4.58)}$$

Through this method, coils have been substituted with permanent magnets with core and the magnetic fields produced by this permanent magnet that are equal to

$$M_x = 0$$
$$M_y = 0 \qquad \textbf{(4.59)}$$
$$M_z = M_0[0.02 - (x^2 + y^2)]$$

Where *0.02* is the outer diameter of the coil. This magnetization is applied from the inner diameter to the outer diameter of the rod made from the copper. There is another rod tangent to this rod that is made with iron as the core of the coil. The magnetic field produce by these coils at *z=-0.12m* is shown in .

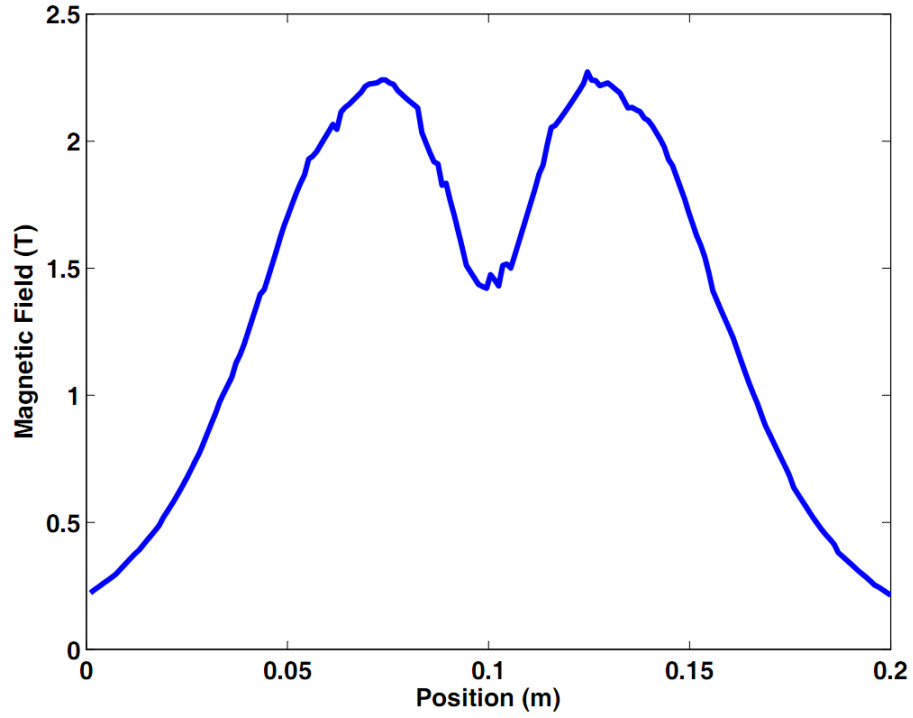

Figure 55 - Magnetic field distribution without pole piece

The magnetic field produced by this model is significantly in agreement with experimentally evaluated field. The magnetic field is maximum at the axis of the magnet and reduces along the radius. The effect of pole piece on the magnetic field in the working space is shown in Figure 56.

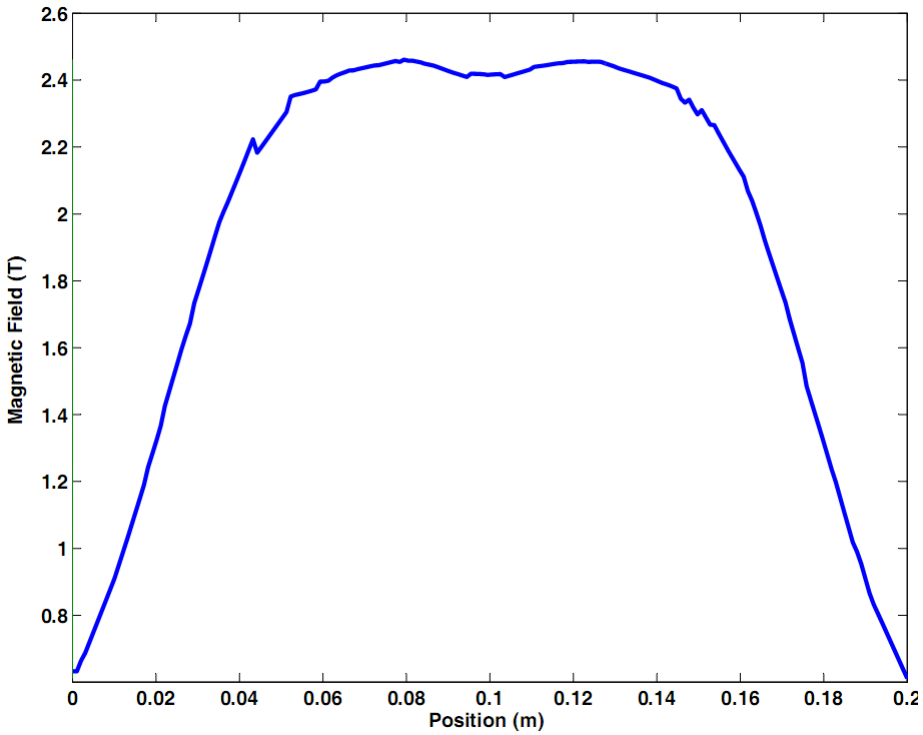

Figure 56 - Magnetic field distribution with pole piece

This figure shows that the peak of the magnetic field has been changed from two peaks to one peak with a large maximum magnetic field area.

4.2.5.3 Electromagnetic field in magnetic drive unit

The permanent magnet modeled above was the key to developing the magnetic drive unit for capsule robot manipulation. Magnetization of the centre permanent magnet is radially applied. For the other coils, magnetization is radially applied with transferring the local coordinate system to the centre of each coil. By this superposition and on basis of Figure 51, magnetization of each coil is explained in Eq. 4.77.

$$
\begin{aligned}
M_1 &= M_0[0.02-\sqrt{(-0.036+x)^2+(-0.02+y)^2}] \\
M_2 &= M_0[0.02-\sqrt{x^2+(-0.042+y)^2}] \\
M_3 &= M_0[0.02-\sqrt{(-0.036-x)^2+(-0.02+y)^2}] \\
M_4 &= M_0[0.02-\sqrt{(-0.036+x)^2+(-0.02-y)^2}] \\
M_5 &= M_0[0.02-\sqrt{x^2+(-0.042-y)^2}] \\
M_6 &= M_0[0.02-\sqrt{(-0.036-x)^2+(-0.02-y)^2}] \\
M_7 &= M_0[0.02-\sqrt{x^2+y^2}]
\end{aligned}
\qquad \textbf{(4.60)}
$$

where M_0 is evaluated from the current density of the real coil, and *x* and *y* are the global coordinates of the Cartesian system.

Magnetic field produced by electromagnets in the working area has been evaluated in different heights to determine the optimum height range for magnetic field manipulation. The FEA model has been shown in Figure 57.

Magnetic field distribution at z=-0.105m under the pole piece is shown in Figure 57.

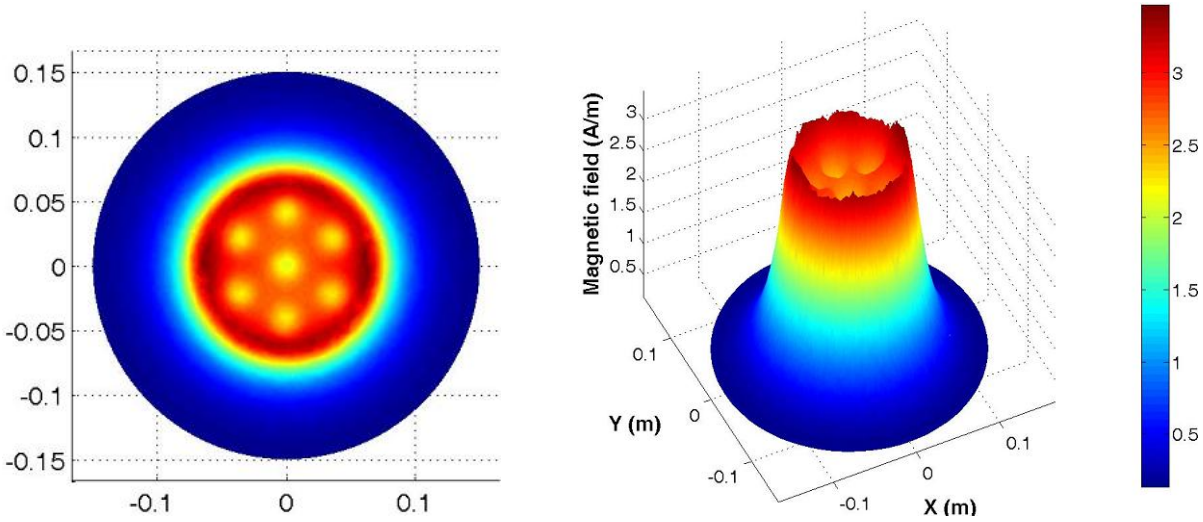

(a) **(b)**

Figure 57 - Magnetic field distribution in MDU working space,

(a) Section view, (b) contour plot

The magnetic field distribution in Figure 57 shows that maximum magnetic field area in not constant on this height. This makes the control system to be unstable on this area. To perform a stable control system, constant magnetic field distribution is desired in working space.

Through this method the optimum magnetic field has been achieved at z=-0.12m in the working space as it is shown in Figure 58.

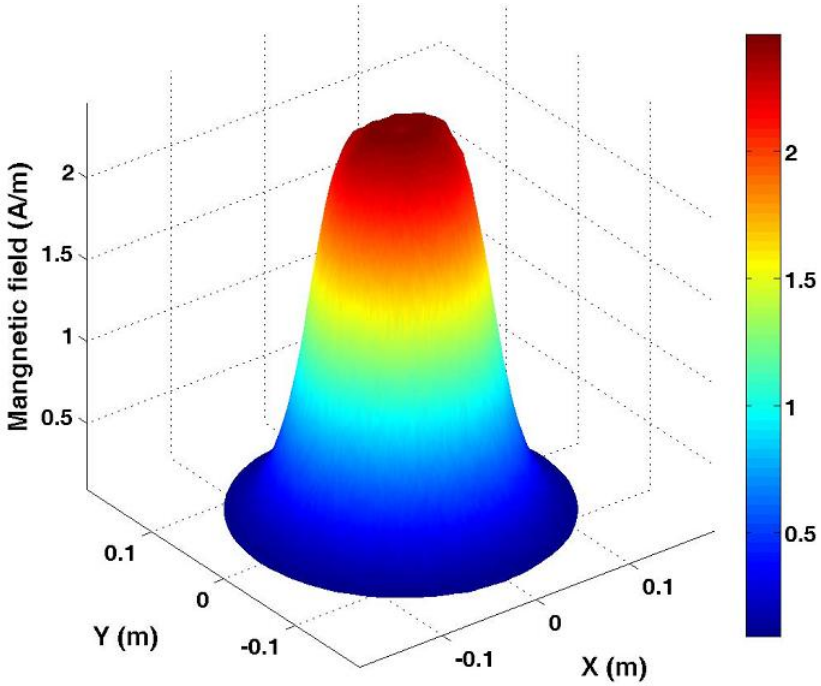

Figure 58 - Magnetic field distribution at z=-0.12m

4.2.5.4 Magnetic field manipulation

The magnetic field manipulation to move the capsule robot is horizontal plane has been modeled in COMSOL. In this model, by changing the current ratio, the maximum point in the maximum magnetic field area is moving which results in the capsule robot moving in horizontal plane. This ratio is the same concept which is used for horizontal open loop controller. This ratio has been shown in Figure 59.

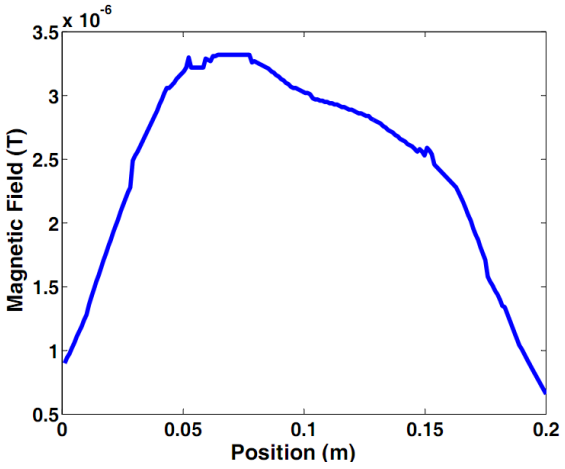
x 10^-6
3.5
3
2.5
2
1.5
1
0.5
Magnetic Field (T)
0
0.05
0.1
0.15
0.2
Position (m)

(a)

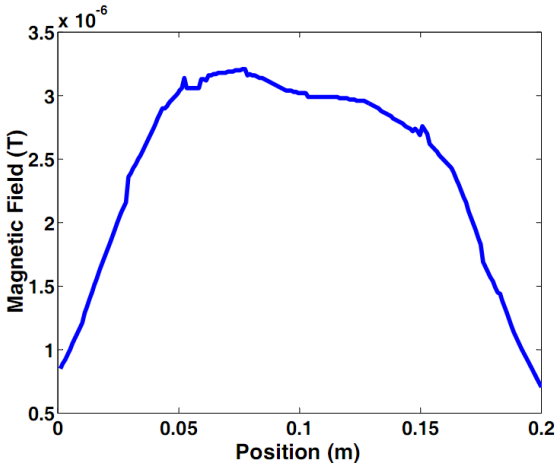
x 10^-6
3.5
3
2.5
2
1.5
1
0.5
Magnetic Field (T)
0
0.05
0.1
0.15
0.2
Position (m)

(b)

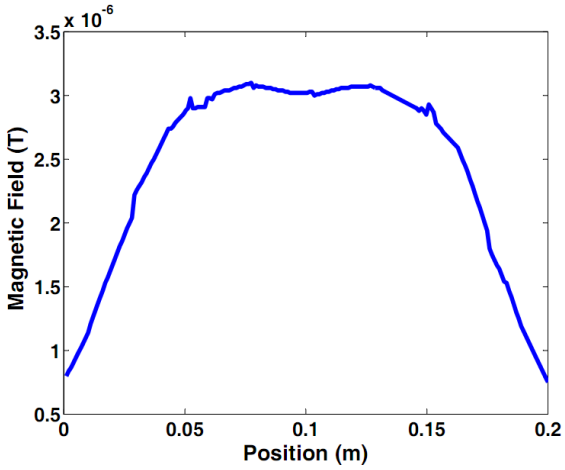
x 10^-6
3.5
3
2.5
2
1.5
1
0.5
Magnetic Field (T)
0
0.05
0.1
0.15
0.2
Position (m)

(c)

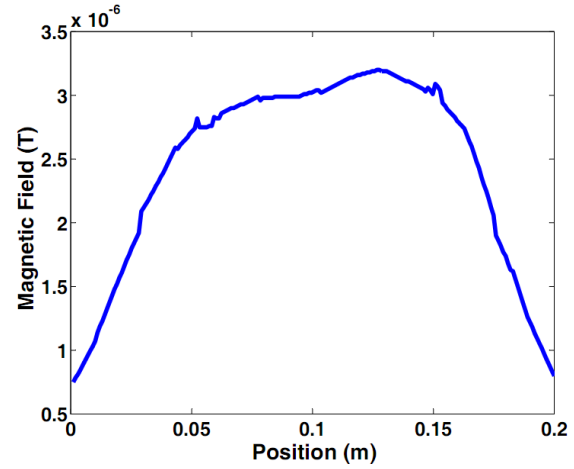

(d)

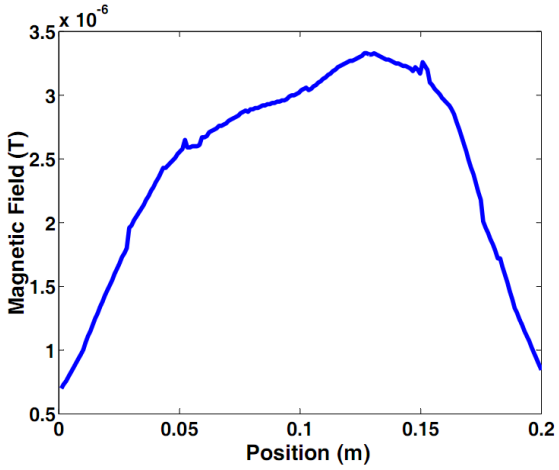

(e)

Figure 59 – Magnetic field manipulation for horizontal motion along *x* direction

As it is shown in Figure 59, magnetic field has been change by different current ratio applied to the electromagnet. Based on the open loop horizontal controller designed, the current ratio has been applied in 5 different steps. In Figure 59- a, maximum magnetic field area is to the right of the centre axis. By changing the ratio, the capsule robot moves close to the centre axis (Figure 59-b). In Figure 59-c, the capsule robot moves to the middle point of the working space and the same ratio of current is applied to move the capsule on the right side of centre axis which is shown in Figure 59-d and Figure 59-e.

4.3 Conclusion

In this Chapter of thesis, electromagnetic system has completely presented. The magnetic control system, consists of 7 electromagnets provide electromagnetic field which manipulate capsule robot in the test bed. This system has been modified to produce the optimized magnetic field for the capsule robot manipulation. The pole piece has been mathematically modeled and the magnetic field is analyzed both with mathematical and numerical methods.

The force field in our system is analytically modeled too. Drag force, magnetic forces and friction force are modeled to design a controller for the system. The electromagnetic force has also been evaluated using numerical method.

Three different control methods have been used for this system. The PID close loop control is used for small horizontal movement. Two open loop controllers are presented for capsule robot manipulation as well. The control equations are derived for the experimental modeling.

At the end of the present chapter, the magnetic manipulation is modeled in COMSOL and the horizontal movement of capsule is numerically explained. The pole piece effect for magnetic field is numerically analyzed to satisfy the analytical analysis of pole piece effect.

Chapter 5

Experimental Results

According to section 4.2.4.4, the PID control system has been implemented for the close loop control manipulation of the capsule robot. For the experiments performed in the present chapter, PID gains are set as

$$K_p = 200$$
$$K_i = 60 \quad \textbf{(5.1)}$$
$$K_d = 0.04$$

The accuracy of lasers used as input for the PID controller is in the range of micrometers. The capsule robot must eventually move inside the esophagus model that is not much larger than the size of the capsule. Therefore, any fluctuation such as smashing of the capsule and inner wall of esophagus thus causing huge errors that makes the controller instable. In order to eliminate this instability, the set of experiments for a close loop controller, are performed in the specific height which the capsule robot would not touch the wall of esophagus. Therefore the capsule robot moves along the axis of the tube at z=-0.0795 which is 0.5mm above the bottom layer of the tube.

5.1 Positive Step Function for *x* coordinate

According to Eq.(4.57), a positive step function has been implemented in the horizontal direction.

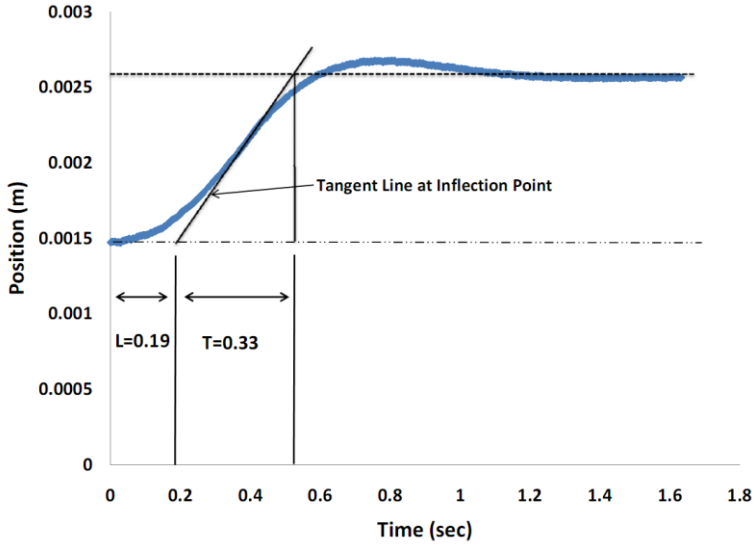

Figure 60 - Step response of the capsule robot for 0.001m step command in the *x* direction

As it is shown in Figure 60 there is no sudden increase in the position of the capsule robot. Elbuken and Shameli (47) have shown that the eddy current effect produced in the aluminum block caused a sudden change in the position of the object. Elbuken (47) has shown that the eddy current effects of the aluminum block are generated in a way to oppose the movements of the levitated object. When a step command is issued, the aluminum block will start to generate a magnetic field to oppose the field change mainly due to the movement of the levitated object (47). However, it has the effect of pole piece had been analytically evaluated in section 4.2.2.It has been proven there that pole piece provide a constant magnetic field for our system. In this way, by changing the current through PID controller, the maximum magnetic field area moves smoothly in the horizontal direction which causes a smooth rising for the capsule robot. The source of eddy current is the magnetic field of the permanent magnet. By moving the capsule robot, the magnetic field inside the aluminum block changes and it produces the current inside the block. The magnetic field produces by electromagnets is very smooth and the frequency of this field is negligible and thus does not have an effect on eddy current.
The existence of a yoke in magnetic drive unit destroys the symmetry of magnetic field produce by electromagnets. This yoke effect can be observed in different horizontal experiments.

5.2 Negative step function for *x* coordinate

The second experiment is the implementation of the negative step response in *x* coordinate system. In this experiment, -0.0015m in the negative direction has been applied to the controller. As it is shown in Figure 61, the time constant in this experiment is more than the positive command. It is supposed to have the same time constant in the x direction based on the symmetry of the electromagnets in magnetic drive unit. The reason is that, in this case, there is the effect of yoke, opposite to the command. Therefore, it takes more time in this case for the controller to stabilize and control the capsule robot. At *t=2.6 s*, the object is settled to the command applied to the system.

The application of the negative and positive motion of the capsule robot in 1 direction is to bombard drug all over the area which is infected. In gastrointestinal diseases, one of the most common diseases is local infection with cells attached to each other like influenza. In this case, localized drug delivery like antibiotic pills is used for patients to deliver the drug in long period of time. With this negative and positive control system, the capsule robot can move back and forth along the infected area and release the drug to this area. In next experiments, it is tried to show both commands are attempted with PID control system.

The negative step response in *x* direction is shown in Figure 61.

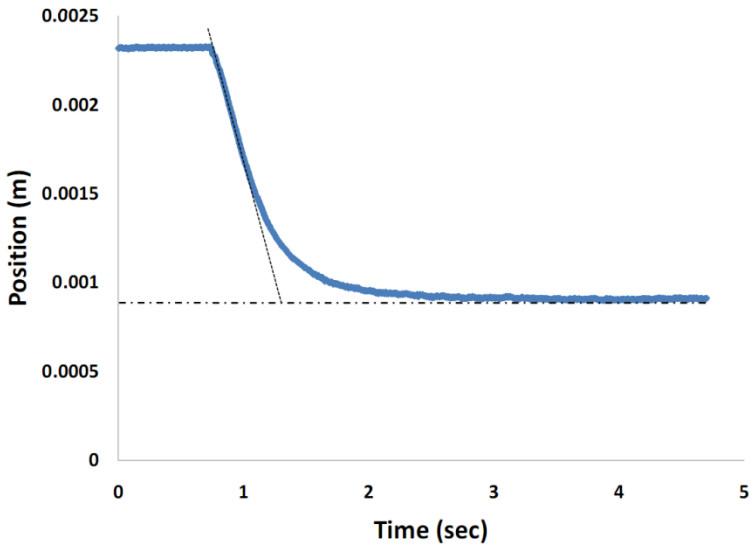

Figure 61 - step response for capsule robot 0.0015m negative command in the x direction

5.3 Step response of two positive command for *x* coordinate

A positive steps command in x coordinate is applied to the capsule robot as well. It is assumed to move the capsule from A to B and hold it on B and move it to C in a short time. The response on these commands is shown in Figure 62.

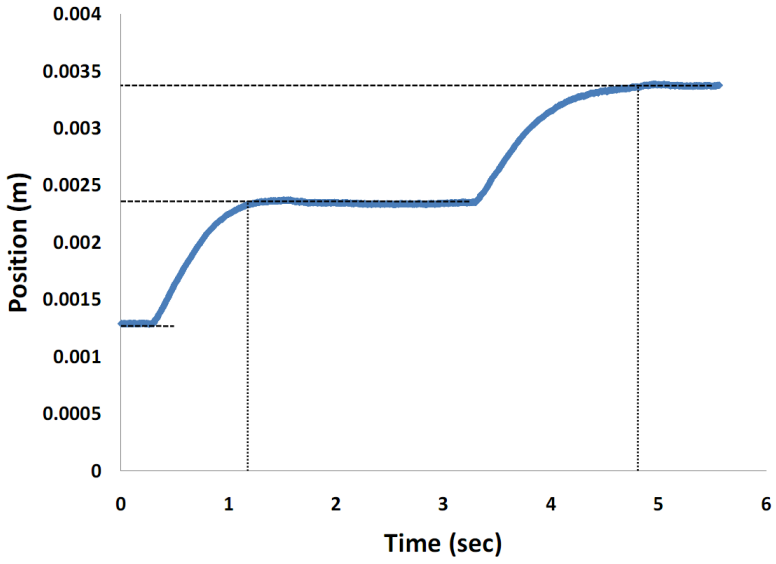

Figure 62 - Step response for two positive commands in *x* direction

The first rise time is 0.9 sec and the second rise time is 1.2 sec. The capsule is stopped at 0.0024m for 2 seconds.

5.4 Step function with positive and negative commands for *x* coordinate

Capsule robot is going to have the ability of multi point drug delivery. This experiment is implemented to move the capsule among three different points. In this experiment, the capsule is going to have a positive command, to the second point from its initial point, and then stopped at its second point for 1 second. After that, the negative position command moves the capsule to the third point. This experiment is set for releasing drug in different desired points.

During the initial second of motion, there is a fluctuation of positioning. This occurs because of the eddy current effect on the aluminum block. The current induced in the block, produces the magnetic field opposite to the motion of the capsule robot. Because of the frequency of the magnetic field fluctuation, the controller could not function properly. This behaviour happened during the negative command as well. The amount of eddy current induction in negative command is less than positive command. This is because of the rate of magnetic field change in negative command.
From 1 - 2.2 s the capsule robot is held at the desired location. During this time the drug is released at the desired point. By keeping the current ratio constant in controller, holding time can be increased up to minutes.

The application of this experiment in biomedical operation is cancer drug delivery. In esophagus cancer, there is the location of cell which requires getting the chemotherapy drug. The capsule robot can move back and forth and release the drug to all the areas of the cancer cells. This up and down steps can be repeated more to release as much of the drug as required for patient. The amount of drug can be controlled as it is mentioned in chapter 3.

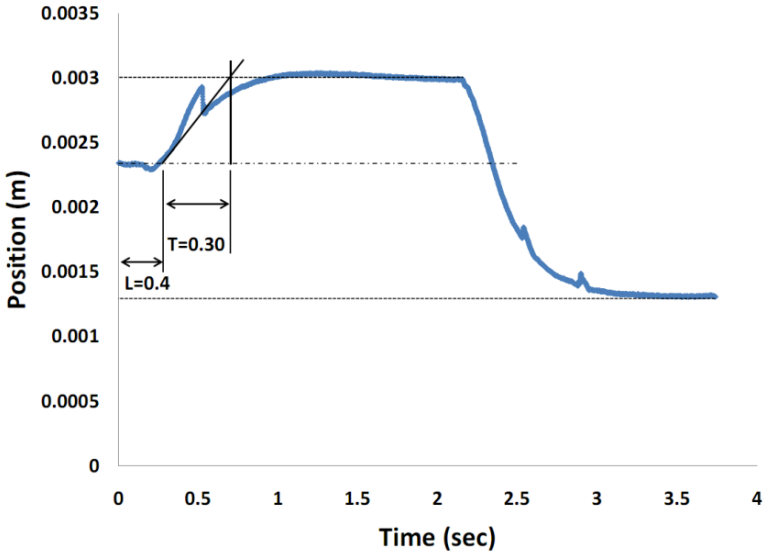

Figure 63 - Step response of the capsule robot for positive and negative commands in *x* direction

5.5 Step response for *y* coordinate

All the data above were referred to *x* direction. The PID controller is set for horizontal coordinates and manipulation in *y* direction need to be done too. The geometry of electromagnets and current manipulation were explained in chapter 4.2.4.3. The positive command of 0.0015m is applied to the capsule robot in *y* direction and the step response is shown in Figure 64.

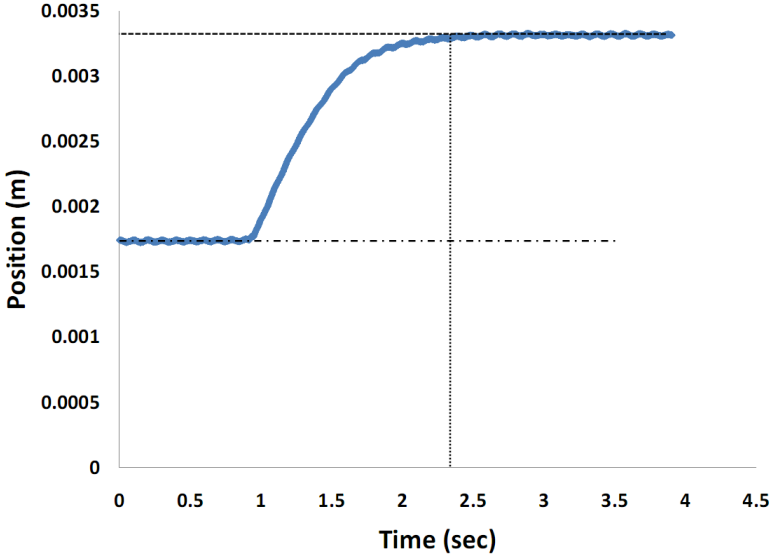

Figure 64 - Step response of the capsule robot for positive command of 0.0015m in *y* direction

According to geometry of the magnetic drive unit and position of yoke in system, the effect of yoke in *y* direction manipulation n is less than *x* direction. It should be mentioned here that the constant time in *y* direction is more than *x* direction. This difference is because of the amount of magnetic field for *y* manipulation which uses fewer coils to move the capsule robot rather than *x* direction. In the next experiment, the other manipulation for *y* direction is expressed.

5.6 Open loop control of capsule robot and drug release in esophagus prototype

The capsule Robot is moved in esophagus by changing the ratio of current in electromagnets. In these experiments, capsule robot is moved 30 mm - 50 mm in esophagus prototype. Our targets in these experiments was to show that the maximum manipulation of the capsule robot.

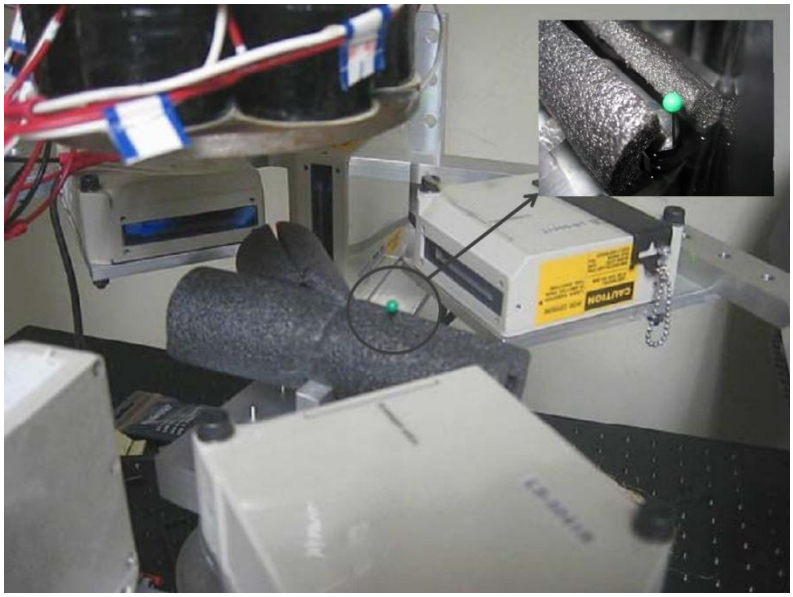

Figure 65 – Capsule robot manipulation in esophagus model

Drug delivery mechanism of capsule robot is completely explained in Chapter 3. This mechanism has been developed experimentally by external magnetic field. With changing the ratio of current distribution the maximum area of magnetic field moves the capsule robot in the esophagus prototype. The four steps of movement is shown in Figure 66.

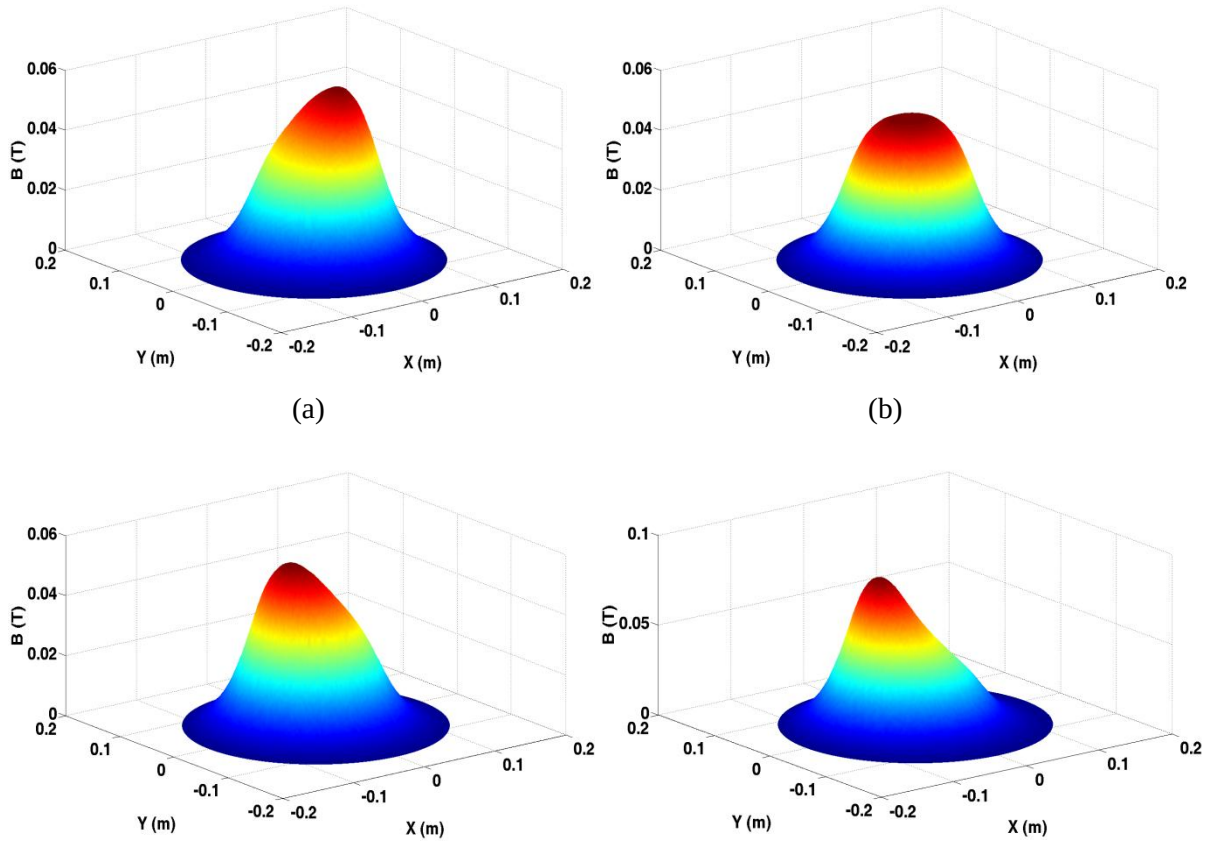

Figure 66 - Magnetic manipulation of capsule robot with current ratio differentiation

In Figure 66-a the maximum area keeps the capsule at the first point which is shown in Figure 67-a. By changing the ratio of current in Figure 66-b, the capsule robot moves to the middle point of the channel (Figure 67-b). Current ratio then rotates the capsule robot to the target channel as it is shown in Figure 66-c and Figure 67-c. The last step is to move the capsule to the target point of drug release and by applying the external force, the capsule robot release the drug at this point (Figure 66-d and Figure 67-d).

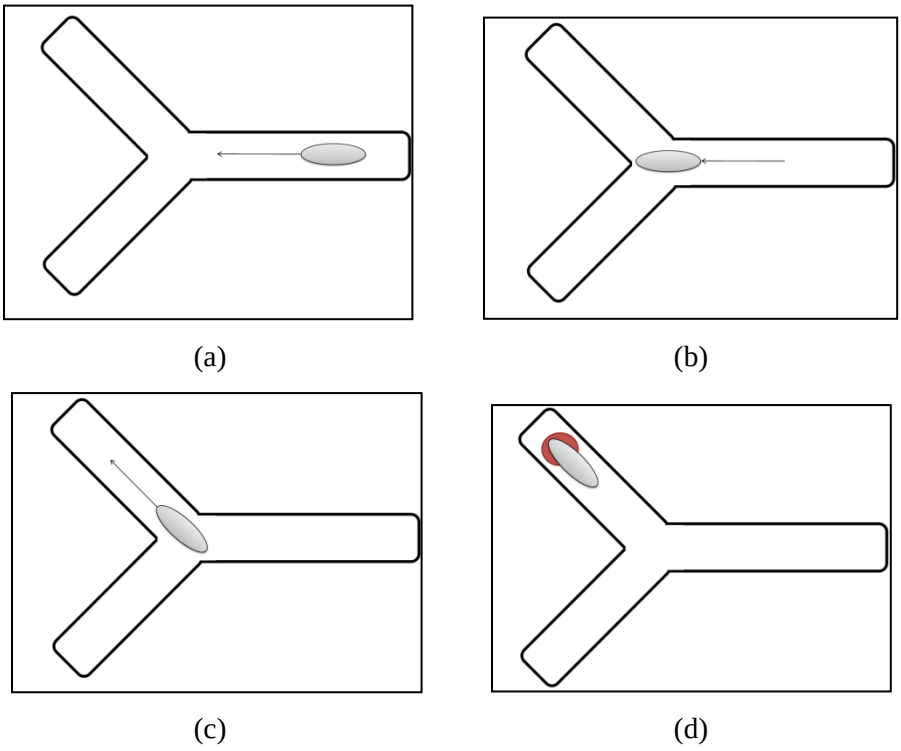

Figure 67 - Capsule robot manipulation diagram

This proof of concept has been experimented and shown in Figure 68.

(a)

(b)

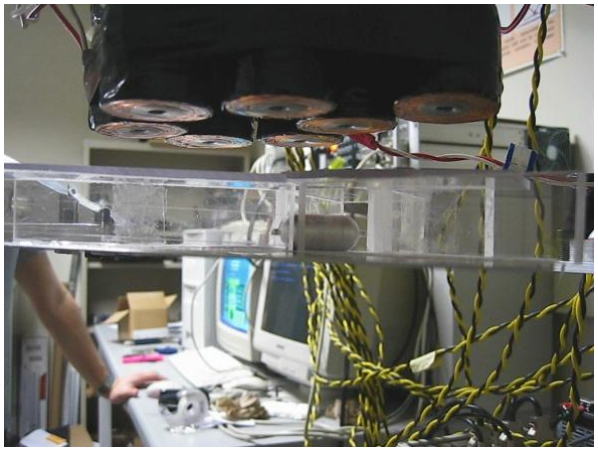

(c)

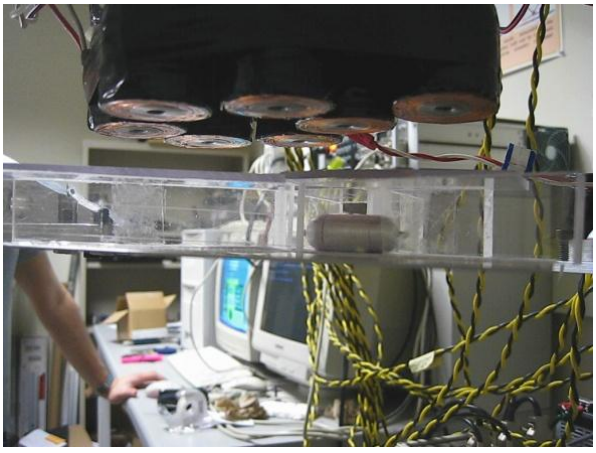

(d)

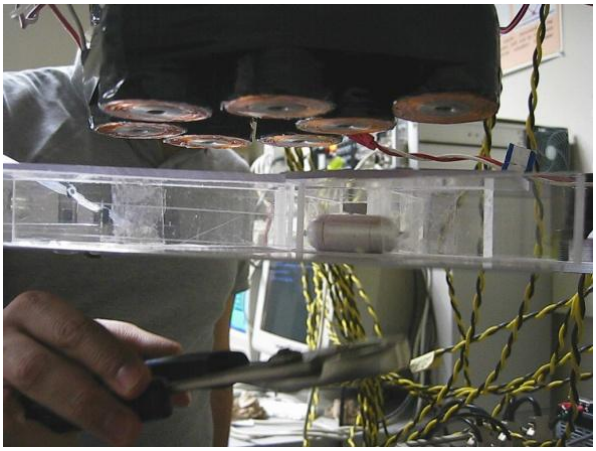

(e)

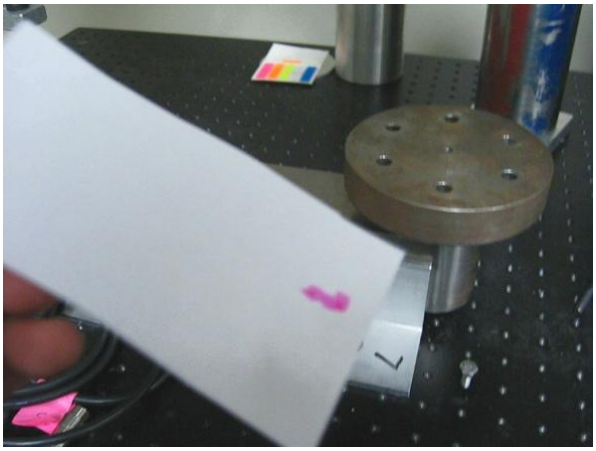

(f)

Figure 68 - Capsule robot manipulation in transparent chamber and drug release

The magnetic field distribution has changed among the coils and controls the capsule to move from the start point (Figure 68-a) and go towards the intersection of two channels (Figure 68-b) in 0.8 sec. Then, the capsule-robot stays at the intersection for 0.6 s (Figure 68-c) and chooses its channel to go. The capsule-robot actively rotates on its location to the selected channel (Figure 68-d) and moves to the specific point set on the second channel. At this step, the drug is going to be released wirelessly. An external magnetic field is applied from the bottom of test bed with an external permanent magnet (Figure 68-e) and after 3 seconds, 0.4mL of drug is released at the specific spot of the paper we put on the test bed (Figure 68-f).

Chapter 6

Conclusion and Recommendations

6.1 Conclusion

This thesis covers a wide range of electromagnetic topics and biomedical application of electromagnetic manipulation system. Biomechanics of the gastrointestinal tract has been presented which led to the design of the human esophagus test bed. The previous capsule robots were completely investigated. The conceptual designs were presented and all of them narrowed to the final design of capsule robot with micro actuator for drug delivery. The target of long term and localized drug delivery are always considered and the drug reservoir with the micro plunger satisfied this target.

The most challenging part of this project was wireless control system. The magnetic levitation setup in MagLev lab at the University of Waterloo was used to control the capsule wirelessly. In this method, electromagnetic field produced by the set of 7 and 14 electromagnets controlled the capsule robot based on the built-in permanent magnet contained inside. Different current ratios in electromagnets moved the capsule robot in the horizontal plane.

The close loop controller was a PID controller with position commands from the capsule robot. These positions were recorded by three sets of lasers and the position feedback produced the error function. The PID controller is coded in Labview and used for 10 mm movement of capsule robot in horizontal plane. For larger displacement of capsule robot, two open loop controllers are presented too. The result of these controllers was to move the capsule robot wirelessly in single and multi channel test beds.

The target of designing the capsule robot is a drug delivery system.. Local wireless drug delivery has been developed for the first time in this project. The mechanism is magnetic-mechanical mechanism. The plunger was designed with a hole which could be opened and closed by external electromagnetic field. The drug chamber was filled with the colored liquid and it is released at desired location of the test bed. This prototype is proven as an active capsule robot for drug delivery within the human body.

6.2 Recommendations

According to the results obtained in this project and thesis, future research can be done on this topic. These potentials are listed here.

1. The test bed presented in Chapter 2 can be studied more and better material or animal tissue can be used for the experiment.
2. The capsule robot can be fully fabricated in the machine shop, including the drug release mechanism.. Micro machining methods are recommended to fabricate this prototype in smaller dimensions and with less weight. In this way, controllability of the operation will be increased too.
3. The magnetic Drive Unit system can be modified based on different applications. If the capsule robot is going to be used for drug delivery inside the human gastrointestinal tract, a moving set of coils can be replaced by fixed setup.
4. According to magnetic field analysis on live human tissue, this experiment can be done on real test bed such as an animal's body. In this way the concept of wireless drug delivery can be proven and commercialized for the next generation of biomedical applications.

Appendix A
Dynamic of double SMA system

Capsule robot with SMA actuator and micro needle as a motion part has four steps of movement. These four steps of movement are explained as followed:

Step 1:

This step of movement is presented in Figure 23. It is assumed that the capsule robot is going to move right. There is no voltage applies to alloys in this step.

Step 2:

In this step by increasing the temperature in the right SMA, the stiffness of SMA changes, it tenses and returns to its normal length. The left SMA is not actuated so it moves based on the right SMA. The clamping system is not working in this step and moves with right SMA. There is not movement for capsule robot in this step.

Step 3:

In step 3 clamping system actuates. The right SMA is not actuating anymore and the left SMA moves the capsule to the right side. Micro needles attached to clamping system help the capsule robot to use the GI tissue as support of clamping system. There is no pain senses with patient because of the small diameter of micro needle.

Step 4:

In this step the left SMA actuates, the capsule robot moves forward a bit more and completes the cycle of movement. The capsule robot is ready for another cycle of movement after this step. As more SMA as connected parallel, the more force will produce.

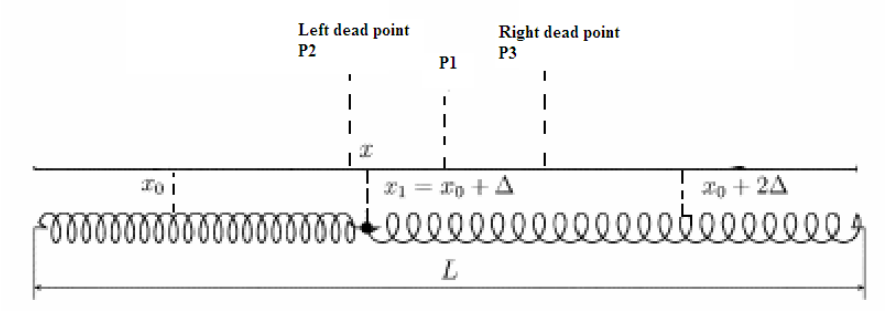

Figure 69 - 3 equilibrium points of SMA system

Double SMA system consist of two similar SMA connected to each other at one point. (Series connection)

In order two model the mathematic behavior of SMA system, equilibrium points are expressed as below:

Equilibrium point x_1

Each SMA in non-load situation and room temperature has the initial length of x_0. If the temperature of two SMA increases as Δ to connect to each other at point x_1, each spring has the length of $x_0 + \Delta$ and the total length would be $L = 2(x_0 + \Delta)$. Since the length change of both SMA and the properties are the same, the force applies from one to the other would be the same too. Therefore, x_1 is called the equilibrium point 1 of the system. This point is presented in Figure 69.

Equilibrium point x_2

The right SMA is actuated (temperature increase) and the left one is not actuated (in room temperature). In this case, the clamping point of both SMA moves left (x_2).

So double force can be written as

$$F_R^h(x) = K_h(x_0 + 2\Delta - x) \quad \textbf{(6.1)}$$

$$F_L^c(x) = K_c(x - x_0) \quad \textbf{(6.2)}$$

Equilibrium point x_3

The left SMA is actuated (temperature increase) and the right one is not actuated (in room temperature). In this case, the clamping point of both SMA moves right (x_3).

So double force can be written as

$$F_L^h(x) = K_h(x - x_0) \quad \textbf{(6.3)}$$

$$F_L^h(x) = K_h(x - x_0) \quad \textbf{(6.4)}$$

$$F_R^c(x) = K_c(x_0 + 2\Delta - x) \quad \textbf{(6.5)}$$

According to equilibrium points, it can be written for forces as:

$$F_L^h(x_2) = F_R^c(x_2) \quad \textbf{(6.6)}$$

And

$$F_R^h(x_3) = F_L^c(x_3) \tag{6.7}$$

Therefore, for SMA at equilibrium points, displacements can be developed as

$$x_2 = \frac{K_c(x_0 + 2\Delta) + K_h x_0}{K_h + K_c} = x_0 + \frac{2K_c\Delta}{K_h + K_c} \tag{6.8}$$

$$x_3 = \frac{K_h(x_0 + 2\Delta) + K_c x_0}{K_h + K_c} = x_0 + \frac{2K_h\Delta}{K_h + K_c} \tag{6.9}$$

Therefore elongation for SMA would be

$$\delta_{\max} = \varepsilon_{\max} x_0 = x_3 - x_0 = \frac{2K_h\Delta}{K_h + K_c} \tag{6.10}$$

And the force need to be applied is

$$f = \frac{Gd^4\delta}{8D^3N} = K\delta \tag{6.11}$$

That N is the number of turns, G is shear modulus and D is diameter of each turn in SMA. This is the force need to apply to SMA for actuating between equilibrium points. This force can be applied either by thermal difference or magnetic field produced by electromagnets. If the permanent magnet located at the connection point SMA, magnetic field can move the magnet and though move the capsule robot.

Appendix B

Magnetized cylinder in an external field

Magnetized cylinder in an external magnetic field is studied to evaluate the change of magnetic field around it. To model the pole piece of our system, and as an example of the phenomenon of magnetic shielding we started with a spherical shell of inner radius *a,* made of material of permeability μ , and placed in a formerly uniform constant magnetic induction B_0 , as shown in Figure 70. **B** and **H** is going to be found everywhere in space, but most particularly in cavity (r<*a*), as function of μ . Since there are no currents present, the magnetic field **H** is drivable from scalar potential

$$H = -\nabla \phi_M \tag{6.12}$$

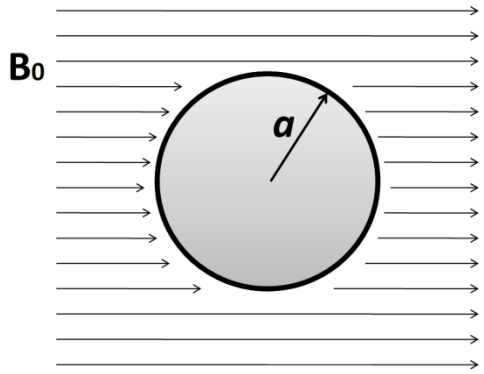

Figure 70 - pole piece sample in magnetic field

It should be mentioned here that, if the current density vanishes in some finite region of space, the Maxwell equation of magnetic field and current density in Eq.(6.13), becomes zero.

$$\nabla \times H = J \tag{6.13}$$

This implies that we can introduce a magnetic scalar potential such that it is presented in Eq. (6.12). With an explicit constitutive relation, this time of B=B [H], the $\nabla . B = 0$ it can be written as

$$\nabla . B[-\mu \nabla \phi_M] = 0 \tag{6.14}$$

Since μ is at least piecewise constant, in each region the magnetic scalar potential satisfies the Laplace equation,

$$\nabla^2 \phi_M = 0 \tag{6.15}$$

Furthermore, since $B = \mu H$, the divergence equation $\nabla.B = 0$ becomes $\nabla.H = 0$ everywhere. The problem reduces to finding the proper solutions in the different regions to satisfy the boundary conditions at *r*=*a*.

To evaluate the potential ϕ_M from Maxwell equation $\nabla.B = 0$ it can be written as

$$\nabla.B = \nabla.(H + 4\pi M) = 0 \qquad \textbf{(6.16)}$$

Then with Eq.**(6.12)**, it becomes magneto static Poisson equation,

$$\nabla^2 \phi_M = -4\pi\rho_M \qquad \textbf{(6.17)}$$

With the effective magnetic charge density,

$$\rho_M = -\nabla.M \qquad \textbf{(6.18)}$$

The solution for the potential ϕ_M if there are no boundary surfaces is

$$\phi_M(x) = -\int \frac{\nabla'.M(x')}{|x - x'|} d^3x' \qquad \textbf{(6.19)}$$

If **M** is well-behaved and localized integration by parts may be performed to yield

$$\phi_M(x) = \int M(x').\nabla'(\frac{1}{|x - x'|}) d^3x' \qquad \textbf{(6.20)}$$

Then

$$\nabla'(\frac{1}{|x - x'|}) = -\nabla(\frac{1}{|x - x'|}) \qquad \textbf{(6.21)}$$

Therefore

$$\phi_M(x) = -\nabla.\int \frac{M(x')}{|x - x'|} d^3x' \qquad \textbf{(6.22)}$$

The simplest way of solution is that of the section shown in Figure 70, via the magnetic scalar potential in cylindrical coordinates and a surface magnetic charge density $\sigma_M(\theta)$. With $M = M_0\varepsilon$ and $\sigma_M = n.M = M_0 \cos\theta$, the solution for the potential in Eq.(6.19) is

$$\phi_M(r,\theta) = M_0 a^2 \int d\Omega' \frac{\cos\theta'}{|x - x'|} \qquad \textbf{(6.23)}$$

An important expansion is that of the potential at **x** due to a unit point charge at x' **:**

$$\frac{1}{|x-x'|}=\sum_{l=0}^{\infty}\frac{r_<^l}{r_>^{l+1}}P_l(\cos\gamma) \tag{6.24}$$

Where $r_<(r_>)$ is the smaller (larger) of $|x|$ and $|x'|$, and γ is the angle between x and x'.

Therefore, Eq. **(6.23)** can be written as

$$\phi_M(r,\theta)=\frac{4\pi}{3}M_0a^2\frac{r_<}{r_>^2}\cos\theta \tag{6.25}$$

And $r_<(r_>)$ are the smaller and larger of (r, a). Inside the cylinder, $r_<=r$ and $r_>=a$. Then

$$\phi_M=(\frac{4\pi}{3})M_0r\cos\theta=(\frac{4\pi}{3})M_0z \tag{6.26}$$

The magnetic field and magnetic induction inside the cylinder are therefore

$$\begin{aligned}H_{in}&=-\frac{4\pi}{3}M\\ B_{in}&=\frac{8\pi}{3}M\end{aligned} \tag{6.27}$$

For $r>a$, the potential must be of the form,

$$\phi_M=-B_0r\cos\theta+\sum_{l=0}^{\infty}\frac{\alpha_1}{r^{l+1}}P_1(\cos\theta) \tag{6.28}$$

And B_0 is the magnetic produced from a long distance source.

In Magnetic Drive Unit, pole piece plays the role of distributing the magnetic field in suitable form for our system. We are dealing with the system which consists of three media with different physical properties. The first media is the coil and wires, the second one are the pole piece and the third one is air. We are studying the conditions that **B** and **H** vectors must satisfy at the interfaces of different media. To derive the magneto static boundary condition for our system, fundamental governing Maxwell equations are applied to a small box and a small closed bath include the interface. The first equation is

$$\nabla.B=0 \tag{6.29}$$

It can be concluded directly that the normal component of **B** is continuous across an interface,

$$B_{1n}=B_{2n} \tag{6.30}$$

It can be inferred for vector **H** that

$$B_1 = \mu_1 H_1$$
$$B_2 = \mu_2 H_2 \qquad \textbf{(6.31)}$$

Therefore

$$\mu_1 H_{1n} = \mu_2 H_{2n} \qquad \textbf{(6.32)}$$

The second Maxwell equation which talks about **H** is

$$\nabla \times H = J \qquad \textbf{(6.33)}$$

The surface integral of both side of Eq. is

$$\int_s (\nabla \times H).ds = \int_S J.ds \qquad \textbf{(6.34)}$$

According to Stoke's theorem it can be written as

$$\oint_C H.dl = I \qquad \textbf{(6.35)}$$

C is the closed path that including the surface of ***S*** and the current ***I*** the amount of free current passing through ***S***. The closed path *abcda* shown in supposed as the contour of ***C***. applying Eq. gives

$$\oint_{abcda} H.dl = H_{1t}.\Delta w + H_{1n}.\Delta h + H_{2t}.(-\Delta w) + H_{2n}.(-\Delta h) = J_{sn}\Delta w \qquad \textbf{(6.36)}$$

And in this case, J_{sn} is the surface current density on the interface normal to the contour ***C***. letting *bc=da* approach zero, Eq. can be written as

$$\oint_{abcda} H.dl = H_{1t}.\Delta w + H_{2t}.(-\Delta w) = J_{sn}\Delta w \qquad \textbf{(6.37)}$$

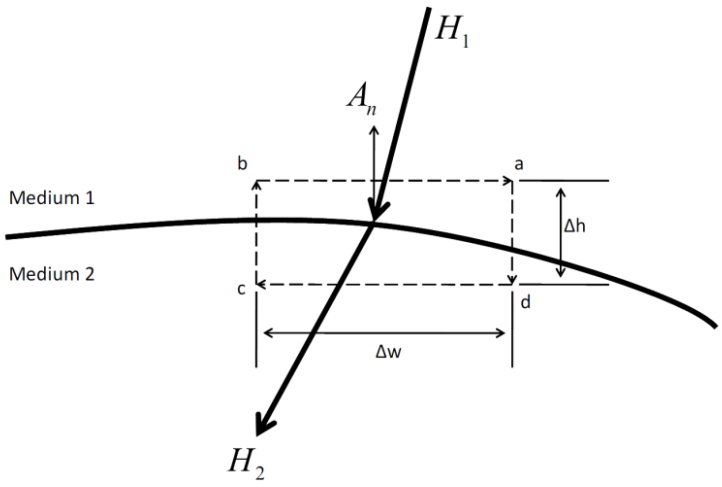

Figure 71 - Closed path about the interface of two media for boundary condition

Considering A_n as the outward unit normal at the interface, Eq. can be written as

$$H_{1t} - H_{2t} = J_{sn} \tag{6.38}$$

Or

$$A_n \times (H_1 - H_2) = J_S \tag{6.39}$$

Thus, the tangential component of ***H*** when it passes through two different media is discontinuous across an interface if the surface current exists. For the magnetic control system this boundary conditions have been explained.

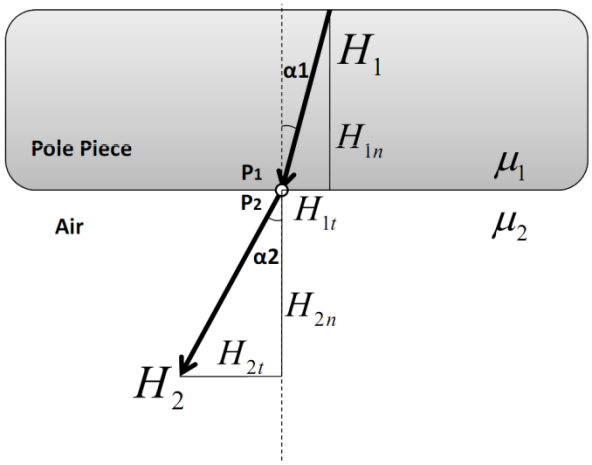

Figure 72 - Boundary conditions for pole piece

Two different media in this case are the pole piece and the working space (air) that we are working in. The magnetic field intensity in the pole piece at point P_1 has a magnitude of H_1 with the angle of α_1 with the normal axis of the section view shown in . The goal is to determine the magnetic field intensity in second media (air) at point to regarding its angle and magnitude. To solve this problem, the continuity of the normal component of ***B*** is required. It can be presented as

$$B_{1n} = B_{2n} \Rightarrow \mu_2 H_2 \cos\alpha_2 = \mu_1 H_1 \cos\alpha_1 \quad \textbf{(6.29)}$$

Since there is no surface current in either media the tangential component of ***H*** is continuous too. Therefore,

$$H_2 \sin\alpha_2 = H_1 \sin\alpha_1 \quad \textbf{(6.40)}$$

By dividing Eq. and, the angle can be represented as

$$\frac{\tan\alpha_2}{\tan\alpha_1} = \frac{\mu_2}{\mu_1} \quad \textbf{(6.41)}$$

Or

$$\alpha_2 = \tan^{-1}\left(\frac{\mu_2}{\mu_1}\tan\alpha_1\right) \quad \textbf{(6.42)}$$

Therefore, magnetic flux intensity can be developed as

$$H_2 = \sqrt{H_{2t}^2 + H_{2n}^2} = \sqrt{(H_2\sin\alpha_2)^2 + (H_2\cos\alpha_2)^2} \quad \textbf{(6.43)}$$

And

$$H_2 = H_1[\sin^2\alpha_1 + (\frac{\mu_1}{\mu_2}\cos\alpha_1)^2]^{1/2} \quad \textbf{(6.44)}$$

Since the one medium in our system is nonmagnetic (air) and the other medium ferromagnetic (iron), then $\mu_2 \gg \mu_1$, and α_2 will be nearly 90°. It somehow says that for any angle of α_1 that is not close to zero; the magnetic field in a ferromagnetic medium (iron) will be parallel to the interface. On the other hand, if $\mu_1 \gg \mu_2$, and then α_2 will be close to zero. The first case happens when the magnetic field produces in coils and passes through the pole piece and the second case happens when the magnetic streamlines pass from the interface of the pole piece to the working space (air). According to the thickness of the pole piece, the magnetic field somehow moves from the middle of the pole piece to the farther radii of the working space. As we know, the locus of the maximum magnetic field produces by coils is located on the axis of the coil. What happens here is that, pole piece makes the

maximum point of magnetic field to the maximum area of magnetic field by the movement of the field distribution.

According to constant thickness of pole piece, the deflection of magnetic streamlines produces a weak magnetic field in outer diameters of pole piece. Therefore the magnetic field in outer diameters of the working space will get damped too. There is a different shape of thickness required for pole piece geometry to keep the field strong enough in outer diameter as well. There is two points required for pole piece analysis:

1- Constant magnetic field area in the middle of the working space.

2- Strong enough magnetic field in outer diameters of working space.

As it is mentioned before, the target of pole piece in magnetic control system is to modify magnetic field and change the maximum point of magnetic field to maximum area of magnetic field. This optimized pole piece is indented to be tested as future work on improving the magnetic controllability.

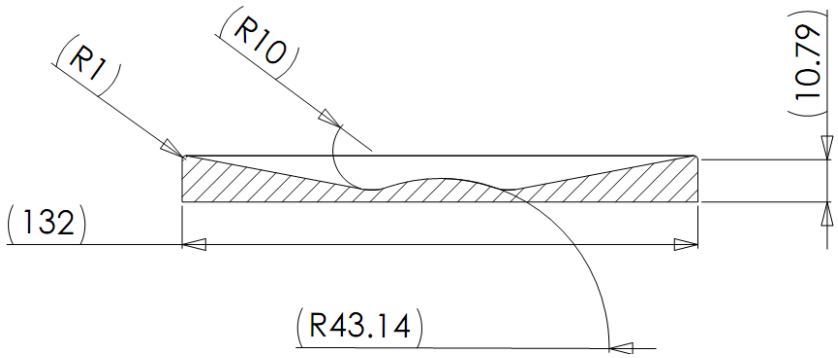

Figure 73 - Cross section of optimized pole piece

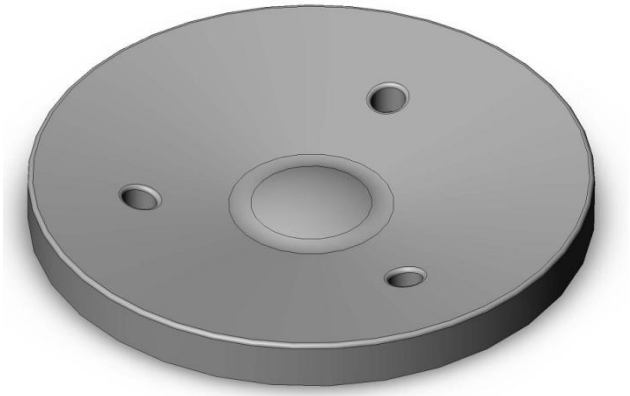

Figure 74 - 3D view of optimized pole piece

References

1. ADAM Lung Needle Biopsy. Retrieved May 18, 2008, from www.averaqueenofpeace.org/aqop/services/Heart/index.aspx. 2008.

2. Gregersen, Hans. Biomechanics of the Gastrointestinal Tract. Aalborg : Springer, Department of Surgical Gastroenterology, Aalborh Hospital, Aalborg University, 2002. 1852335203.

3. Schwarz, Y., Greif, J., Becker, H., Ernst, A., and Mehta, A.Real-Time Electromagnetic navigation Bronchoscopy to Peripheral Lung Lessions Using Overlaid CT Images. ARCHIVOS DE BRONCONEUMOLOGÍA Journal, Volume 43, Issue 8, 2007, Pages 460-463.

4. Schwarz, Y., Mehta, A., Ernst, A., Herth, F., Engel, A, Besser, D., Becker, H.Electromagnetic navigation during Flexible Bronchoscopy. Am J Respir Crit Care Med. 2006 November 1; Published online 2006 July 27.

5. Johns, C.Bronchosocpy. Retrieved May 18, 2008, from www.myoptumhealth.com/portal/ADAM/item/Bronchoscopy, 2008.

6. Sheilds, T., loCicero, J., Ponn, R., and Rusch, V. General thoracic surgery. p. 235. 2004.

7. Moglia A, Menciassi A, Schurr MO, Dario P Wireless capsule endoscopy from diagnostic devices to multipurpose robotic systems., Journal: BIOMEDICAL MICRODEVICES, Publisher: Springer Netherlands ISSN, Issue Volume 9, Number 2 , April, 2007 Pages 235-243.

8. Yoav C Metzger, Samuel N Adler, Ariella Bar-Gil Shitrit, Binyamin Koslowsky, Ingvar Bjarnason

Comparison of a new PillCam™ SB2 video capsule versus the standard PillCam™ SB for detection of small bowel disease Published Date February 2009 , Volume 2009:2. Journal: REPORTS IN MEDICAL IMAGING

9. Aman Ali, MD, Janice M, Santisi, RN, John Vargo, MD, MPH , Video capsule endoscopy: A voyage beyond the end of the scope.. s.l. : CLEVELAND CLINIC JOURNAL OF MEDICINE VOLUME 71, Number 5, May 2004.

10. M., Pennazio.Capsule endoscopy: where are we after 6 years of clinical use?

Gastroenterology Unit 2, Department of Gastroenterology and Clinical Nutrition, S. Giovanni A.S. Hospital, Via Cavour 31, 10123 Turin, Italy

Received 4 September 2006; accepted 5 September 2006. Available online 11 October 2006.

11. Appleyard M, Fireman Z, Glukhovsky A, et al randomized trial comparing wireless capsule endoscopy with push enteroscopy for the detection of small-bowel lesions. Department of Gastroenterology, Renji Hospital, Shanghai Institute of Digestive Disease, Shanghai Second

Medical University, Shanghai 200001, China, CHINESE MEDICAL JOURNAL, 2004, Vol. 117 No. 7 2004.

12. Zuckerman G et. AGA technical review on the evaluation and management of occult and obscure gastrointestinal bleeding, Gastroenterology, *Volume 118, Issue 1, Pages 201-221 G.Zuckerman, C.Prakash, M.Askin, B.Lewis 2000.*

13. S., Lahoti.The small bowel as a source of gastrointestinal blood loss. Journal:CURRENT GASTROENTEROLOGY REPORTS, Publisher Current Medicine Group LLC, ISSN1522-8037 (Print) 1534-312X (Online),Issue Volume 1, Number 5 / October, 1999, DOI10.1007/11894-999-0025-3

Pages 424-430, SpringerLink Date:Wednesday, May 23, 2007 . 1999.

14. Lewis B, Swain P.Capsule endoscopy in the evaluation of patients with suspected small intestinal bleeding, a blinded analysis: the results of the first clinical trial. . 2001.

15. Andrea Moglia, Arianna Menciassi and Paolo Dario. Recent Patents on Wireless Capsule Endoscopy. Pisa, Italy : Center for Applied Research in Micro Engineering (CRIM Lab), Scuola Superiore, November 21, 2007 .

16. http://www.olympus-europa.com/endoscopy/2001_5491.html. . Endocapsule, Olympus. 2005.

17. Kuth, R., Reinschke, J., Roeckelein. R.: DE102005032370 . 2007.

18. Nakamura, T., Yoshizawa, F., Matsumoto, K., Shimizu, http://www.bentham.org/biomeng/samples/biomeng1-1/Moglia.pdf, US2007065407.. 2007.

19. Topolsky, J. s.l.Mini-robot Swims through Bloodsream. . : www.endadget.com/2007/06/27/mini-robot-swims-through-bloodstream/, 2007.

20. Chung, E., Karagozler, M, Park, S., Kim, B., and Sitti, M. A new endoscopic microcapsule robot using beetle inspired microfibrillar adhesives. Proc. IEEE/ASME Int. Conf. Advanced Intelligent Mechatronics.Online available at http://ieeexplore.ieee.org/stamp/stamp.jsp?arnumber=01639068, 2005.

21. Meniassi, A. Gorini, S., Moglin, A., Pernorio, G., Stefanini, C., and Dario. s.l.Clamping tools of a capsule for monitoring the gastrointestinal tract probem analysis and preliminary technological activity. Proceedings of the 2005 IEEE, International Conference on Robotics and Automation

Barcelona, Spain, Online available at, http://ieeexplore.ieee.org/stamp/stamp.jsp?arnumber=01570296

22. Guo S., Pan Q., and Khamesee MB.,. s.l. : "Development of a novel type of microrobot for biomedical application"., JOURNAL OF MICROSYSTEM TECHNOLOGIES, Publisher

Springer Berlin / Heidelberg, ISSN 0946-7076 (Print) 1432-1858 (Online), Issue Volume 14, Number 3 / March, 2008, Category Technical Paper, DOI 10.1007/s00542-007-0430-1, Pages 307-314, Subject Collection Engineering, SpringerLink Date Monday, September 17, 2007 , 2008, Vols. 14, Number 3, .

23. Shingo, S., Masafumi, M., Yorinobu, M., Shigeki, T., and Yasuhiro, K. s.l. Development of micro robot used in wireless liquid. : Mekatoronikusu Koenkai Koen Ronbunshu, Affiliation: Department of Chemical Engineering, Ben-Gurion University of the Negev, Israel. DOI:10.1080/00150190490508927 Published in: Ferroelectrics, Volume 308, Issue 1 2004 , pages 193 - 304 Subjects: Chemical Physics; Materials Science;2006.

24. Cole, E. s.l. Fantastic Voyage. : www.wired.com/medtech/health/news/2007/01/72448., 2009.

25. Menciassi, A., Gorini, S., Moglia, A., Pernorio, G., Stefanini, C., and Dario.Deign, fabrication, and performances of a biomimic robotic earthworm. IEEE Int. Conf. on Robotics and Biomimetics. pp. 274-8, 2007 online available at http://www.iop.org/EJ/article/0967-3334/28/3/N01/pm7_3_n01.pdf?request-id=6ac2974e-e011-49ac-8ac3-73f09955e1fa.

26. Kim, B., Lee, S., and Park, J. s.l.Design and fabrication of a locomotive mechanism for capsule type endoscopes using shape memory alloys. IEEE/ASME Trans. Mechatron 10. pp. 77-86. , 2005 online available at http://ieeexplore.ieee.org/stamp/stamp.jsp?arnumber=01395870.

27. Bergh, J. s.l. Is pharmacokinetically guided chemotherapy dosage a better way forward? : Annals of Oncology 13, 2002 online available at http://annonc.oxfordjournals.org/cgi/content/full/13/3/343.

28. Bruinewoud, H. s.l Ultrasound-Induced Drug Release from Polymer Matrices [Online].. : Retrieved from http://alexandria.tue.nl/extra2/200513447.pdf, 2005.

29. Ishihara, K., Furukawa, T. s.l.Intelligent microrobot dds (drug delivery system) measured and controlled by ultrasonics. Ieee/rsj international workshop on intelligent robots and systems lros. : Osaka, Japan. IEEE cat., 1991 online available at http://pre.aps.org/pdf/PRE/v50/i2/p1629_1.

30. Yamazaki, A., Sendoh, M., Ishiyama, K., Ara, K., Kato, R., Nakano, M., and Fulunag, H. s.l.Wireless micro swimming machine with magnetic thin film. JOURNAL OF MAGNETISM AND MAGNETIC MATERIALS., 2004.

31. Marin, A., Muniruzzaman, M., and Rapoport, N. s.l. : Acoustic activation of drug delivery from polymeric micelles: effect of pulsed ultrasound. JOURNAL OF CONTROLLED RELEASE 71. pp. 239–249., 2001.

32. Edelman, E., Fiorino, A., Grodzinsky, A., and Langer, R. s.l.Mechanical deformation of polymer matrix controlled release devices modulates drug release. JOURNAL OF BIOMEDICAL MATERIALS Research Part A, Volume 35 Issue 4, Pages 433 - 441 Published Online: 6 Dec 1998 1619-1631., 1991.

33. Rapoport, N., Pitt, W., Sun, H., and Nelson, J. s.l. Drug delivery in polymeric micelles: from in vitro to in vivo. JOURNAL OF CONTROLLED RELEASE 91. pp. 85–95., 2002.

34. Santini, J., Richards, A., Scheidt, R., Cima, M., Langer, R. s.l. Microchips as controlled drug-delivery devices.: Angew. Chem.. Int. Ed 39. pp. 2396-2407. 2000.available online at http://informahealthcare.com/doi/pdf/10.1517/17425247.3.3.379

35. Li, Y., Shawgo, R., Tyler, B., Henderson, P., Vogel, J., Rosenberg, A., Storm, P., Langer, R., Brem, H., Cima, M. s.l. In vivo release from a drug delivery MEMS device.: JOURNAL OF CONTROLLED RELEASE 100. pp. 211-219., 2004.

36. zhang, M., Tarn, T., and Xi, N. s.l. : Intelligent drug delivery system using UML diagrams analysis, JOURNAL OF SHANGHAI JIAOTONG UNIVERSITY (Science), ISSN 1007-1172 (Print) 1995-8188 (Online), Issue Volume 13, Number 3 / June, 2008, DOI 10.1007/12204-008-0312-4, Pages 312-317, Subject Collection Engineering, SpringerLink Date Thursday, July 24, 2008

37. Shameli S.E., Craig D.G., and Khamesee M.B.,. s.l. : Design and implementation of a magnetically suspended microrobotic pick-and-place system. ", JOURNAL OF APPLIED PHYSICS 99, 08P509, 2006.

38. A Passive tag, www.technovelgy.com/ct/Technology-Article.asp?ArtNum=47. s.l. : Technology.com, 2008.

39. Margery Conner, Nice Engineering Demo of Wireless Power Transmission. http://www.edn.com/article/CA6455599.html?text=wireless+power+transmission, 2007.

40. Soljacic, M. Cutting the Cord. Engineering & Technology. 2007, INTERNATIONAL JOURNAL OF CLOTHING SCIENCE ANDTECHNOLOGY, ISSN 0955-6222, Volume 20, Number 6, 2008 Power Source, Vols. Vol 2. issue 6. pp. 30-33.available online at http://www.emeraldinsight.com/Insight/ViewContentServlet?Filename=/published/emeraldfulltextarticle/pdf/0580200601.pdf

41. Guanying, M., Guozheng, Y., and Xiu, H. s.l. Power transmission for gastrointestinal microsystems using inductive coupling.: Physiological Measurement 28. pp. N9-N18., 2007.

42. P.A. Voltairas, D.I. Fotiadis, L.K. Michalis. s.l.Hydrodynamics of Magnetic Drug Targeting. : J. Biomech, 2002, Vol. 35 online available at http://medlab.cs.uoi.gr/Papers_Fotiadis/A45.pdf.

43. C.M. Oldenburg, S.E. Borglin, G.J. Moridis. s.l.Numerical Simulation of Ferrofluid Flow for subsurface Environmental Engineering Applications. : Transport in Porous Media, 2000, Vol. 38.

44. Rosensweig, R.E. Ferrohydrodynamics. New York : Dover Publications, ISBN 5QAH-S74-ETOC 1997 .

45. B. D. Cullity, C. D. Graham. s.l.Introduction to Magnetic Materials. : Wiley-IEEE, 2008, Vol. p. 103. 0471477419 online available at http://sun025.sun.ac.za/portal/page/portal/Administrative_Divisions/Navorsing/Research%20Home/Research%20Report/2008.pdf.

46. Sorensen DCS series Data Sheet. http://www.sorensen.com/products/DCS/DCS_Specifications.htm. [Online] 2006.

47. Elbuken C., Shameli E., Khamesee B. s.l. : Modeling and analysis of eddy-current damping for high-precision magnetic levitation of a small magnet. IEEE Transactions on Magnetics, 2007, Vol. 43.

48. Development of capsule endoscopes and peripheral technologies for further expansion and progress in endoscope applications. s.l. : from http://www.olympuscanada.com/msg_section/msg_endoscopy_capsulescopes.asp, 2008.

49. Hussenini, G., Myrup, G., Pitt, W., Christensen, D., and Rapoport, N. s.l.Factors affecting acoustically triggered release of drugs from polymer micelles. : JOURNAL OF CONTROLLED Release 69. pp. 43-52.April, 2001.

50. Khamesee, Mir Behrad et al. s.l. Design and Control of a Microrobotic System Using Magnetic Levitation.: JOURNAL OF APPLIED SCIENCE, IEEE/ASME Transactions on Mechatronics , 2002 ISSN 00218979.